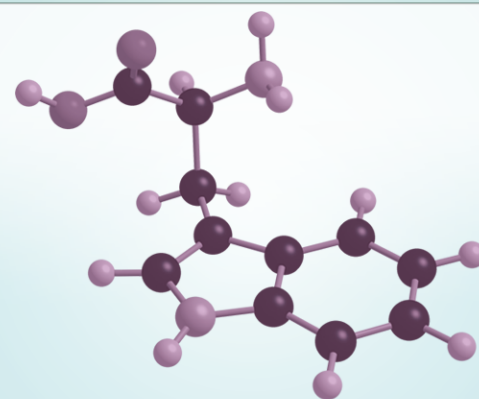
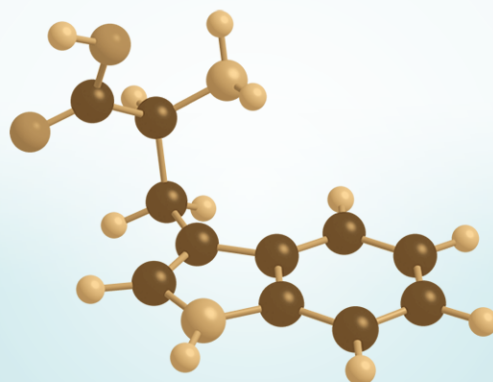
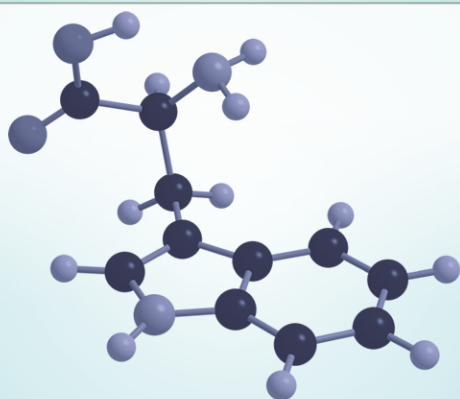


STRUCTURAL IDENTIFICATION OF GAS-PHASE BIOMOLECULES USING INFRARED SPECTROSCOPY

JOOST M. BAKKER



STRUCTURAL IDENTIFICATION OF GAS-PHASE BIOMOLECULES USING INFRARED SPECTROSCOPY

JOOST BAKKER

Structural identification of gas-phase biomolecules using infrared spectroscopy

J.M. Bakker

Thesis Radboud Universiteit Nijmegen - Illustrated

With references - With summary in Dutch

ISBN 90-9018659-X

NUR 926

Subject headings: physical chemistry / infrared spectroscopy
/ biomolecules / conformational structure

Cover design by Louise Thomas.

STRUCTURAL IDENTIFICATION OF GAS-PHASE BIOMOLECULES USING INFRARED SPECTROSCOPY

EEN WETENSCHAPPELIJKE PROEVE OP HET GEBIED VAN DE
NATUURWETENSCHAPPEN, WISKUNDE EN INFORMATICA

PROEFSCHRIFT

TER VERKRIJGING VAN DE GRAAD VAN DOCTOR
AAN DE RADBOUD UNIVERSITEIT NIJMEGEN
OP GEZAG VAN DE RECTOR MAGNIFICUS PROF. DR. C.W.P.M. BLOM
VOLGENS BESLUIT VAN HET COLLEGE VAN DECANEN
IN HET OPENBAAR TE VERDEDIGEN
OP VRIJDAG 10 DECEMBER 2004,
DES NAMIDDAGS OM 1:30 UUR PRECIES

DOOR

JOOST MIENTE BAKKER

GEBOREN OP 8 OKTOBER 1975
TE UITGEEST

PROMOTOR : PROF. DR. G.J.M. MEIJER

CO-PROMOTOR : G. VON HELDEN, PH. D.
FRITZ-HABER-INSTITUT DER MAX-PLANCK-GESELLSCHAFT,
BERLIJN, DUITSLAND

MANUSCRIPTCOMMISSIE : DR. L.C. SNOEK
OXFORD UNIVERSITY, OXFORD, GROOT-BRITTANNIË

: PROF. DR. M.S. DE VRIES
UNIVERSITY OF CALIFORNIA, SANTA BARBARA, VERENIGDE STATEN

: PROF. DR. W.J. VAN DER ZANDE

The work described in this thesis was performed as part of the research program of the “Stichting voor Fundamenteel Onderzoek der Materie” (FOM), which is financially supported by the “Nederlandse organisatie voor Wetenschappelijk Onderzoek” (NWO). The research was also financed by the NWO council for Chemical Sciences (CW).

Contents

1	Introduction	1
1.1	Motivation	2
1.2	Instrumentation	4
1.2.1	The Free-Electron Laser FELIX	4
1.2.2	The molecular beam machine	7
1.2.3	Sources	8
1.3	Spectroscopic techniques	10
1.3.1	UV spectroscopy	11
1.3.2	Infrared ion-dip spectroscopy	12
1.3.3	Infrared photodissociation spectroscopy	13
1.4	Signal interpretation	13
1.4.1	A two- and three-level approximation	13
1.4.2	Application to an experimental ion-dip spectrum	15
1.5	Theoretical methods	17
1.5.1	Conformational search	17
1.5.2	Electronic structure calculations	18
1.5.3	Harmonic vibration frequency calculations	20
2	The benzene–Ne and –Ar complex cations	23
2.1	Introduction	24
2.2	Spectroscopic details	25
2.3	Results and Discussion	29
2.3.1	Benzene–Ne	29
2.3.2	Van der Waals sidebands	33
2.3.3	Symmetry breaking effects	35
2.3.4	Deuterated benzene	38
2.3.5	Hot band spectroscopy of benzene–Ar	40
2.4	Conclusions	42
3	The benzene dimer	49
3.1	Introduction	50
3.2	Experiment	51
3.3	Results	52
3.4	Conclusions	58

4	The benzoic acid monomer and dimer	61
4.1	Introduction	62
4.2	Experiment	62
4.3	Results	63
4.3.1	The benzoic acid monomer	63
4.3.2	The benzoic acid dimer	65
4.4	Conclusions	68
5	Conformations of tryptophan	71
5.1	Introduction	72
5.2	Experiment	73
5.3	Results and Discussion	74
5.3.1	Calculations	74
5.3.2	IR spectra	74
5.3.3	Discussion	78
5.4	Conclusions	78
6	The nucleobase pair guanine-cytosine	81
6.1	Introduction	82
6.2	Experimental	84
6.3	Theoretical methods	84
6.4	Results and discussion	85
6.5	Conclusions	89
7	Benzyl-β-lactoside	93
7.1	Introduction	94
7.2	Results and discussion	95
7.3	Conclusions	101
8	Summary and outlook	105
9	Samenvatting	107
10	Dankwoord	113
11	Curriculum Vitae	117
12	Publicatielijst	119

CHAPTER 1

INTRODUCTION

A motivation of the experimental work in this thesis is presented, followed by an overview of the employed experimental and theoretical techniques.

1.1 Motivation

Bridging such scientific areas as biology, chemistry and physics, the field of biochemistry studies the microscopic interactions that determine macroscopic processes in living matter. By relating macroscopic processes to those on the inter- and intramolecular scale a better fundamental understanding of the mechanisms of life can be gained.

To understand processes that take place on the molecular scale it is imperative to have knowledge of the three-dimensional structure of the individual molecules. Generally, biomolecules are rather large. A typical protein, for instance, consists of hundreds or thousands of atoms that are arranged in a chainlike fashion. Such an arrangement brings about a great flexibility of the macromolecule, which allows the molecule to arrange itself in a vast variety of folded higher order structures. The specific higher order structure of a biomolecule determines the type of interactions it can engage in, simply by the fact that only functional groups that are exposed to the surface of the folded molecule can interact with external bodies. Usually, the interaction then takes place based on a match of the patterns of the molecules' conformation. This type of molecular pattern recognition is well illustrated in the interaction between the nucleic acid molecules of DNA and RNA, where the unique interactions between the nucleobase molecules allow for the inheritance of genetic code. The functions of proteins, saccharides and lipids are also determined by the three-dimensional structures. Interestingly, despite the numerous degrees of freedom biomolecules possess, they are almost always observed in a single conformation. For a fundamental understanding of the properties and function of biomolecules it is thus of great interest to study the intermolecular forces that govern the formation and stability of conformational structure.

To allow for a description of the three-dimensional structure of biomolecules a classification of the structure into increasingly larger ordering exists: first, the primary structure describes the way a molecule is built from individual atoms using covalent bonds. This description also includes the way in which longer molecules consist of molecular subunits or building blocks. A sequence of these building blocks in the molecular chain is then sufficient to characterize the primary structure of a biomolecule. The secondary structure describes the local orientation of molecular side groups with respect to each other. The secondary structure is mostly determined by weaker interatomic interactions, such as electrostatic and dispersive interactions. Typically, they are an order of magnitude weaker than the covalent interactions that determine the primary structure. Since these weaker interactions between side groups determine the (local) folding structure, they are responsible for the formation of well-known structural organizations, such as the α -helix and β -pleated sheet structures and the various turns that characterize a biomolecule. The macromolecules are further characterized by the tertiary structure, describing the larger substructures and longer-range interactions. Finally, the quaternary structure describes conformations of multiple entangled biomolecules. The conformational structure of biomolecules is thus described by the secondary, tertiary and quaternary structures.

Several techniques are employed to study the conformational structure of biomolecules. From the early 1950s X-ray crystallography emerged as a first reliable technique. In this method biomolecules are crystallized and studied using X-ray diffraction, from which structural information can be extracted. A drawback for this technique is the difficulty to crystallize biomolecules, and the uncertainty whether the crystalline form of the molecule is the same as the one in solution.

In the late 1980s, the development of Matrix-Assisted Laser Desorption Ionization (MALDI) and ElectroSpray Ionization (ESI) allowed mass-spectrometrists to bring large molecules (of masses up to typically 10^6 amu) intact into the gas phase [1, 2]. This led to a dramatic increase in the number

of biomolecules that can be studied, and has become a routine tool in analytical biochemistry to determine mass and sequences of biomolecules. However, little information on the conformational structure is obtained. Some mass-spectrometric techniques have been developed for evaluation of the conformational structure. Among these are the development of ion chromatography, in which the conformation is deduced from the measured collision cross-section of the molecule with a buffer gas of inert atoms [3–5]. In other gas-phase mass-spectrometric experiments, the H-D exchange rate of a molecule is measured, which is a measure of the surface area of the molecule, and thus of its conformation. The drawback that all mass-spectrometric techniques have in common is that they involve (often multiply) charged molecules, which could influence the conformational structure of the system under study.

Recently, a different approach has been introduced. This approach involves the determination of the conformational structure of biomolecules by measuring their spectroscopic properties [6, 7]. The aim of this method is to study the effects of inter- and intramolecular interactions on the spectral properties of biomolecules on a basic level, *i.e.*, starting from the building blocks. To isolate inherent properties of the molecules from solvent effects, the molecules are studied in the gas-phase. Later, the effects of the addition of solvent molecules can then be studied by adding them in a controlled fashion in so-called microsolvation experiments. Initially, the spectral properties of gas-phase biomolecules were studied solely in the UV, where information of the nuclear structure of the molecules is mixed with information on the electronic structure. Recently, the infrared (IR) properties of biomolecules have drawn more interest, as they are a more direct probe of the (nuclear) structure.

The general strategy for such experiments is the following: first, the UV spectrum of a biomolecule brought into the gas phase is obtained. This UV spectrum consists of contributions of several stable conformational isomers, or conformers, of the studied molecule. These contributions can then be disentangled by the performance of UV-UV hole burning spectroscopy [8]. The IR spectral properties of individually selected conformers can then be probed by IR–UV hole burning experiments. Finally, the combination of these experimental data with high-level ab-initio calculations can lead to a structural assignment.

The scope of systems that are studied using these techniques undergoes a constant evolution into larger and more complex systems. Initially, single amino acid molecules or mimic systems were studied, nowadays more involved systems are studied. The systems under study range from nucleobase molecules and the pairing of them in the gas phase, to di-, tri- and larger peptides (where the first signs of model secondary structure formation are observed), to the complexation in the gas-phase of the molecules with water molecules to study microsolvation effects. The results from these studies in general terms allow for an evaluation of the importance of several intramolecular interactions in the formation of higher order structure. They also form a large set of experimental data that theoretical chemists can use to improve quantum chemical calculations and to parametrize force fields used in semi-classical trajectory calculations.

While the IR spectroscopic studies have proven to be highly successful at determining the stable gas-phase structures of biomolecules, they have so-far been limited to a rather narrow spectral regime. Almost all work has been performed using table-top laser systems that produce light in the near-IR spectral region up to $\sim 7 \mu\text{m}$. In this wavelength region the stretching vibrations of C=O, O–H, N–H and C–H groups are probed. Due to the importance of the intramolecular hydrogens bonds in the formation of higher order structure, and due to the sensitivity of the stretching vibrations to the presence of these hydrogen bonds, these studies have had great success. Consequently, the benchmarking of

quantum chemical methods has mainly been performed using the stretching vibrations. However, the main body of molecular vibrations is found at lower energies, and it is in the mid-IR spectral region that a wealth of information lies hidden that is still to be uncovered.

The main limitation for studies in the mid-IR regime has been the lack of a suitable laser source that produces widely tunable, pulsed IR radiation. In previous studies, it has been shown that a Free-Electron Laser (FEL) is a highly suitable apparatus for performing molecular spectroscopy throughout the mid-IR spectral region [9]. The aim of this thesis is to investigate whether information on the conformational structure of gas-phase biomolecules can be obtained using FEL-based molecular double-resonance spectroscopic methods. The central questions in this work are thus the following:

- can differences in conformational structure be observed in the mid-IR spectral range with FEL-based molecular spectroscopy?
- do the current theoretical methods accurately describe the vibrations to allow structural identification from the mid-IR spectra?

In the present work these questions are investigated by evaluating several molecular systems, which are prototypes for the interactions that play a role in conformational structure formation and stabilization. In Chapter 2 a classical chemistry problem, that of the Jahn-Teller effect in the benzene cation, is studied to investigate the capabilities of the present experimental setup in conjunction with the Free-Electron Laser for Infrared eXperiments (FELIX). Next, the effects of dispersive forces and hydrogen bonding on the IR spectral properties are probed by studying the benzene dimer (Chapter 3) and the benzoic acid monomer and dimer (Chapter 4), respectively. Then the applicability of IR spectroscopy in the mid- and far-IR to probe the conformational structure of highly flexible molecules is explored by studying the amino acid tryptophan (Chapter 5). Finally, in Chapters 6 and 7, IR spectroscopy is applied to more exotic species: to the isolated nucleobase pair of guanine and cytosine, and to a model disaccharide system benzyl- β -lactoside.

First, however, it is imperative to describe the experimental and theoretical methods that are used in this thesis. This introductory chapter starts out with a description of the unique and unrivaled capabilities that the free-electron laser FELIX possesses in the mid- and far-IR. After that, the techniques that are used to prepare the molecules under study are described, followed by a discussion on the spectroscopic techniques and on the interpretation of the obtained data.

1.2 Instrumentation

1.2.1 The Free-Electron Laser FELIX

Central in this work is the possibility to perform mid- and far-infrared (IR) spectroscopic studies on molecular species. Although there exist several table-top sources that can produce radiation in the wavelength range up to 10 μm and even longer wavelengths, only few are able to produce a high enough fluence and a narrow enough bandwidth to effectively study absorptions in dilute samples of gas-phase molecules. A common approach to produce tunable IR radiation is to combine the outputs of pulsed dye lasers and of a Nd:YAG laser at 1064 nm in a nonlinear crystal and produce radiation with the difference frequency of the two input frequencies. The resulting difference frequency can typically reach wavelengths of up to 3-4 μm . For longer wavelengths, usually an optical parametric oscillator (OPO) system is employed where wavelengths of up to 7 μm can be reached.

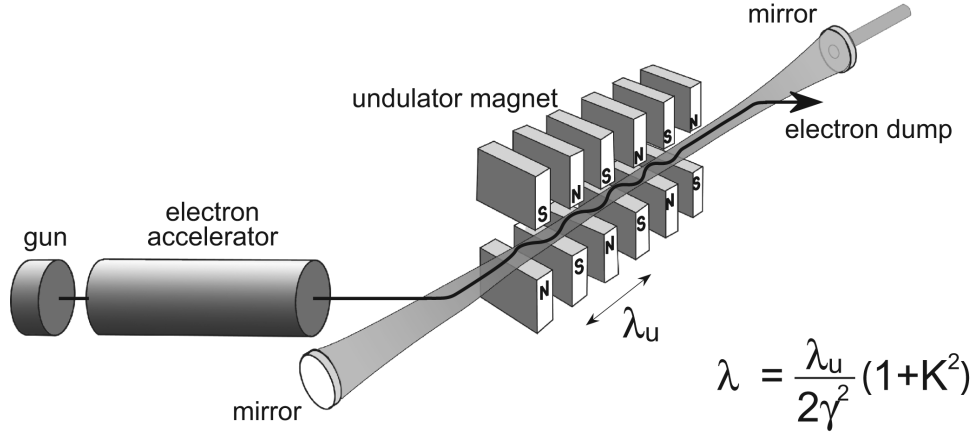


Figure 1.1: Schematic layout of a Free-Electron Laser (FEL)

For longer wavelengths, no feasible tabletop systems are in existence and a different type of laser is required. In this work, IR radiation is produced by the Free-Electron Laser for Infrared eXperiments (FELIX), based at the FOM institute for Plasma Physics Rijnhuizen in Nieuwegein, the Netherlands. This type of laser is unique in that it has no atomic, molecular or solid state system as a gain medium. Rather, the gain medium consists of free electrons that are traveling at relativistic energies through a periodically alternating magnetic field [10]. Therefore, there are no intrinsic absorptions in the gain medium and radiation can (in principle) be produced at any wavelength, from the far-IR to the XUV.

A schematic of the operation of this laser is depicted in Figure 1.1: bunched relativistic electrons, usually produced by an RF accelerator, are injected into a magnetic field that is produced by a set of alternately poled permanent magnets, called an undulator. A Lorentz force is exerted on the electrons by the magnetic field, of which the orientation is perpendicular to the motion of the electrons and the magnitude is periodically reversed. The force makes the electrons perform a wiggling motion perpendicular to the propagation direction. The oscillatory motion of the electrons is analogous to the motion of electrons in a stationary dipole antenna, and likewise, these electrons emit radiation. The relativistic nature of the electrons causes the radiation to be emitted in the forward direction concentrated in a narrow opening angle, often referred to as the “head-light” effect. Furthermore, it shifts up the frequency of the radiation by a factor γ^2 , with γ the Lorentz factor of the electron ($\gamma \gg 1$). The resonance condition under which an electron radiates spontaneously is that the radiation, propagating at the speed of light, should advance with respect to the electron an integer number of wavelengths per undulator wavelength λ_u :

$$n\lambda = \frac{\lambda_u}{2\gamma^2}(1 + K^2)$$

where K is a dimensionless parameter, proportional to the on-axis undulator field strength, that accounts for the path length difference between the path of the radiation and the path of the electron.

The moving electron couples to the radiation field and, depending on the phase between the propagating radiation field and electron, will transfer energy to or from the radiation field. Given an isotropic distribution of the electrons in a bunch over all phases, no net energy transfer is achieved after an undulator traverse, yielding no optical gain. However, since the energy transfer causes a velocity modulation, a phase dependent density modulation is created which makes a net energy transfer

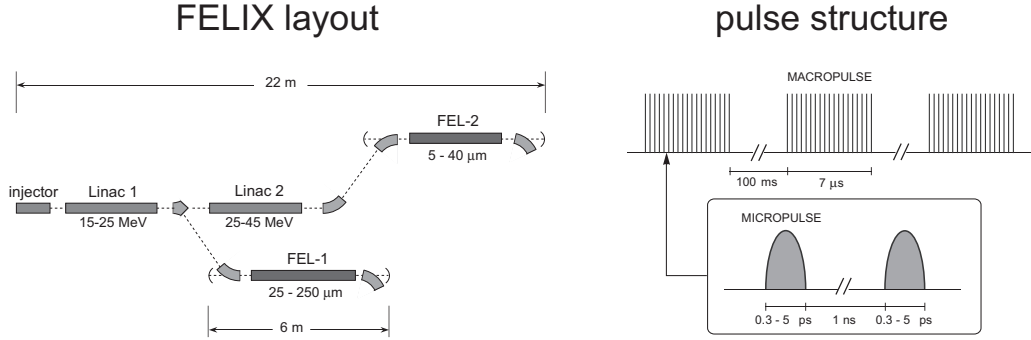


Figure 1.2: Schematic layout of FELIX and its temporal pulse structure.

from electron beam to the radiation field possible. As the density modulation will be 90° out of phase with the spontaneous radiation field, and no coupling will take place, optical gain will result at a wavelength slightly detuned to the red. Saturation will set in when an electron is so strongly coupled to the radiation field that, where it enters the undulator under conditions that energy is transferred *to* the field, it gets slowed down so much that it starts transferring energy *from* the field. There exist FELs where a single pass of an electron bunch can already lead to saturation [11]. However, in FELIX this saturation is not reached within a single pass and the produced radiation is captured in an optical cavity built around the undulator that is matched to the electron bunch spacing, ensuring that eventually saturation is reached. Adjustment of the length of the optical cavity determines the importance of so-called slippage effects: the slippage length is the distance the electron bunch lags with respect to the optical radiation field after passing through the undulator. These effects determine among others the number of optical cycles in one laser pulse and saturation power.

In Figure 1.2 the physical layout of FELIX is shown: two FEL cavities (aptly named FEL1 and FEL2), consisting of two high-quality copper coated mirrors of which one has a hole in it for out-coupling purposes, are fed with electron bunches produced by one or two accelerator stages. The accelerators and FEL cavities are designed for different IR wavelength ranges: FEL1 covers the 25–250 μm far-IR range and FEL2 the 5–40 μm region. Additionally, the range between 2 and 5 μm can be covered as well by optimizing FELIX to lase on the third harmonic [12]. This is accomplished by replacing the copper coated cavity mirrors by dielectric mirrors that have a high reflectivity in a narrow spectral region around the desired wavelength range. Lasing on the fundamental is thus suppressed and the gain that is present at three times the photon energy is used to produce laser light.

The temporal structure of the optical output of FELIX mimics that of the incoming electron beam. The RF accelerator(s) produces a typically 7 μs long pulse of ps-long electron bunches, that individually produce ps-duration laser pulses. The individual laser pulses are tagged “micropulses”, whereas the pulse train of laser pulses, usually shorter than 7 μs due to a light pulse energy build-up required by the low-gain single-pass conditions in the FELIX cavity, is called a “macropulse”. The macropulse period can be set to 100 ms or any integer multiple of 100 ms, and the micropulse repetition rate can be either 25 MHz or 1 GHz. This corresponds to one or 40 optical pulses circulating in the 6 m long cavity of FEL1 or FEL2, respectively. The micropulse duration ranges from 300 fs (broad bandwidth) to several ps (narrow bandwidth), depending on the cavity determined slippage length. The bandwidth of the produced radiation is near-transform limited and can range from less than 0.5 % to several percent full width at half maximum (FWHM) of the central wavelength.

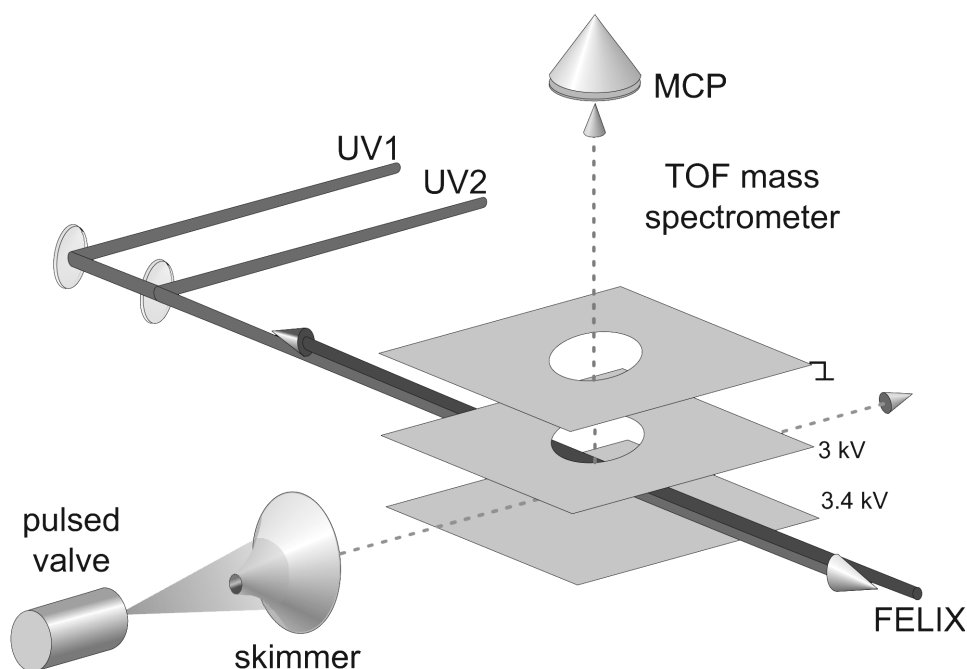


Figure 1.3: Scheme of the experimental set-up used for all IR photodissociation and IR ion-dip spectroscopy experiments described in this thesis.

The resulting output wavelength of FELIX is determined by the electron beam energy (γ) and the strength of the undulator magnetic field (K). Both parameters can in principle be changed to vary the wavelength. In FELIX the wavelength is changed by adjusting the distance between the magnets that are placed on two sides of the electron beam, thus by varying the magnetic field strength. This is implemented in an extremely flexible fashion making spectroscopy using FELIX very feasible. Only for large wavelength changes the electron beam energy is adjusted. During one experimental session using FELIX the electron beam energy is usually optimized for a certain wavelength range and only the inter-magnets distance is varied. Typically, a factor of three in wavelength can be covered using one electron beam energy setting.

A typical macropulse energy at narrow bandwidth settings and 1 GHz micropulse repetition rate is 30 to 50 mJ, but energies of 100 to 150 mJ are routinely available when the cavity is adjusted for shorter micropulse duration (and larger bandwidth).

A transport system consisting of evacuated tubing (to minimize atmospheric absorption) and several refocusing mirrors is in use to direct the FELIX output to user experiments. Although the distance between the FELIX cavity and an experiment is typically 30 m, the stability of the transport system is such that no realignments are needed over periods of hours.

1.2.2 The molecular beam machine

All experiments described in this work are performed in a molecular beam machine. The setup that is used in this work is schematically shown in Figure 1.3. A rare gas is expanded from a certain backing pressure through a pulsed valve into a vacuum chamber. Either before the release of the gas sample into the vacuum chamber or very shortly after it, a sample of molecules is in a variety of ways

vaporized and mixed with the rare gas. The vaporization sources are described in section 1.2.3. In the expansion process, the atom-molecule gas mixture is cooled adiabatically, *i.e.*, internal energy of the gas is transferred into kinetic energy of the atoms. On a microscopic level, the molecules are cooled through inelastic collisions with the carrier gas atoms. Several inert gases are used of which Ar, Ne and He are the most frequently used. The cooling properties of the so-called carrier gas are determined by its mass (and thus its ability for momentum transfer). Typically, the molecules are vibrationally and rotationally cooled to some 5 K. The expansion conditions enable the formation of weakly bonded molecular Van der Waals complexes, complexes of molecules with rare gas atoms, and hydrogen bonded complexes and these complexes are internally cooled as well.

After the expansion, all particles travel at rather high speed (typically 500 ms^{-1}) and with a rather narrow velocity distribution, which is a measure of the translational temperature of the sample. The molecules then enter an interaction region after being skimmed by a conically shaped skimmer. The distance from the nozzle of the pulsed valve to the skimmer, some 50 mm, and the skimmer diameter, 1 mm, determine the geometry of the beam, that interacts with various laser sources in the source region of a Wiley-McLaren type linear Time-Of-Flight (TOF) mass spectrometer. The molecules in the beam interact with incoming UV laser beams as well as with the IR laser beam at the crossing point of the mutually perpendicular molecular beam axis, laser beam axis and TOF tube axis. Ions are produced in this region and subsequently pulse extracted and accelerated toward a Micro Channel Plate (MCP) detector, yielding mass spectra with a resolution of $M/\Delta M \approx 200$. The signal from the MCP detector is amplified and fed into a 10 bit, 100 Ms/s digital oscilloscope that is read out by a PC. The experiment is running at a 10 Hz repetition rate; digital delay/pulse generators are used to synchronize the molecular beam to the various laser sources.

1.2.3 Sources

The experiments described in this thesis are all studies of gas-phase species. For crystalline or liquid samples with a substantial vapor pressure at room temperature the sample can directly be mixed with the carrier gas. Other molecules can be heated to produce a reasonable vapor pressure and are then seeded into the carrier gas before the expansion into the vacuum chamber. Temperatures that can be employed are limited by the properties of the pulsed valve; the Jordan type valve can be heated to a maximum of 75°C . For experiments with benzene (Chapters 2 and 3) and the benzoic acid molecule (see Chapter 4), no higher temperatures are required and the standard equipment available is used. When higher temperatures are needed, an oven that is placed *after* the nozzle and where thermal contact between valve body and oven is minimized, can be used. It is less trivial to study systems that have both a low vapor pressure and are thermally labile. For these molecules the method of laser-desorption is employed.

A sublimation oven

To heat samples of low vapor pressure that are thermally stable an oven is constructed, based on a design from Dr. L.C. Snoek [13]. Schematically, the oven is shown in Figure 1.4, part A. The oven is placed behind the nozzle of a General Valve (series 9), a pulsed valve that can be heated to 200°C . The oven body is heated by heating coils, while the temperatures of both the valve and oven bodies are monitored using thermocouple gauges. Typically, the oven can be heated to 250°C without exceeding the temperature limit of the valve, due to the poor thermal contact between oven and valve, both of

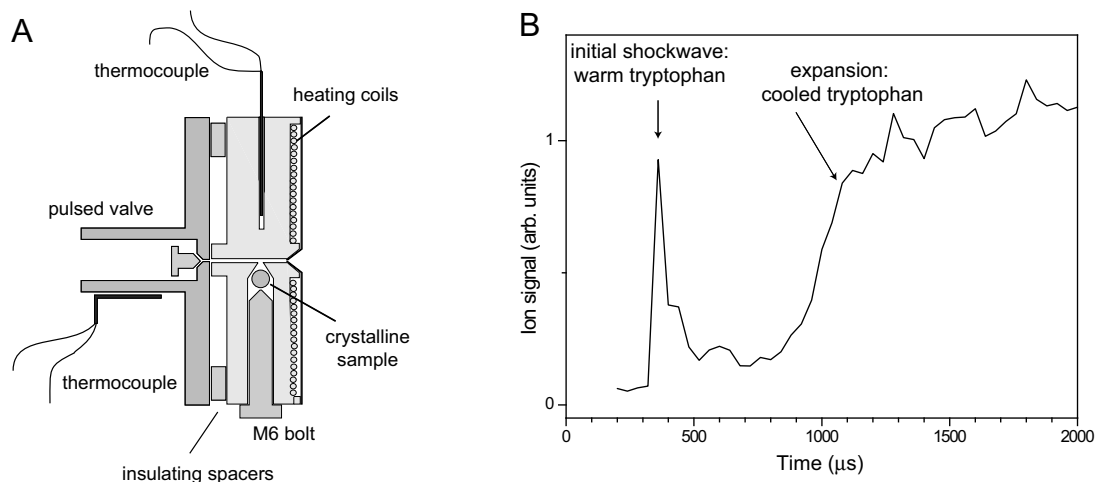


Figure 1.4: Schematic drawing of the oven used for the sublimation of molecular species at temperatures higher than the pulsed valve can withstand (part A). In part B, a temporal profile of detected tryptophan molecules, seeded in an argon beam, is depicted.

which are made of stainless steel.

The species of interest is inserted into a sample compartment in the oven, which is closed to one side. The oven thus produces a vapor plume, which is then entrained by the gas pulse and expands after the oven. In Figure 1.4, part B, a typical temporal profile of the molecular beam as produced by the oven is depicted. In the figure, the ion current due to tryptophan molecules is probed as a function of time delay between the trigger pulse that starts the valve opening and the firing of the laser downstream. The laser is tuned to a resonance for cold tryptophan. The temporal structure is slightly strange: it appears as if there are two pulses of molecules coming out of the oven. Inspection of the UV spectra taken at the maxima of the two peaks learns that for the first peak there is no structure at all, whereas the second peak does exhibit a resonant spectrum. From this it is inferred that the first tryptophan peak is the result of warm tryptophan molecules that are blown out of the oven by the shock wave of the gas pulse. Hardly any mixing with the rare gas atoms which could collisionally cool down the molecules takes place and broadband absorption of the UV light leads to ionization of the molecules.

Different is the situation if the UV spectrum is recorded on the maximum of the second peak. Here, a UV spectrum with clearly separated resonance structure is observed. The proposed mechanism for the expansion properties of this second pulse is the following: the initial pulse of rare gas atoms fills the channel in the oven body thereby pushing out the plume of tryptophan molecules that will be detected as 'hot'. It also fills the sample compartment where the already present tryptophan vapor mixes thoroughly with the carrier gas. In this process, pressure is built up in the sample compartment (and in the oven channel) which leads to, indeed, a second expansion. The expansion conditions are evidently less ideal than in the situation where nothing blocks the pulsed valve. The resulting beam temperature could be some 15 K or even higher, but is still low enough to allow for a resonant and conformer-specific detection scheme (see section 1.3.2).

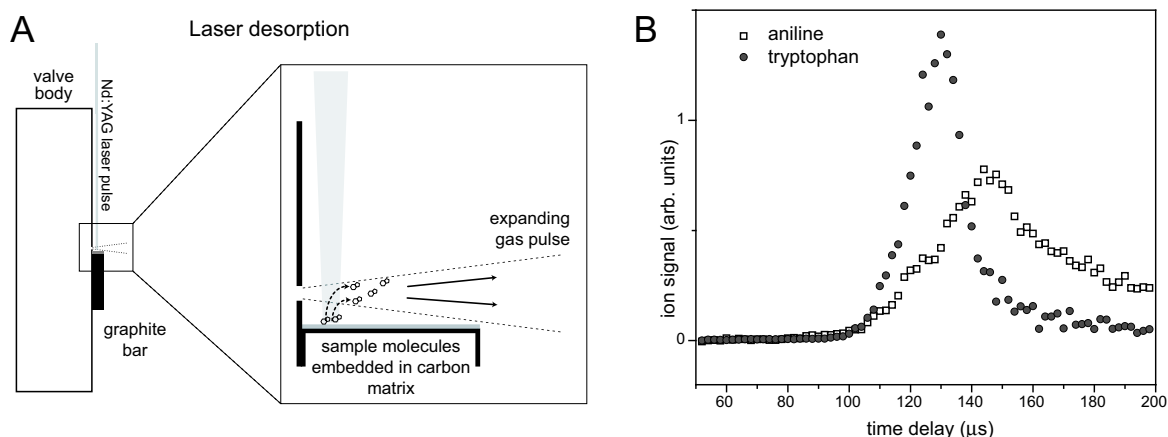


Figure 1.5: Schematic overview of laser desorption (top): a pulsed Nd:YAG laser (1064 nm) desorbs molecules that are embedded in a graphite matrix. The – intact – molecules are then entrained by a passing gas pulse and are cooled adiabatically. Next to the schematic a time dependence of a gas pulse with desorbed molecules is shown for optimum cooling conditions. Plotted is the yield of ions produced downstream by a 1+1 REMPI process as a function of the delay of the probe pulse with respect to the opening of the valve.

Laser desorption

A second method to bring molecules that have a low vapor pressure at room temperature into the gas phase is laser desorption [14]. The method is schematically described in Figure 1.5, part A. In the laser desorption source a crystalline sample of the molecules under study is mixed with fine graphite powder and applied onto a surface of a bar of solid graphite (50x15x2 mm) that is placed directly under the orifice of a pulsed valve. The 10 Hz pulsed Jordan valve releases gas pulses of argon (typically 50 μs long) through a 0.5 mm diameter nozzle into vacuum at a backing pressure of 3.5 bar. Directly after opening the nozzle a pulsed Nd:YAG laser (Thales Diva-2, 1064 nm, 5 ns, < 1 mJ per pulse) desorbs sample molecules from the graphite matrix. The desorbed molecules are entrained in the supersonically expanding carrier gas. In the adiabatic expansion the internal degrees of freedom in the nucleobase molecules are cooled to some 10 K.

In part B of Figure 1.5 a time dependence of the gas pulse is shown under optimal cooling conditions. The yield of ions produced downstream by a 1+1 REMPI process is plotted as a function of the delay of the probe pulse with respect to the opening of the valve. The squared, open symbols represent the yield of ionized test molecules (aniline) that are seeded into the beam prior to the expansion to detect the gas pulse. The round, full symbols represent the tryptophan molecules that are desorbed from the sample bar and seeded into the beam. It is experimentally observed that the optimum probe laser delay is shorter for desorbed material than for molecules seeded into the beam before expansion.

1.3 Spectroscopic techniques

The techniques that are used in this thesis to record IR absorption spectra of dilute samples of gas-phase molecules are double-resonance techniques, *i.e.*, they are based on the presence of two well-synchronized lasers that interact with the same sample. Mostly, these double-resonance techniques are based on already existing techniques that probe the electronic structure of the molecules under

study. Therefore, these techniques are introduced first, and after that the natural extension to usage in the IR is discussed.

1.3.1 UV spectroscopy

There are two spectroscopic techniques that are commonly used in the spectroscopy of dilute samples. The applicability of both is dependent on the electronic structure of the molecule under investigation. The first technique, Laser-Induced Fluorescence (LIF), is not used in this work and only a short description is given. In LIF, the molecule of interest interacts with an incoming (UV) photon and is excited to an electronically excited state. After initial excitation, the excited state may spontaneously get de-excited while emitting a photon that carries off the energy associated with the excited state. The emitted light can then be collected and detected. By recording the flux of emitted light as a function of excitation wavelength, information on the electronic and rovibronic structure of the molecule is obtained. This method is in principle universally applicable, as long as the excited state has a sufficiently large quantum yield for fluorescence.

The second technique that is used to study the electronic structure of molecules is based on ionization of the molecule. In this process, the molecule is initially excited to a rovibronic level in an electronically excited state and then a second photon is absorbed that ionizes the molecule. Molecular ions can then be detected in a mass spectrometer (cf. section 1.2.2) and by monitoring the number of detected ions (in one mass channel) while varying the excitation laser an electronic excitation spectrum is obtained. In

an alternative detection scheme, the simultaneously produced electrons are collected, but here the mass-selectivity is lost. The source of the second photon can be the same laser as used for excitation; this method is called (1+1)-Resonance-Enhanced Multi-Photon Ionization (REMPI). Another possibility is to employ a second laser and to tune that to a convenient frequency that maximizes the ionization rate. This method is called Resonant Two-Photon Ionization (R2PI) and has the advantage that not only the excitation frequency can be changed, and thus the electronic structure of the molecule can be probed, but also the ionization frequency can be varied, which allows for a mapping of the electronic and vibrational structure of the ion. When R2PI is combined with smart electronic detection methods, one can separate molecular ions in different vibrational states and obtain a clean picture of

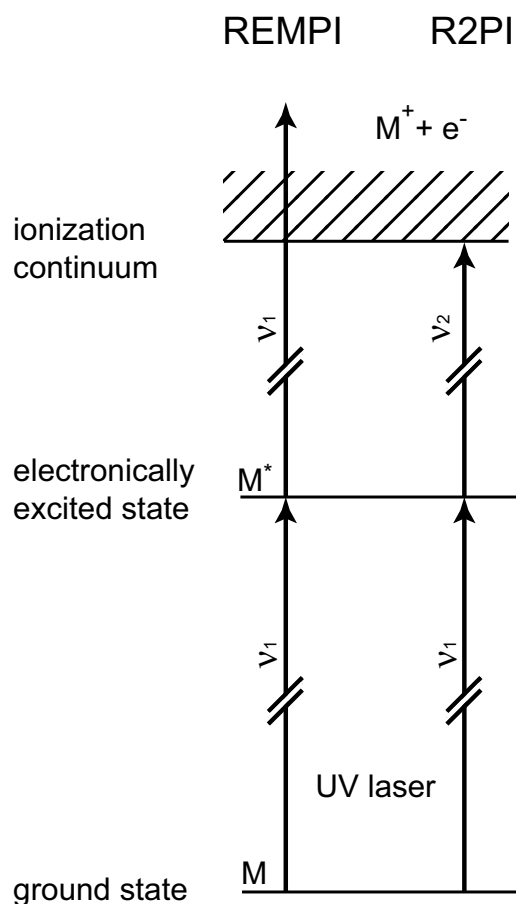


Figure 1.6: Schematic overview of Resonance-Enhanced Multiphoton Ionization (REMPI) and Resonance-enhanced 2-color Multiphoton Ionization (R2PI).

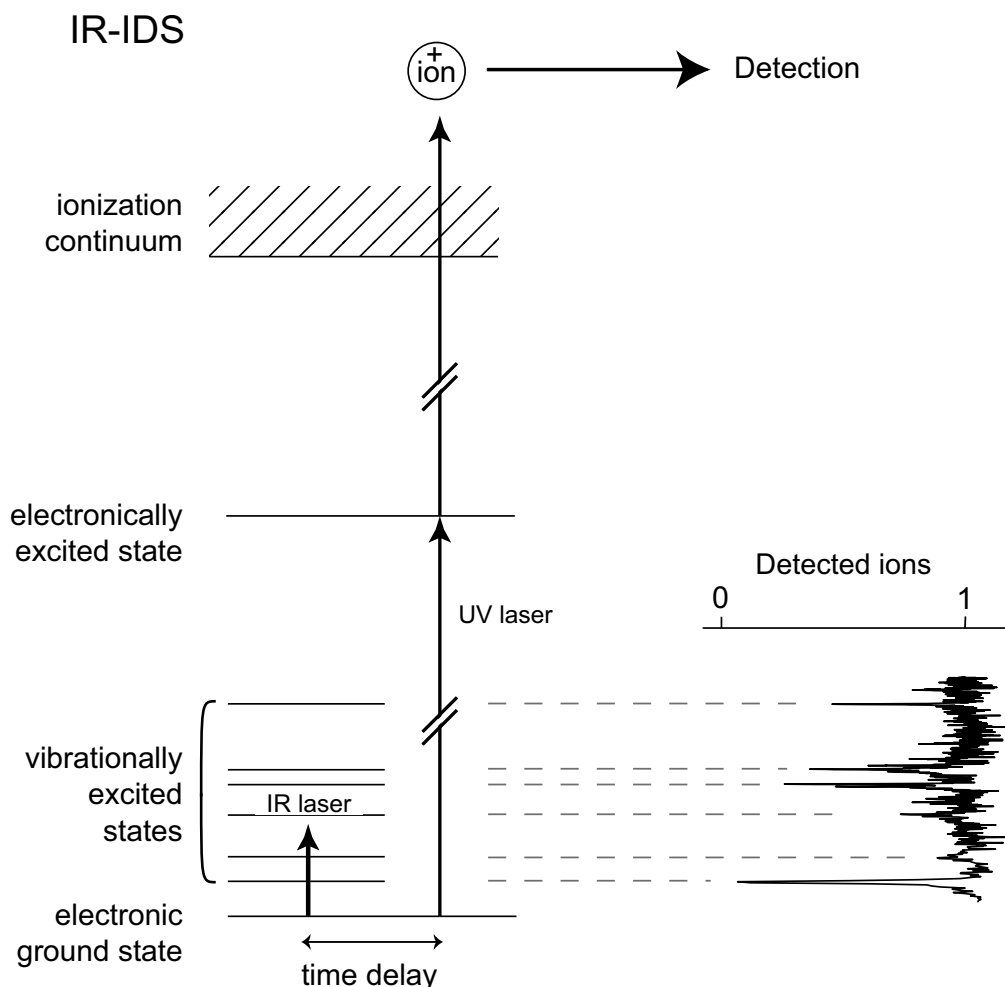


Figure 1.7: Schematic overview of IR-ion-dip spectroscopy

the vibrational structure of the ion. This is applied in the so-called threshold techniques, Zero Electron Kinetic Energy (ZEKE) spectroscopy and Mass-Analyzed Threshold Ionization (MATI) spectroscopy [15, 16]. The applicability of REMPI or R2PI depends on the lifetime of the excited state, which has to be as long as the laser pulse duration. If the molecule exhibits a very fast inter-system crossing into a different electronically excited state from where the second photon cannot efficiently ionize, this method cannot be applied.

1.3.2 Infrared ion-dip spectroscopy

The method that is employed to measure the IR absorption spectra of jet-cooled, neutral molecules is IR ion-dip spectroscopy (IR-IDS). This technique is applicable for the measurement of the IR absorption spectrum of any neutral molecule. In IR ion-dip spectroscopy ions are produced from ground state molecules using a one- or two-color ionization scheme, ionizing only molecules in the vibrationless ground state of the neutral molecules. A few μs before the excitation laser is fired, an IR laser interacts with the molecules. If a vibrational transition is induced by the IR light, molecular population is transferred from the ground state into an excited vibrational state, leading to a depletion

of ground state molecules. This results in a dip in the number of produced ions. By measuring the ion yield, while varying the wavelength of the IR laser, the ion-dip spectrum is obtained. Similar to IR-IDS, IR fluorescence-dip spectroscopy is often applied [6].

1.3.3 Infrared photodissociation spectroscopy

To record the IR absorption spectrum of gas-phase ions, IR photodissociation of a complex of the species of interest with a rare gas atom is a very suitable technique [17]. The technique makes use of the fact that the interaction between the inert rare gas atom and the molecule is of little or no influence on the structure of the molecule. IR photodissociation requires a well-defined initial ion distribution of molecular complex ions. Such a population could for instance be prepared in an electron-impact (EI)-source [18] but a more controlled way is to make use of a complex specific R2PI scheme. The transition frequencies for the complex in general are shifted from those of the isolated molecule, enabling a complex-specific excitation. The ionizing photon is then chosen such that the molecular complex is ionized and all ionic population is in the vibrational ground state. Directly after creation of the ionic population, an IR laser interacts with the molecules. The IR laser can induce a transition of the molecules into a vibrationally excited state. If the vibrational energy is larger than the dissociation of the complex there is a probability that the complex will dissociate. In this case the charge will remain localized on the molecule and a bare molecular ion will be detected. If the number of bare molecular ions is recorded while varying the IR frequency the IR photodissociation spectrum is obtained. Because there is initially no population of the bare ion, this method is background free, which makes it very sensitive. Additionally, contrary to threshold techniques it has the advantage of being subject to the selection rules that govern IR absorption processes. Using FELIX, this method has been successfully demonstrated to study the IR absorption spectra of aniline- Ar^+ , naphthalene- Ar^+ , phenanthrene- Ar^+ and benzene- Ar^+ [9, 19–22].

1.4 Signal interpretation

1.4.1 A two- and three-level approximation

In a first-order approximation, IR absorption spectroscopy is governed by the rate equations for a closed two-level system (see Figure 1.8). Since the FELIX macropulse duration is long compared to decoherence times of excited vibrational states, of which the full rotational envelopes can be covered with the FELIX bandwidth, coherent effects such as Rabi oscillations can be neglected. In the rate equations, the populations $N_1(\nu, t)$ of the initial state 1, and $N_2(t)$ of the final state 2 are coupled by the radiation field, represented by a time-dependent fluence $\rho(\nu, t)$, and an absorption cross-section $\sigma(\nu)$, both functions of frequency ν . Spontaneous emission is neglected as, in general, vibrational lifetimes are on the order of milliseconds, which is well out of the experimental time window. Additionally, in the cold

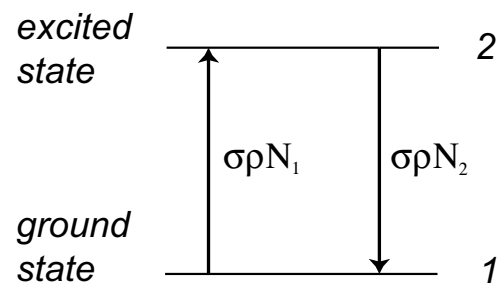


Figure 1.8: Schematic two-level system, neglecting spontaneous emission.

order of milliseconds, which is well out of the experimental time window. Additionally, in the cold

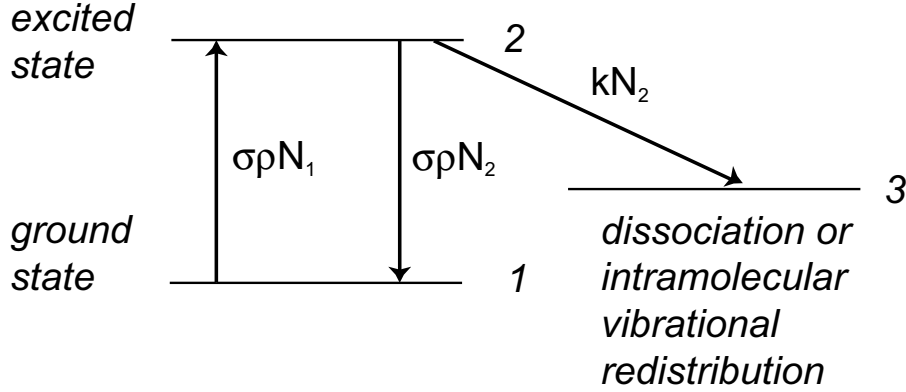


Figure 1.9: Schematic three-level system, as applicable to IRPD and IR-IDS

beam environment, conditions preclude collisional relaxation. This simplifies the two-level picture to yield the coupled differential equations:

$$\begin{aligned}\dot{N}_2(\nu, t) &= \sigma(\nu)\rho(\nu, t) (N_1(\nu, t) - N_2(\nu, t)) \\ \dot{N}_1(\nu, t) &= \sigma(\nu)\rho(\nu, t) (N_2(\nu, t) - N_1(\nu, t))\end{aligned}$$

With the initial conditions at $t = 0$, the start of the macropulse, of $N_2(t = 0) = 0$ and $N_1(t = 0) = 1$, these equations yield

$$\begin{aligned}N_1(\nu, t) &= \frac{N_0}{2} [1 + \exp(-\sigma(\nu)\rho(\nu, t))] \\ N_2(\nu, t) &= \frac{N_0}{2} [1 - \exp(-\sigma(\nu)\rho(\nu, t))]\end{aligned}$$

where the total population $N_0 = N_1(\nu, t) + N_2(\nu, t)$. The bandwidth of FELIX is much larger than that of a vibrational transition, and can be assumed to be constant over the macropulse. The energy density $\rho(\nu, t)$ can then be approximated by a constant $P(\nu)$, which is the fluence of the macropulse at frequency ν . The molecular populations, after interaction with a FELIX macropulse can then be described by (dropping the time dependence)

$$\begin{aligned}N_1(\nu) &= \frac{N_0}{2} [1 + \exp(-\sigma(\nu)P(\nu))] \\ N_2(\nu) &= \frac{N_0}{2} [1 - \exp(-\sigma(\nu)P(\nu))]\end{aligned}$$

For large fluences the equilibrium population in both states will converge to $N_0/2$.

All this is derived for a closed, two-level system. In the techniques that are used in this work, the vibrational states cannot be regarded as isolated states. In the IRPD experiments, there is a high probability that the molecular complex in the vibrationally excited state dissociates. This is an extension to a three-level system with unidirectional decay described by a decay constant $k(\nu)$ (cf. Figure 1.9):

$$\begin{aligned}\dot{N}_1(\nu, t) &= \sigma(\nu)\rho(\nu, t) (N_2(\nu, t) - N_1(\nu, t)) \\ \dot{N}_2(\nu, t) &= \sigma(\nu)\rho(\nu, t) (N_1(\nu, t) - N_2(\nu, t)) - k(\nu)N_2(\nu, t) \\ \dot{N}_3(\nu, t) &= k(\nu)N_2(\nu, t)\end{aligned}$$

The solutions of this three level system can be solved analytically. As the decay process in IRPD for all ν takes place well within the experimental timescale [23], the approximation $k(\nu) \gg \sigma(\nu)\rho(\nu, t)$ is introduced. With this approximation one gets:

$$\begin{aligned} N_1(\nu) &= N_0(\exp(-\sigma(\nu)P(\nu))) \\ N_2(\nu) &= 0 \\ N_3(\nu) &= N_0(1 - \exp(-\sigma(\nu)P(\nu))) \end{aligned}$$

Again, $N_0 = N_1(\nu) + N_2(\nu) + N_3(\nu)$ is the total population. From this it is clear that the population in the intermediate, excited state is negligible and is directly transferred into the dissociated state. The relative cross-section can then be retrieved by:

$$\sigma(\nu) = -\frac{1}{P(\nu)} \ln\left(\frac{N_1(\nu)}{N_1(\nu) + N_3(\nu)}\right)$$

The relative cross-section can of course also be obtained from the population in state I only, but inclusion of the dissociated state 3 will reduce the experimental noise substantially since the shot-to-shot noise in the initially created total population N_0 is factored out.

For IR-IDS a similar picture can be drawn: there is no decay channel for dissociation or fragmentation, but there is Intramolecular Vibrational Redistribution (IVR). The density of states for larger molecules becomes rapidly so large that the probability of accidental degeneracies between different vibrational states becomes rather high. It is then possible to redistribute the population that is transferred from the initially excited state to isoenergetic vibrational states [24]. Now the three-level approximation is technically no longer valid, since redistribution does not necessarily completely depopulate the initially excited state. If there are many levels over which population is redistributed, however, the states over which this is done can be described as a *bath* to which the population is decaying. In this approach, the description of the population in states I , 2 and 3 is valid, and the relative cross-section is retrieved by

$$\sigma(\nu) = -\frac{1}{P(\nu)} \ln(N_1(\nu))$$

In this approach, the fluctuations in the total population are not factored out, and care should be taken that the ion signal for state I is normalized to a constant background of ions. Experimentally this is done by running FELIX at half the repetition rate of the UV laser(s) and recording alternating IR-*on* and IR-*off* signals so that the former can be normalized to the latter.

1.4.2 Application to an experimental ion-dip spectrum

To demonstrate the applicability of the previously discussed three-level system to retrieve relative cross-sections from IR-IDS data, a typical IR-IDS spectrum, recorded for the benzoic acid monomer, is shown in Figure 1.10. The trace shows the detected ion signal due to benzoic acid monomer ions, corrected for source and UV laser intensity fluctuations. The signal is thus proportional to the population remaining in the vibrational ground state after interaction with the IR light. One can identify a large number of *dips*, where the vibrationless ground state population is depleted. The dips are the signatures of vibrational states accessible with IR radiation from the ground state.

It is observed that for a number of dips, the population decrease is more than 50 %. In particular, the resonance at 1752 cm^{-1} can result in a depletion as high as 80 %. This is quite an interesting

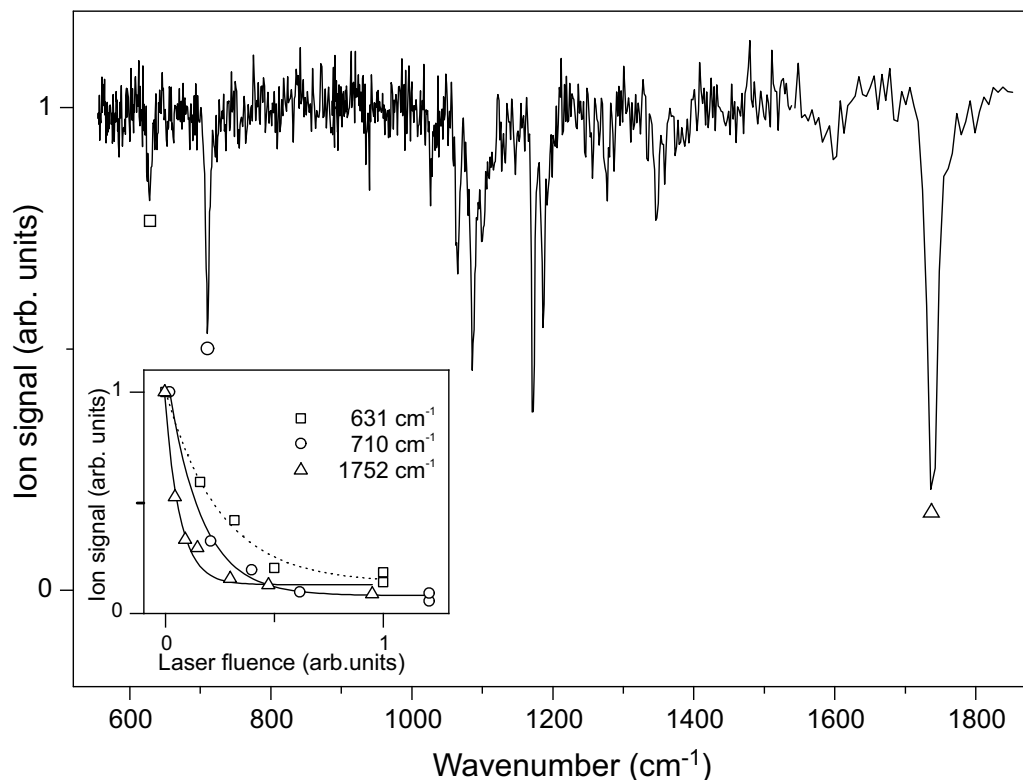


Figure 1.10: Observed IR ion-dip spectrum of the benzoic acid monomer. In the inset the laser fluence dependence of the ion depletion on the resonances marked with symbols is shown.

observation, as in the interaction of an isolated, non-degenerate two-level system with electromagnetic radiation population transfer is limited to 50 %, as discussed above. Apparently, there is an extra channel into which population is transferred after excitation to this vibrational state. One possibility is the occurrence of IVR, by which vibrational energy is redistributed over "dark" states that are iso-energetic with the excited vibrational state. Through this coupling, a more than 50 % depletion of the ground state population is possible. Depletions of over 50 % are even reached at wavenumbers below 1000 cm^{-1} , although it appears to be quite unlikely that the BA monomer will exhibit IVR here, as molecules of this (still rather limited) size simply lack the required density of states that allows for IVR to take place.

To be able to convert the observed IR-IDS spectra to IR absorption spectra, one needs to know the maximum possible depletion signal at each frequency, *i.e.*, one needs to know where the baseline of the spectrum is. The formulas for signal interpretation, as derived in the previous section, represent the ideal case. Here, experimental imperfections, such as a slight misalignment, cannot be ruled out. They can be taken into account by introducing an experimental parameter $a(\nu)$ describing the signal baseline. The remaining population in the ground state is then described by:

$$\begin{aligned} N_1(\nu) &= N_0(a(\nu) + (1 - a(\nu))\exp(-\sigma(\nu)P(\nu))) \\ &= N_0\exp(-\sigma(\nu)P(\nu)) + N_0a(\nu)[1 - \exp(-\sigma(\nu)P(\nu))] \end{aligned}$$

In addition, one needs to verify that the observed depletion signals are due to single-photon absorptions. In order to test this, the population decrease as a function of laser fluence is measured for a few

selected resonances. This is done by varying the laser fluence with a set of fixed-value attenuators. The results of these measurements are displayed in the inset in Figure 1.10, where the population decreases for the resonances at 631 cm^{-1} , 710 cm^{-1} and 1752 cm^{-1} are plotted as a function of laser fluence. As the observed curves are well described by the functional dependence it is concluded that we indeed deal with single-photon absorptions. In the high laser power limit, the population for all resonances converges to about 0.1, setting a base line value $a(\nu) = a = 0.1$.

The IR-IDS data can thus directly be interpreted as a measurement of the (relative) IR absorption cross-section. However, since the IR laser has a finite bandwidth that is larger than the line width of the vibrational transitions, the cross-section is smeared out over the full laser bandwidth and an IR absorption intensity is measured, of which the integral equals the absorption cross-section. Furthermore, although the obtained data could be corrected for variation of the FEL bandwidth, it is chosen to present them as recorded in the experiment, and correct the theoretically calculated spectra instead to facilitate direct comparison.

1.5 Theoretical methods

The work presented in this thesis consists largely of results from experimental studies. However, for the interpretation of experimental data several theoretical studies have been performed. As numerical methods available in quantum chemistry can become rather demanding on computational resources one usually has to compromise between accuracy and computational cost. In this work, the calculations necessary for the structural identification of gas-phase biomolecules can be divided into two parts: conformational search and electronic structure calculations.

Most of the studies performed here are done using commercial quantum chemistry packages such as Gaussian 98 [25], the Turbomole suite [26] and force-field based molecular mechanics program bundles like Tinker [27] and Sybyl [28]. Although these programs contain computational tools that nowadays can be considered standard for both experimental as well as for theoretical chemists, one cannot deny that a certain air of “black box” methods hangs around them. It therefore seems appropriate to shortly discuss the fundamental principles behind the used methods.

1.5.1 Conformational search

As biomolecules possess numerous bonds over which subgroups can rather freely be rotated, a large number of possible geometries results. It is the aim of the conformational search to find all these possible geometries and to define criteria based upon which a found geometry is further investigated, and eventually submitted to the more costly quantum chemical methods. The results of those calculations are then compared to the experimental data.

The conformational search is performed using two methods. The first method involves the use of classical molecular dynamics (MD) simulations. Here, the interactions between different atoms is described in a parametrized force field. The classical Newtonian equations of motion are solved for a set of atoms with pre-defined interaction parameters. The procedure used is the following: with a given temperature the MD simulation is run for some time. After a suitable time the structure’s temperature is slowly lowered to zero. The thus obtained structure is then optimized to obtain the lowest potential energy of the system. It is then stored for later evaluation, and the MD simulation is restarted to generate a next structure. With sensibly chosen MD run times, temperatures and dura-

tion of the cool-down period, the phase space can effectively be sampled. This method yields large numbers of different geometries, the stabilities of these structures are mainly determined by the force field parameters, which are not known accurately. As a result, the most stable geometries found with MD simulations are thus not guaranteed to be the lowest energy conformers found at higher levels of theory or even a potential energy minimum at all. Added to that, there is still the possibility that the lowest energy conformer is not that which is observed in the experiment. Force fields that are used in the calculations in this work are MM3 [29] and Sybyl [28].

The second method to probe the multidimensional phase space is by performing a systematic scan over all freely rotatable bonds. Geometries that exhibit major steric hindrance are rejected. The structure of all other resulting geometries are optimized at a theoretical level which is both acceptable in predicting structure and stability and at the same time cheap enough to optimize multiple geometries. As is the case with the force field search, not all geometries optimized at lower theoretical level are guaranteed to be stable minima on the potential energy surface (PES). Additionally, the cost of such systematic scans is growing enormously when more rotatable bonds are included. In this work, conformers for tryptophan were investigated using the semi-empirical method AM1 [30].

1.5.2 Electronic structure calculations

For the interpretation of experimentally obtained IR absorption spectra electronic structure calculations are performed. Geometries obtained from the conformational search are submitted to a full structural optimization by *ab initio* methods. These methods evaluate for the geometry the electronic Schrödinger equation to find equilibrium structures.

The Hamiltonian for a many body system, ignoring relativistic and spin-orbit interactions is

$$H = -\frac{\hbar^2}{2} \sum_a \frac{1}{m_a} \nabla_a^2 - \frac{\hbar^2}{2} \sum_i \nabla_i^2 + \sum_a \sum_{b>a} \frac{Z_a Z_b e^2}{r_{ab}} - \sum_a \sum_i \frac{Z_a e^2}{r_{ai}} + \sum_i \sum_{j>i} \frac{e^2}{r_{ij}}$$

where a and b are the nuclear indices and i and j are the electron indices, m_e the electron mass, m_a the nuclear masses, r the distances between the various particles and Z the nuclear charges. The first two terms describe the kinetic energy of the nuclei and electrons, respectively, the fourth term the Coulombic electron-nucleus attraction and the third and fifth terms the Coulombic repulsion of the nuclei and electrons, respectively.

To solve the molecular Schrödinger equation an *Ansatz* in the form of the Born-Oppenheimer approximation is made. The Born-Oppenheimer approximation implies that the masses of the nuclei make them move much slower than the electrons and as a result the electrons instantaneously follow the nuclear motion. This results in a separation between the wavefunctions and Hamiltonian operators of the nuclei and of the electrons:

$$\begin{aligned} \psi(\mathbf{R}, \mathbf{r}) &= \psi_e(\mathbf{R}, \mathbf{r}) \psi_n(\mathbf{R}) \\ H(\mathbf{R}, \mathbf{r}) &= H_e(\mathbf{R}, \mathbf{r}) + H_n(\mathbf{R}) \end{aligned}$$

where \mathbf{R} are the coordinates of the nuclei and \mathbf{r} the coordinates of the electrons. The implication of this separation is that for a given solution for the electronic Schrödinger equation

$$H_e(\mathbf{R}, \mathbf{r}) \psi_e(\mathbf{R}, \mathbf{r}) = E_e \psi_e(\mathbf{R}, \mathbf{r})$$

Consulted literature includes refs [31] and [32]

the equivalent nuclear Schrödinger equation can be solved to yield the vibrational energy levels. Reversely, for any configuration of the nuclei, the electronic Schrödinger equation can be solved. By evaluating the electronic Schrödinger equation for a given set of configurations the PES, on which the nuclei move, can be sampled.

For the theoretical treatment of the systems under study two classes of methods are used. The first is that based on the Hartree-Fock self-consistent field approach, in which the energy of a system is calculated using the Hartree-Fock equations. These equations yield a set of so-called orbitals which determine the energy of the system, but also determine the exact form of the aforementioned Hartree-Fock equations. By an iterative procedure starting with a wavefunction set up from trial orbitals a set of self-consistent orbitals is obtained. The basic form of this method is generally referred to as the Hartree-Fock (HF) level of theory. Among further refined methods that take the HF level as a starting point is the second-order Møller-Plesset (MP2) perturbation theory [33], which is used in this thesis. It must be pointed out that the semi-empirical AM1 method mentioned before is also a HF method, although some of the electron-electron interactions are parametrized here.

The second method used is Density Functional Theory (DFT). In this method, the electronic structure is not described by electronic wavefunctions, but by a general electron probability density. The energy is then a *functional* of the electron probability density function [34]. The Kohn-Sham equations, central in DFT, are solved in a similar fashion as the HF equations, (by applying a self-consistent field method) to yield orbitals from which the energy is determined. Many different functionals exist, mainly differing in their description of the electron exchange energy. In this work, use is made of the popular Becke3 hybrid functional [35] with the Lee-Yang-Parr correlation functional [36], or shortly B3LYP.

In both methods orbitals are constructed using a pre-defined basis set. In principle, any basis set that consists of an infinite number of orthogonal basis functions will describe the orbitals exact. However, as the computational cost rises dramatically with the number of basis functions, a finite basis set needs to be employed. In this thesis, among the basis functions that are used are Dunning's D95(d,p), and the Pople style basis sets 6-31G, 6-31G* and 6-31G**. These basis sets are all double-zeta sets, indicating a more flexible spatial extent. For an increased level of accuracy, as desirable in the calculations on the nucleobase pair guanine-cytosine, use is made of even larger basis sets, the triple-zeta basis sets, where even more flexibility in the spatial extents of the basis functions is incorporated.

DFT has proven to be a reliable method to study systems that are governed by covalent interactions [9] and is with success applied to investigate the structure of flexible biomolecules of which the structures are mainly determined by electrostatic interactions [7]. Good examples for systems studied in this work which can successfully be treated with DFT are the benzoic acid monomer and dimer. As DFT is considerably cheaper in computational effort than HF calculations with added correlation treatment, it is the preferred method to study flexible molecules. However, the very nature of DFT, where the properties of individual electrons are smeared out over a general electron density, makes a satisfactory treatment of dispersive interactions difficult. It is for systems of which the structures are dominated by these interactions that MP2 calculations are carried out. An example of the use of MP2 is in the calculations for the most stable geometry of the benzene dimer, which is mostly determined by dispersive interactions.

1.5.3 Harmonic vibration frequency calculations

When the electronic structure calculations have determined a stable structure, the harmonic energies of the normal mode vibrations are calculated by solving the nuclear Schrödinger equation. The potential energy of the molecule is approximated by a second-order Taylor expansion as

$$V(\mathbf{R}) = V(\mathbf{R}_0) + \left(\frac{dV}{d\mathbf{R}} \right)_0^T (\mathbf{R} - \mathbf{R}_0) + \frac{1}{2} (\mathbf{R} - \mathbf{R}_0)^T \left(\frac{d^2V}{d\mathbf{R}^2} \right)_0 (\mathbf{R} - \mathbf{R}_0)$$

where \mathbf{R} is a $3N$ dimensional vector containing all N nuclear coordinates and $\left(\frac{dV}{d\mathbf{R}} \right)_0$ and $\left(\frac{d^2V}{d\mathbf{R}^2} \right)_0$ are $3N \times 3N$ matrices, evaluated at the equilibrium position. (The superscript T denotes the transposed matrix.) Since a stable structure is found at a minimum of the PES, the first derivative vanishes. Translating the equilibrium position to the origin and introducing the displacement $\mathbf{x} = \mathbf{R} - \mathbf{R}_0$ one gets the harmonic approximation of the vibrational potential (in matrix notation):

$$V(\mathbf{x}) = \mathbf{x}^T \mathbf{F} \mathbf{x}$$

with \mathbf{F} the $3N \times 3N$ force constant or *Hessian* matrix. Now, the nuclear Schrödinger equation can be solved, by first applying a coordinate transformation $y_i = \sqrt{m_i} x_i$, which makes the nuclear Schrödinger equation mass-independent. By diagonalizing the mass-weighted Hessian the vibrational eigenfrequencies and eigenvectors are obtained, constituting the normal modes. The IR intensities associated with the normal modes are calculated as the second derivative of the dipole moment μ with respect to the normal coordinates.

In the calculations two important approximations are introduced. First, the Born-Oppenheimer approximation assumes separation between electronic and nuclear coordinates. However, when two PES's come close together energetically, vibrational energies become comparable to inter-PES energy differences and couplings between nuclear motion and electronic structure can occur. At that point the Born-Oppenheimer breaks down. This is the case for the benzene cation, which has two iso-energetic PES's and electronic-vibrational coupling distorts both (Chapter 2). The second approximation is that the PES can be considered harmonic along every normal coordinate. Although this approximation is often good, there exist regions on the PES where the anharmonicity is so large that one or more vibrational modes are not well described in the harmonic approximation. A good example of this is the NH_2 inversion mode in aniline, for which the potential is strongly anharmonic [19].

References

- [1] F. Hillenkamp, M. Karas, R. Beavis, and B. Chait, *Anal. Chem.* **63**, A1193 (1991).
- [2] J. Fenn, M. Mann, C. Meng, S. Wong, and C. Whitehouse, *Science* **246**, 64 (1989).
- [3] G. von Helden, T. Wyttenbach, and M. T. Bowers, *Science* **267**, 1483 (1995).
- [4] D. E. Clemmer, R. Hudgins, and M. F. Jarrold, *J. Am. Chem. Soc.* **117**, 10141 (1995).
- [5] C. S. Hoaglund-Hyzer, Y. J. Lee, A. E. Counterman, and D. E. Clemmer, *Anal. Chem.* **74**, 992 (2002).
- [6] T. S. Zwier, *J. Phys. Chem. A* **105**, 8827 (2001).
- [7] E. G. Robertson and J. P. Simons, *Phys. Chem. Chem. Phys.* **3**, 1 (2001).
- [8] F. Huiskens, A. Kulcke, C. Laush, and J. M. Lisy, *J. Chem. Phys.* **95**, 3924 (1991).
- [9] H. Piest, Ph.D. thesis, Katholieke Universiteit Nijmegen (2002).
- [10] L. Elias, W. Fairbank, J. Madey, H. Schwettman, and T. Smith, *Phys. Rev. Lett.* **36**, 717 (1976).
- [11] J. Andruszkow and *et al.*, *Phys. Rev. Lett.* **85**, 3825 (2000).
- [12] S. V. Benson and J. M. J. Madey, *Phys. Rev. A* **39**, 1579 (1989).
- [13] L. C. Snoek, private communication.
- [14] G. Meijer, M. de Vries, H. Hunziker, and H. R. Wendt, *Appl Phys. B* **51**, 395 (1990).
- [15] K. Müller-Dethlefs, M. Sander, and E. Schlag, *Chem. Phys. Lett.* **112**, 291 (1984).
- [16] L. Zhu and P. Johnson, *J. Chem. Phys.* **94**, 5769 (1991).
- [17] M. Okumura, L. Yeh, J. Myers, and Y. Lee, *J. Phys. Chem.* **94**, 3416 (1990).
- [18] O. Dopfer, R. V. Olkhov, and J. P. Maier, *J. Chem. Phys.* **111**, 10754 (1999).
- [19] H. Piest, G. von Helden, and G. Meijer, *J. Chem. Phys.* **110**, 2010 (1999).
- [20] H. Piest, G. von Helden, and G. Meijer, *Ap. J.* **520**, L75 (1999).
- [21] J. H. Piest, J. Oomens, J. Bakker, G. von Helden, and G. Meijer, *Spec. Acta A* **57**, 717 (2001).
- [22] R. G. Satink, H. Piest, G. von Helden, and G. Meijer, *J. Chem. Phys.* **111**, 10750 (1999).
- [23] R. G. Satink, J. M. Bakker, G. Meijer, and G. von Helden, *Chem. Phys. Lett.* **359**, 163 (2002).
- [24] A. Beil, D. Luckhaus, M. Quack, and J. Stohner, *Ber. Bunsenges. Phys. Chem.* **101**, 311 (1997).
- [25] M. J. Frisch, G. W. Trucks, H. B. Schlegel, G. E. Scuseria, M. A. Robb, J. R. Cheeseman, V. G. Zakrzewski, J. J. A. Montgomery, R. E. Stratmann, J. C. Burant, et al., *Gaussian 98, Revision A.7*, Pittsburgh, PA (1998).
- [26] R. Ahlrichs, M. Bar, M. Haser, H. Horn, and C. Kolmel, *Chem. Phys. Lett.* **162**, 165 (1989).

- [27] URL <http://dasher.wustl.edu/tinker/>.
- [28] M. Clark, R. Cramer, and N. Opdenbosch, *J. Comput. Chem.* **10**, 982 (1989).
- [29] N. L. Allinger, Y. H. Yuh, and J.-H. Lii, *J. Am. Chem. Soc.* **111**, 8551 (1989).
- [30] M. Dewar, E. Zoebisch, E. Healy, and J. Stewart, *J. Am. Chem. Soc.* **107**, 3902 (1985).
- [31] P. Atkins and R. Friedman, *Molecular quantum mechanics* (Oxford University Press, Oxford, Great Britain, 1997), 3rd ed.
- [32] F. Jensen, *Introduction to computational chemistry* (John Wiley & Sons, Chichester, Great Britain, 1999).
- [33] C. Møller and M. Plesset, *Phys. Rev.* **46**, 618 (1934).
- [34] P. Hohenberg and W. Kohn, *Phys. Rev.* **136**, B864 (1964).
- [35] A. Becke, *J. Chem. Phys.* **107**, 8554 (1997).
- [36] C. Lee, W. Yang, and R. Parr, *Phys. Rev. B* **37**, 785 (1988).

CHAPTER 2

INFRARED PHOTODISSOCIATION SPECTROSCOPY OF BENZENE–NE AND BENZENE–AR COMPLEX CATIONS

The infrared (IR) absorption spectrum of the jet-cooled benzene cation complexed with Ne has been recorded throughout the 275–1900 cm⁻¹ and the 2800–3200 cm⁻¹ range via IR-laser induced vibrational dissociation spectroscopy. Measuring the spectrum of the complex ion rather than the spectrum of the bare benzene cation, leads to the appearance of weak Van der Waals sidebands. In addition, subtle effects of the symmetry lowering in the complex, giving rise to additional lines in the spectrum, have been observed for the benzene-Ar complex. The recorded IR absorption spectrum of the deuterated benzene-Ar complex as well as the IR absorption spectra of benzene complex cations prepared in selected low-lying vibrationally excited levels yield a more detailed picture of the vibrational structure of the benzene cation.

Adapted from: J. M. Bakker, R. G. Satink, G. von Helden, and G. Meijer, *Phys. Chem. Chem. Phys.* **4**, 24–33 (2002)

2.1 Introduction

A detailed understanding of the vibrational structure of the benzene cation is both interesting and relevant for a variety of reasons. The benzene cation, with its doubly degenerate electronic ground state, is of fundamental interest as it is the prototypical system for studies of the Jahn-Teller interaction [1, 2]. In the vibrational spectrum the Jahn-Teller effect manifests itself as a splitting of certain vibrational modes. This splitting can be rather large, on the order of the vibrational energy, and it is often difficult to discern a clear vibrational energy level pattern, complicating assignment of vibrational modes. The benzene cation might also be of astrophysical interest. Recently, neutral benzene has been identified as an emitter of infrared (IR) radiation in a proto-planetary nebula [3]. It is therefore not unlikely that the benzene cation can be identified in astrophysical objects via its IR emission spectrum as well. After all, the polycyclic aromatic hydrocarbons (PAHs), and specifically their cations, have been proposed as carriers of the Unidentified Infrared Bands (UIBs), a series of distinct IR emission bands observed from the interstellar medium [4, 5].

The use of direct IR absorption techniques to obtain information on the vibrational structure of the benzene cation, for instance on benzene cations deposited in rare gas matrices, has thus far not been successful. Another commonly used method to study vibrational structure, Laser Induced Fluorescence (LIF) on ionic species either in the gas phase or in matrices, has not proven to be viable for the benzene cation either, due to an unfavorably low quantum yield for fluorescence [6]. As a consequence, much of the early experimental work on benzenoid systems consisted of dispersed fluorescence studies of partly or completely halogenated benzene ions, for which the fluorescence quantum yield is close to one. For an overview, the reader is referred to the work by Miller and Bondybey [7].

With the advent of the dye laser and with the development of supersonic molecular beam cooling techniques, other methods for studying benzene cations became available. By recording the gas phase one color (1+1) photoelectron spectrum, Long, Meek and Reilly identified several low-lying fundamental vibrational frequencies in the benzene cation [8]. The spectral resolution in this original work was limited by the resolution of the electron energy analyzer to about 3 meV. In later studies, in which a second tunable dye laser photon was used to induce ionization, the resolution was largely improved, making a more detailed analysis possible. These studies include accurate determination of photoionization thresholds via Resonance Enhanced Multi Photon Ionization (REMPI) spectroscopy [9, 10], Zero Electron Kinetic Energy (ZEKE) spectroscopy [11], and Mass Analyzed Threshold Ionization (MATI) spectroscopy [12, 13]. The measurement of rotationally resolved high- n Rydberg spectra of neutral benzene allowed for the extrapolation to the various ionization thresholds, leading to a very precise determination of some vibrational frequencies in the ion [14]. The most recent threshold technique studies on the benzene cation include MATI studies of the benzene cation using either vacuum UV to directly probe the ion from the neutral ground state [15] or by using the $^3B_{1u}$ triplet state of benzene (populated in a discharge source) as the initial state [16].

Although the methods mentioned above yield accurate vibrational frequencies, definite assignment of the modes involved might nevertheless be complicated. This is because in the electronic transitions involved in the detection process, the relative line intensities are mainly governed by Franck-Condon overlap and there are no strict vibrational selection rules. Additional information can therefore be obtained when the true vibrational absorption spectrum of the cation is measured instead. For this, a sensitive IR absorption detection scheme is required, for instance a scheme based on the IR induced photodissociation of weakly bonded complexes of the benzene cations with rare

gas atoms. Although the IR absorption spectrum of the complex ions, rather than of the bare ions, is measured in this case, it is expected that these spectra will closely resemble each other; this is substantiated by the good agreement between the observed MATI spectra for bare benzene and those of its argon complexes [17]. To be able to efficiently induce photodissociation of these complexes, an intense (pulsed) IR source, tunable throughout the relevant portion of the spectrum, is required. Using a pulsed laser system tunable in the 3 μm region, Dopfer *et al.* measured the IR active C–H stretch mode via IR laser induced photodissociation of the benzene-Ar cation [18]. In a complementary study, using a Free Electron Laser (FEL) as a source of widely tunable IR radiation, Satink *et al.* reported on the IR absorption spectrum of the same species in the 450–1500 cm^{-1} range [19].

The experimental activity in the recent years has led to a refinement in the theoretical models [20, 21]. While most spectroscopic information in the spectral region below 1000 cm^{-1} can satisfactorily be explained by invoking only the Jahn-Teller activity of two low energy modes (see section 2.2), new studies have attempted to assign all observed resonances making use of spectral information available at that time [22, 23].

In this chapter the results of a study on the IR spectrum of the benzene cation complexed with either Ne or Ar are presented. There are two main advantages of using Ne over Ar as a messenger atom. First, the binding energy of the benzene-Ne complex is significantly lower than that of benzene-Ar, enabling the detection of IR absorption lines at lower frequencies. Second, the lower polarizability of Ne is expected to yield a spectrum that is more closely resembling the spectrum of the bare benzene cation. In the spectra of the complex ions Van der Waals sidebands have been observed, yielding information on the intermolecular potential energy surface. Finally, the IR spectrum of the deuterated benzene cation, complexed with argon, and IR absorption spectra of benzene-Ar cations prepared in selected low-lying vibrationally excited levels have been recorded to obtain a more detailed picture of the complex vibrational structure of the benzene cation in the region up to 1800 cm^{-1} .

2.2 Spectroscopic details

The neutral benzene molecule in its electronic ground state belongs to the D_{6h} molecular symmetry group. Its 30 vibrational modes are of the species

$$\Gamma_{\nu} = 2a_{1g} \oplus 1a_{2g} \oplus 2b_{2g} \oplus 1e_{1g} \oplus 4e_{2g} \oplus 1a_{2u} \oplus 2b_{1u} \oplus 2b_{2u} \oplus 3e_{1u} \oplus 2e_{2u}. \quad (2.1)$$

Throughout this chapter the commonly used Wilson notation [24] is adopted. In the neutral ground state there are four IR active modes, one of a_{2u} and three of e_{1u} symmetries. The fundamental frequencies of these modes are experimentally found at 671 cm^{-1} for the a_{2u} ν_{11} mode [out-of-plane C–H bending], at 1037 cm^{-1} for the e_{1u} ν_{18} mode [in-plane C–H bending], at 1485 cm^{-1} for the e_{1u} ν_{19} mode [C–C stretching] and at 3099 cm^{-1} for the e_{1u} ν_{20} mode [C–H stretching] [25]. The electronic configuration of neutral benzene is $(a_{2u})^2(e_{2g})^4(e_{1g})^4$ and upon removal of one electron from one of the e_{1g} orbitals, the cation is left in a degenerate E_{1g} state. When the vibrational symmetry is combined with the E_{1g} electronic symmetry of the ground state of the cation, the number of vibrational states is greatly increased. In particular, six ungerade states of electronic-vibrational A symmetry and ten of E symmetry result; all are expected to lie in the spectral range covered in this study.

In a classic paper published in 1937, Jahn and Teller pointed out that for any nonlinear molecule with a threefold (or higher) rotational symmetry axis in an orbitally degenerate electronic state there will be at least one normal coordinate for which the potential energy minimum does not coincide with

the symmetrical position, thus effectively distorting the nuclear framework, lowering the symmetry and lifting the degeneracy [1]. The benzene cation in its electronic ground is a prototypical system for this. For molecules of D_{6h} symmetry, vibrations of e_{2g} symmetry will cause a distortion that is linear in the corresponding normal coordinate whereas vibrations of e_{1g} , e_{1u} and e_{2u} symmetry will cause a quadratical distortion. In the benzene cation, there are four e_{2g} modes that are linearly Jahn-Teller active. Of course, none of these four modes can be directly observed in IR absorption spectroscopy of the bare cation. Using photoelectron spectroscopy and the more sophisticated ZEKE and MATI methods, only the frequency and Jahn-Teller activity of the lowest energy e_{2g} mode, the ν_6 in-plane ring-bending mode, have been identified thus far. The benzene molecule is distorted along this coordinate and two possible structures of D_{2h} symmetry result. No theoretical agreement has been reached so far as to which of the two structures has the lowest energy [2, 26]. Experimentally, however, ZEKE spectroscopy studies revealed that the barriers between these structures are so low that ν_6 acts as a pseudorotational coordinate linking the two. The resulting system as a whole is then necessarily viewed as D_{6h} [11], a conclusion that has recently been confirmed by rotationally resolved ZEKE spectra of the ionic vibrational ground state [27]. Of the quadratically Jahn-Teller active modes, only the lowest frequency e_{2u} mode, the ν_{16} out-of-plane ring bending mode around 300 cm^{-1} , has been identified. It is split up into two non-degenerate and one doubly degenerate mode, of which only the latter is IR active [11].

The low frequencies of the linear and quadratical Jahn-Teller active ν_6 and ν_{16} modes give rise to a rich energy level structure in the ion, even when only overtones and combinations of these two modes are included. Due to the possibility of interaction of such combination modes with IR active fundamental modes via Fermi resonances, this might lead to unexpected features in the IR spectrum of the ion [19]. In Figure 2.1, a schematic representation of the energy level structure originating from the ν_6 and ν_{16} modes of the benzene ion is given. The two-mode interaction model we have used to produce this figure is the same as used by Goode *et al.* [13]. For interpretation of their spectroscopic data on halogenated benzenoid systems, Miller and Bondybey developed a theoretical framework, based on a treatment by Longuet-Higgins [28], to explain the observed energy level structure [7]. This work was used and refined for the benzene cation by various groups [8, 11, 13]. The method consists of diagonalization of a Hamiltonian matrix representing the two degenerate electronic states coupled through the Jahn-Teller active vibrational states. For a complete treatment the reader is referred to the original work [7]. In Figure 2.1, the linear and quadratic Jahn-Teller coupling parameters are simultaneously increased from left to right, going from the situation of no Jahn-Teller interaction (left axis) to the situation that is in best agreement with experimental observations (right axis) [13]. From this figure, level assignments can be deduced.

Based on the experimental work that was available at the time, Applegate and Miller proposed a full assignment for the data observed via threshold techniques and via IR photodissociation [22]. For completeness, all presently known vibrational frequencies are listed in Tables 2.1 and 2.2, both for $C_6H_6^+$ and for $C_6D_6^+$. The numbers in these tables are taken from MATI studies by Krause *et al.* [12, 29] and Goode *et al.* [13], ZEKE spectroscopy by Lindner *et al.* [11, 30], Rydberg spectroscopy by Siglow *et al.* [14, 31] and recent vacuum UV MATI work by Kwon *et al.* [15] as well as from the present work. The photoelectron studies by Long *et al.* [8] are among the landmark works on benzene, but the values obtained from these low-resolution studies have not been included. Mode assignments are given in the table, both based on assignments previously made in the literature and on the present work, as will be discussed below. Although the assignment put forward by Applegate and Miller

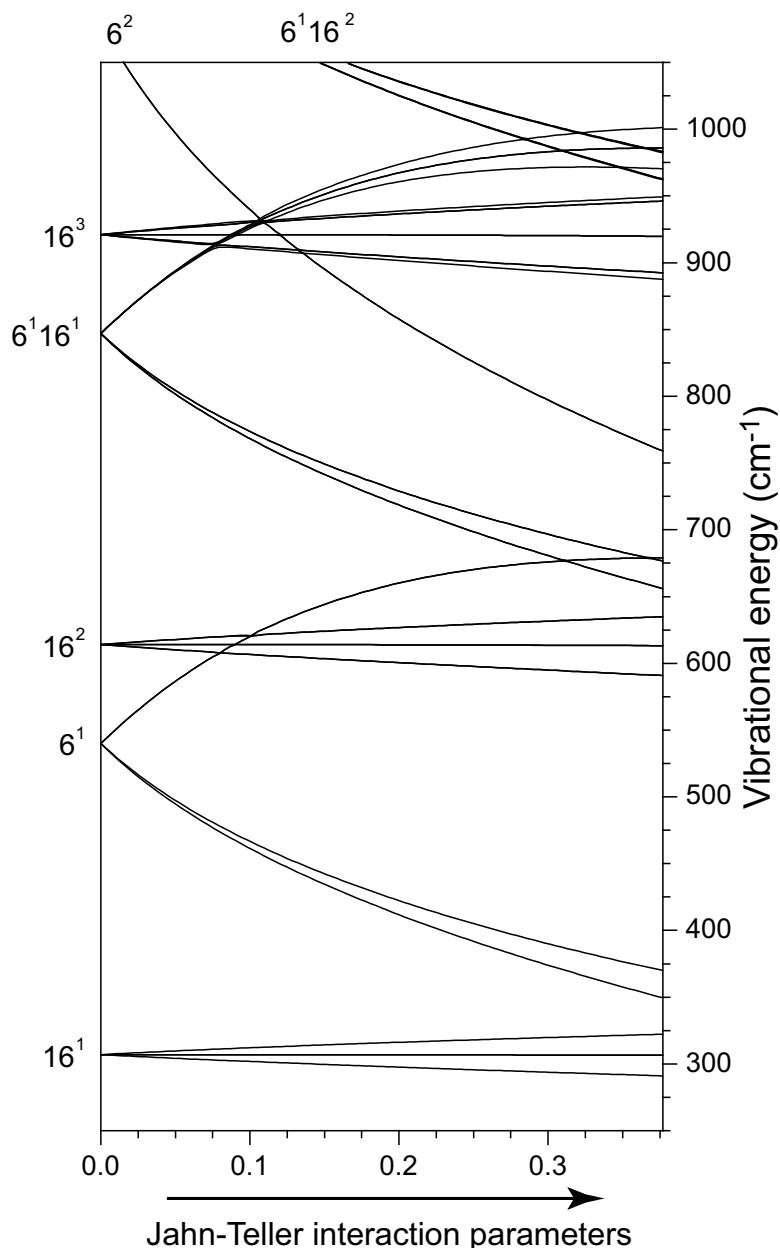


Figure 2.1: Correlation diagram, linking the energy levels in the benzene cation with Jahn-Teller interaction (right axis) to those expected in the absence of Jahn-Teller interaction (left axis). In the two-mode interaction model that is used, only the ν_6 and ν_{16} vibrations have been included. From left to right the Jahn-Teller interaction parameters are linearly increased to their experimentally determined values [13].

is still open for debate, most of the assignments in the tables are based upon their interpretation. Additionally, in the table it has been recognized that all linearly Jahn-Teller active modes are coupled to each other through the ground state. This is reflected in the notation, where all resonances due to linearly Jahn-Teller active modes are labeled by a vibronic angular momentum quantum number $j = l_v + \frac{1}{2}\Lambda$ where l_v is the vibrational angular quantum number for Jahn-Teller active mode ν_v ; $\Lambda = \pm 1$ the electronic angular momentum quantum number associated with the two degenerate electronic

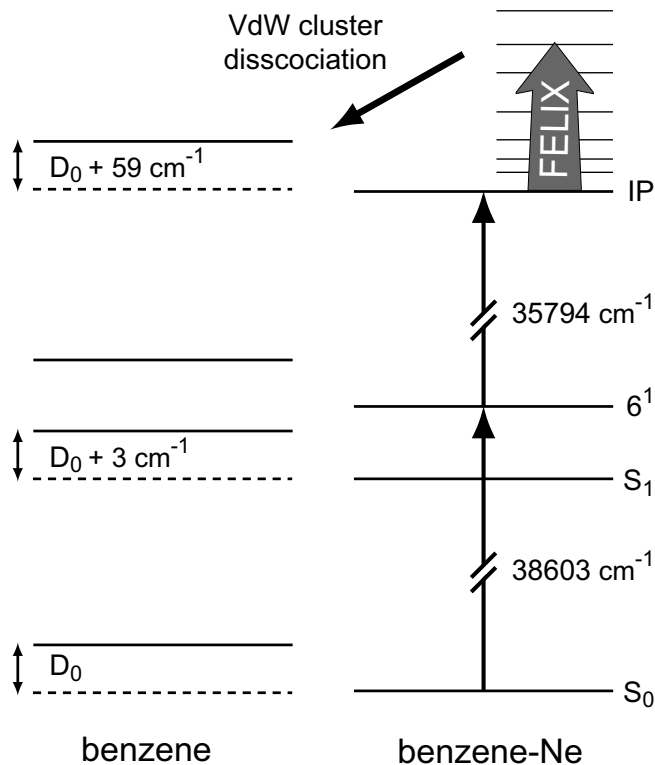


Figure 2.2: Energy level scheme for benzene and benzene-Ne. The redshifts of the transitions used to prepare the vibrationally cold benzene-Ne complex ions relative to the transitions in the bare benzene molecules correspond to an increased binding energy of the complex of 3 cm^{-1} upon excitation to the S_1 state and of 59 cm^{-1} upon ionization [32, 33].

potential energy surfaces. Due to the coupling through the ground state the original character of the mode is lost and all modes are labeled $|j, n_j\rangle$, introducing n_j as an accounting integer, keeping track of the number of modes with equal j . For completeness it should be mentioned that the vibrational ground state is labeled $|1/2, 1\rangle$ in this notation. In the discussion of the spectrum, however, the ν_6 vibration is explicitly mentioned, because it is assumed that the Jahn-Teller active mode involved has mainly ν_6 character and because the one-mode analysis presented in Figure 2.1 allows for an accurate description of the spectrum below 1000 cm^{-1} ; it certainly makes the discussion more intuitive.

To study the IR absorption spectrum of benzene-rare gas atom complex ions the technique of IR photodissociation is used. A mixture of approximately 1% benzene vapor in a rare gas (Ne or Ar) at a backing pressure of 2 atm. is expanded through the nozzle into vacuum. The adiabatic expansion conditions enable the formation of weakly bonded Van der Waals complexes of benzene with rare gas atoms, and these complexes are internally cooled to some 5 K. To prepare the complex ions for the dissociation experiment a UV double-resonance scheme is used. In Figure 2.2, this scheme is explicitly shown for the benzene-Ne cation. A first UV laser, referred to as the excitation laser, excites the neutral benzene-Ne complexes to the ν_6 vibrationally excited level in the first electronically excited (S_1) state. The single photon excitation spectrum for this, as well as that for the other Van der Waals complexes studied in this work, is well-characterized in rotationally resolved high-resolution UV spectroscopy [32, 34, 35]. The frequency-doubled dye (Coumarin 500) laser is tuned to the center of the (unresolved) rotational envelope. The electronically excited complexes are subsequently

ionized with a second tunable UV laser (Rhodamine 6G), pumped by the same Nd:YAG laser but optically delayed relative to the excitation laser by a few ns. The ions are produced in zero electric field, and the photon energy of the ionization laser is chosen to bring the Van der Waals complexes just barely above their ionization threshold [33]. With an excess energy of less than 5 cm^{-1} there is a possibility that one Van der Waals mode of the complex ion, which is predicted within 2 cm^{-1} in the case of benzene-Ar, is excited [36]. Typically, the population in states with excited Van der Waals modes is at least an order of magnitude smaller than in the vibrationless ground state and for the purpose of spectroscopy, the resulting population can thus well be described as consisting solely of ground state ions. The temperature of the ions will be about as low as that of the neutral benzene-Ne complexes that they originate from.

2.3 Results and Discussion

2.3.1 Benzene-Ne

The IR absorption spectrum of the benzene-Ne cation is displayed in Figure 2.3. The observed frequencies of a total of eighteen spectral lines are indicated in the figure. The absolute frequency accuracy is about 1 cm^{-1} at the low frequency end of the spectrum, gradually deteriorating to 5 cm^{-1} at the high frequency end. The line width observed in the spectrum is almost exclusively determined by the bandwidth of the laser, although it could be partly broadened due to the presence of molecular ions with a low-frequency Van der Waals mode excited at the time of preparation. As more than a factor of 10 in frequency is covered in this study, it is rather difficult to accurately determine relative intensities of widely separated lines in the spectrum. Within a limited spectral region, for instance in the $600\text{--}800\text{ cm}^{-1}$ region, relative intensities are accurate to within 20%. The relative intensity between the two outermost lines in the spectrum, however, might be off by as much as a factor five. As already discussed in section 2.2, a maximum of sixteen fundamental modes of the benzene cation are expected in the IR spectrum. The lowest frequency mode is the E_{1u} central one of the quadratically Jahn-Teller split triad of ν_{16} modes. This mode, already known from MATI spectroscopy to lie near 306 cm^{-1} , is observed at 305 cm^{-1} in this spectrum. The ν_{16} vibration could not be observed in the IR photodissociation study of the benzene-Ar cation, as it is located significantly below the dissociation limit of the ionic complex in that case [19]. From the observation of the resonance in the present spectrum, it is evident that the dissociation limit of the ionic benzene-Ne complex is below 305 cm^{-1} . This implies an upper value for the dissociation limit D_0 for the neutral benzene-Ne complex in its electronic ground state of $D_0 = 305 - 59 = 246\text{ cm}^{-1}$ (cf. Figure 2.2). The actual value for the dissociation limit is expected to be significantly lower than this, however; theoretically a value of $D_0 = 99\text{ cm}^{-1}$ is found [37].

The spectrum is dominated by intense resonances in the $600\text{--}700\text{ cm}^{-1}$ region. As mentioned in section 2.2, the IR active ν_{11} mode [out-of-plane C–H bending] of vibronic E_{1u} symmetry is expected in this region, but no other fundamental IR active modes. In a previous study on the benzene-Ar cation it was already indicated that the three strongest resonances in this spectral region can be attributed to the occurrence of a Fermi resonance [19]. It is seen from Figure 2.1 that the two lowest frequency $\nu_6 + \nu_{16}$ combination modes, both of E_{1u} symmetry as well, are expected to be very close in energy to the ν_{11} mode. Interaction of these three modes leads to a textbook example of Fermi-resonance, an interaction between different, accidentally degenerate, vibrations of the same symmetry [25]. This Fermi resonance is shown on an expanded scale in inset A in Figure 2.3.

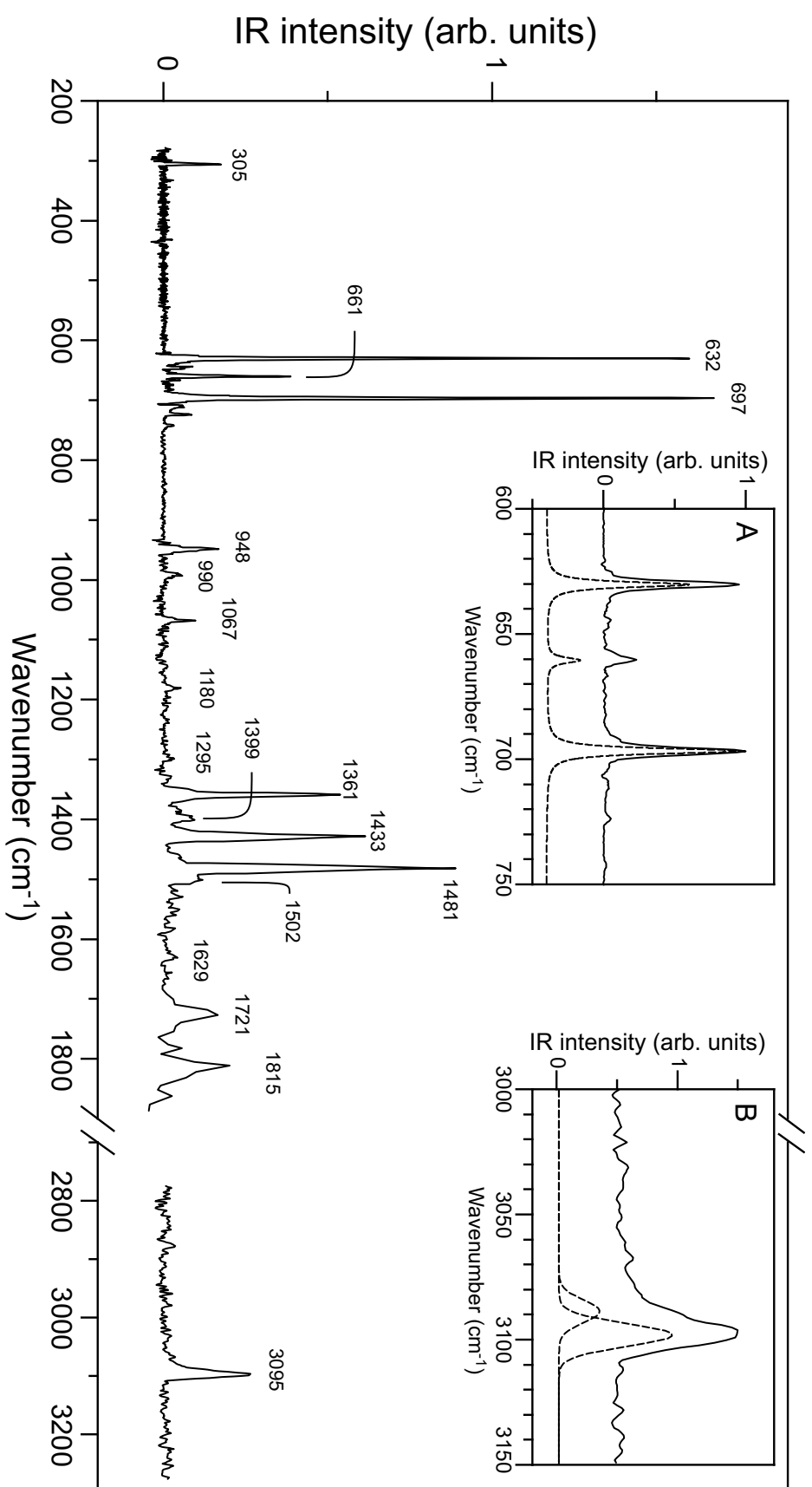


Figure 2.3: IR absorption spectrum of the benzene-Ne complex cation. In inset **A** the spectral region from 600–750 cm⁻¹ is shown on an expanded scale together with a simulation (dashed curve) of the Fermi-resonance between the IR active ν_{11} mode and the $\nu_6 + \nu_{16}$ combination modes. In inset **B** the highest frequency resonance is shown on an expanded scale, together with a decomposition into two 11 cm⁻¹ wide resonances (dashed curves).

In the most simplified model of the Fermi resonance, it is assumed that both $\nu_6 + \nu_{16}$ combination modes couple only to the ν_{11} mode with the same coupling parameter, and that only the ν_{11} mode carries IR intensity. These assumptions result in four parameters (three unperturbed line positions and one coupling parameter α) to fit five observables from the experimental spectrum (three line positions and two relative line intensities). The best fit to the experimentally observed spectrum is shown as the lower (dashed) trace in inset A of Figure 2.3; the calculated stick spectrum is convoluted with a line shape function representing the laser line width. As can be seen, fairly good agreement is obtained, and a coupling parameter α of 22 cm^{-1} is found. The unperturbed line position for the ν_{11} mode is 668 cm^{-1} , whereas the two $\nu_6 + \nu_{16}$ combination modes are found at 650 cm^{-1} and 669 cm^{-1} . The latter values are in good agreement with the expected unperturbed frequencies as depicted in Figure 2.1.

In the high-frequency C–H stretching region the e_{1u} ν_{20} vibration, resulting in A_{1u} , A_{2u} and E_{2u} modes, as well as the b_{1u} ν_{13} vibration, resulting in an IR active mode of E_{2u} vibronic symmetry, are expected. In Figure 2.3 a single absorption feature centered at 3097 cm^{-1} is observed. The full width at half maximum (FWHM) of this absorption is approximately 14 cm^{-1} , mainly determined by the spectral profile of the IR radiation. As shown more clearly in inset B, a slight asymmetry can be recognized in the line shape, hinting at a possible overlap of more absorption lines. The absorption can be deconvoluted into two 11 cm^{-1} wide components centered at 3089 cm^{-1} and 3098 cm^{-1} with a 1:3 intensity ratio, as shown by the dashed curves in the inset. For the benzene-Ar cation, a significantly wider absorption feature centered at 3094 cm^{-1} was recently reported by Dopfer *et al.* [18]. In their experiment, Van der Waals complex ions are produced after electron impact ionization of neutral benzene in the expansion region of a pulsed gas jet. The complex ions that are thus produced can be at relatively high internal temperatures, leading to a broadening of the absorption lines.

Based on the known vibrational frequencies in the ground state of neutral benzene [25], the ten remaining IR active fundamental modes in the cation are all expected to lie in the $800\text{--}1600\text{ cm}^{-1}$ spectral region. In this region of the spectrum, the peak absorption frequency of ten recognizable absorption lines is indicated in Figure 2.3. To obtain a better understanding of the observed spectral structure in this region, density functional theory calculations are performed using the B3LYP method with the 6-31G* basis set, as implemented in GAUSSIAN 98 [38]. Starting with the two D_{2h} benzene cation structures that were calculated by Raghavachari *et al.* [2] the results obtained earlier by Müller-Dethlefs and Peel were reproduced [26]; for a more detailed discussion on the methods used and the interpretation of the D_{2h} calculations the reader is referred to ref. [26].

The calculated IR spectra for these two structures incorporate a convolution of the stick spectrum with a Gaussian function representing the FELIX spectral profile and are displayed in Figure 2.4. It is clearly visible that the four resonances in the $900\text{--}1200\text{ cm}^{-1}$ region are well reproduced in both calculated spectra and could thus be attributed to four fundamental vibrational modes of the benzene cation. A visual inspection of the calculated normal modes unfortunately does not allow for a full assignment to specific fundamentals. The character of the calculated mode around 1045 cm^{-1} is that of the ν_{18} vibration, which seems a perfectly reasonable assignment as the neutral benzene ν_{18} vibration is found at 970 cm^{-1} . On the other hand it is expected that ν_{18} , the only IR active mode in this region for the neutral species, would be the strongest resonance. Since none of the other three calculated modes in this region could be assigned based on their motions, they are included in Table 2.1 as unspecified fundamental modes.

In the region between 1300 cm^{-1} and 1600 cm^{-1} , only two benzene fundamental modes are

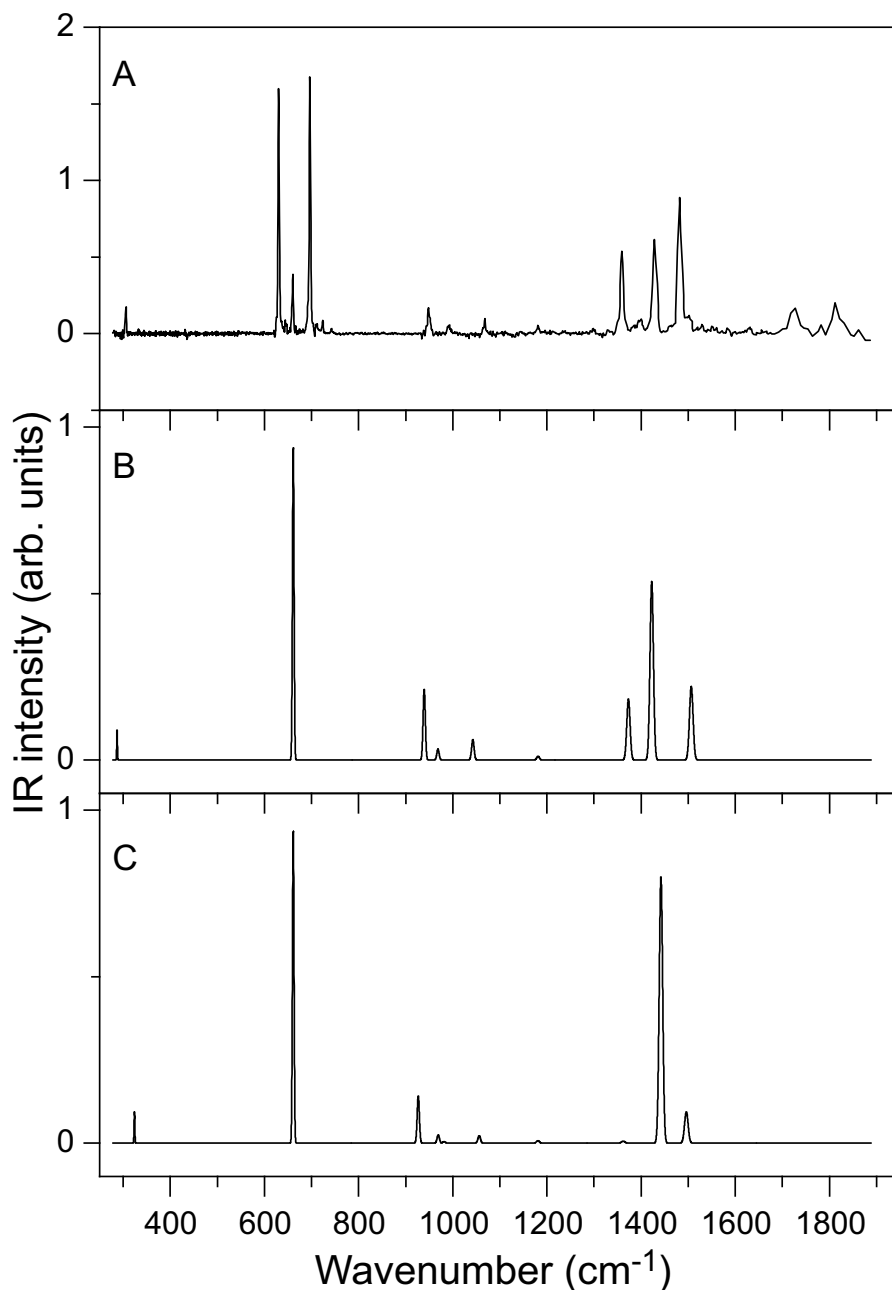


Figure 2.4: Density functional calculations of the IR absorption spectrum of the benzene cation. The experimentally obtained spectrum is given in trace **A**. Traces **B** and **C** represent the calculated spectra for the elongated benzene structure of electronic B_{2g} symmetry and for the compressed structure of B_{3g} symmetry, respectively.

expected based on their frequencies in neutral benzene. One of these, the strong neutral mode ν_{19} , could be split up due to the quadratic Jahn-Teller interaction into three IR active modes, leading to a total of four resonances. However, no symmetric splitting signature (as for the quadratically split ν_{16}) is observed. The calculated spectrum in Figure 2.4 exhibits only three resonances in this region, none of which can be assigned based on the molecular motion, further complicating a full assignment. The

assignment by Applegate and Miller of the resonances at 1361 , 1433 and 1481 cm^{-1} to ν_{14} , ν_{19} and $\nu_4 + \nu_{18}$ seems unlikely for two reasons: first, the strongest neutral mode in this region ν_{19} , is not the strongest here and second, the assignment of the 1481 cm^{-1} resonance to a combination of ν_4 (418 cm^{-1}) and ν_{18} (previously assigned 948 cm^{-1}) would imply a negative cross-anharmonicity, a rare phenomenon. It would also have implied that the combination mode of the rather weak ν_{18} (with ν_4) is in fact much stronger than the fundamental itself. An alternative assignment is therefore proposed: the 1361 resonance is still assigned to ν_{14} , but could overlap with $\nu_4 + \nu_{18}$ which is energetically much more reasonable ($418 + 948 = 1366$). The strongest transition at 1481 cm^{-1} is then assigned to the fundamental ν_{19} , and the shoulder of this resonance, centered at 1501 cm^{-1} , to the combination mode $\nu_{10} + \nu_{11}$. The most uncertain assignment is that of the resonance at 1433 cm^{-1} . An energetically plausible assignment would involve ν_{11} (665 cm^{-1}) and the Jahn-Teller component $|1/2, 3\rangle$ (763 cm^{-1} ; cf. ν_6^2 in Figure 2.1). Finally, the resonance at 1399 cm^{-1} remains assigned to $\nu_4 + \nu_{17}$.

Above 1550 cm^{-1} , no fundamental vibrations are expected. Still, two clear, but broad resonances are observed at 1721 cm^{-1} and 1815 cm^{-1} , together with a weak one at 1629 cm^{-1} . Applegate and Miller have in fact attributed these resonances to combination modes, and these can be found in Table 2.1.

The high energy region between 1600 cm^{-1} and 1900 cm^{-1} was not investigated in the work by Satink *et al.*. To compare the benzene-Ne spectrum with that of benzene-Ar, the latter is also measured. The result, depicted in Figure 2.5, shows a very similar picture: strong lines are observed at 1720 and 1815 cm^{-1} , and a weak one at 1629 cm^{-1} . Moreover, the benzene-

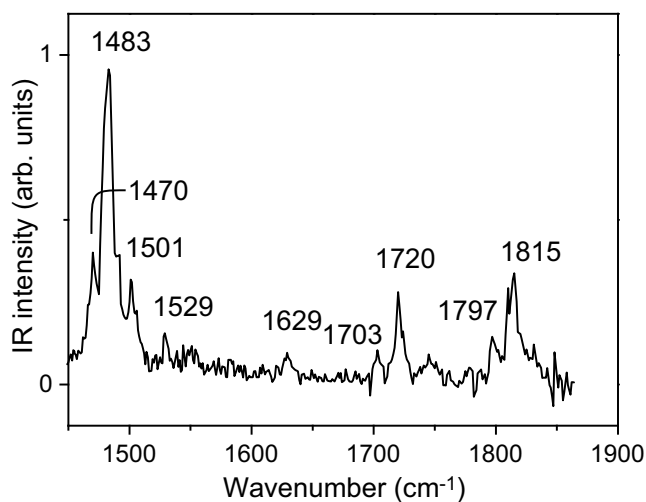


Figure 2.5: IR absorption spectrum of benzene-Ar, recorded in the $1450\text{--}1850\text{ cm}^{-1}$ region

Ar spectrum also reveals some additional, weaker lines. These extra lines could well also be present in the benzene-Ne spectrum, but the somewhat less favorable signal-to-noise conditions under which the benzene-Ne spectrum is recorded prevent the observation of all resonances. Although one would suspect that the repetitive pattern observed for the doublets at 1720 cm^{-1} and at 1815 cm^{-1} is a signature of the quadratic Jahn-Teller splitting, no combination modes could be found to yield a satisfactory assignment.

2.3.2 Van der Waals sidebands

In the IR absorption spectrum shown in Figure 2.3, additional weak absorption lines are seen at the high frequency side of the strong resonance at 697 cm^{-1} . This is shown more clearly on an expanded scale in the upper part of Figure 2.6. As no IR active fundamental modes are expected in the $700\text{--}750\text{ cm}^{-1}$ spectral region, these weak additional lines are attributed to Van der Waals sidebands, *i.e.*, combination modes of the IR active mode at 697 cm^{-1} with low-frequency intermolecular benzene-Ne

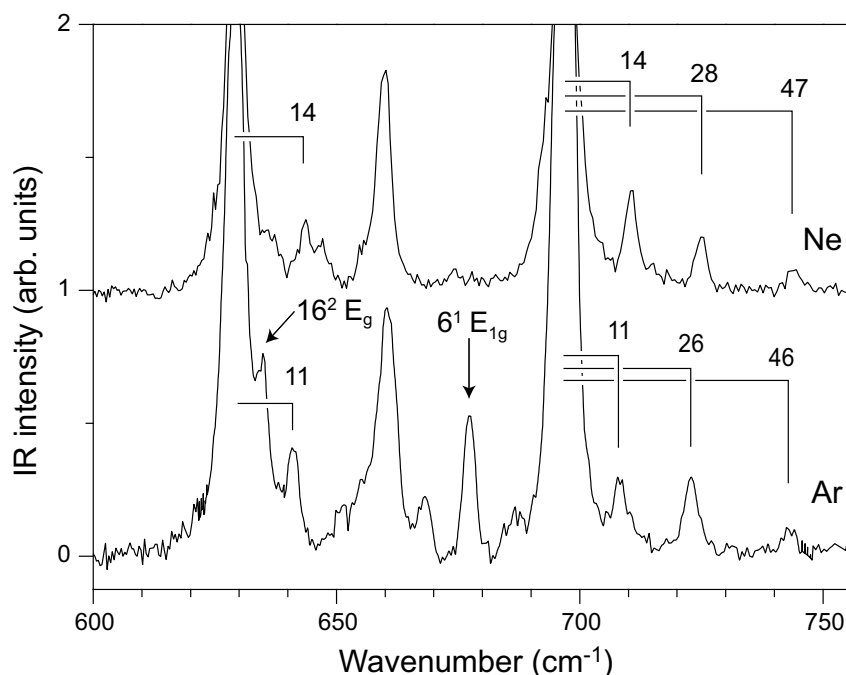


Figure 2.6: Expanded view of the 600-750 cm^{-1} region of the IR absorption spectrum of benzene-Ne (upper trace) and benzene-Ar (lower trace) complex cations. In both spectra distinct Van der Waals sidebands are observed, and the Van der Waals frequencies, i.e., the frequency shift of the sidebands relative to the IR active mode of the benzene cation chromophore, are indicated. In the benzene-Ar spectrum the ν_6 mode and the ν_{16} overtone mode are observed (indicated by arrows); both modes are of gerade symmetry, and therefore not IR allowed, for the bare benzene cation.

modes. The frequency shift of these sidebands relative to the 697 cm^{-1} mode, directly indicating the frequency of the corresponding Van der Waals mode, is given in the spectrum. It is noted that no Van der Waals sidebands are visible at the low-frequency side of the 697 cm^{-1} resonance, confirming that the complex ions are originally only present in their vibrational ground state, or with the lowest Van der Waals mode excited. A sideband originating from this lowest Van der Waals mode would be dipole allowed [36], but could at best result in a slight broadening of the linewidths, as the spectral properties of FELIX preclude a full resolution of structure that is within 2 cm^{-1} from the main resonance. The 14 cm^{-1} Van der Waals mode also appears as a distinct sideband at the second strong IR active mode at 632 cm^{-1} .

Another possible assignment for these weak additional lines is that they originate from the three $\nu_4 + \nu_{16}$ combination modes. These combination modes are IR allowed, although it is *a priori* not clear what their intensity would be; normally combination modes are at least an order of magnitude weaker than the fundamental modes, and the ν_{16} fundamental mode is already rather weak. Nevertheless, these combination modes are expected to nearly coincide, depending on their (unknown) cross-anharmonicity, with the presently found lines (cf. Table 2.1). A similar study is therefore performed on the benzene-Ar cation, the result of which is shown in the lower part of Figure 2.6. For this complex, a similar pattern of weak additional lines is observed, but the lines are significantly shifted relative to the strong peak at 697 cm^{-1} . This is consistent with an interpretation of these additional lines as Van der Waals sidebands since a significant shift in absolute frequency would not be expected

if these lines originated from the $\nu_4 + \nu_{16}$ combination modes. Also for the benzene-Ar complex cation, the lowest frequency Van der Waals mode can be recognized on the high frequency side of the 632 cm^{-1} mode. The corresponding Van der Waals frequencies are therefore again indicated in the figure. The frequencies of the benzene-Ar cation are slightly smaller than those of the Ne complex and are – with frequencies of 11 cm^{-1} , 26 cm^{-1} and 46 cm^{-1} – considerably lower than the Van der Waals frequencies in the neutral benzene-Ar complex [39].

IR selection rules are not very helpful in trying to identify the observed Van der Waals modes. In the complex, the mirror symmetry in the plane of the benzene molecule is no longer present, lowering the symmetry from D_{6h} to C_{6v} . The IR active ν_{11} mode of a_{2u} symmetry in D_{6h} is of a_1 symmetry in C_{6v} . Motion of the noble gas atom in the plane of the benzene chromophore is of e_1 symmetry, while motion perpendicular to the plane is of a_1 symmetry. Character multiplication then reveals that both bending and stretching modes are IR allowed as Van der Waals sidebands. Recent calculations, performed by Van der Avoird and Lotrich, predict a bending mode at 10.1 cm^{-1} and a stretching mode at 47.9 cm^{-1} [36]. These computed values, surprisingly low due to the flatness of the intermolecular potential, are in excellent agreement with the frequencies observed here. Moreover, they compare well to an earlier experimentally determined value of 48 cm^{-1} [40]. Van der Avoird and Lotrich also predict an intense intermolecular mode at 1.7 cm^{-1} . Although an IR induced transition to a combination mode involving this low-frequency mode would be dipole allowed, it has not been observed. This could of course be due to the fact that the combination band could be indiscernible from such strong resonances as the Fermi-triplet components. Additionally, Van der Avoird and Lotrich predict a dissociation energy $E_0 = 5.74\text{ kJ/mole}$ (480 cm^{-1}) for deuterated benzene-Ar, which is in good agreement with the experimentally found upper limit of $E_0 = 5.80\text{ kJ/mole}$ (485 cm^{-1}) [19].

2.3.3 Symmetry breaking effects

As already mentioned above, the mirror symmetry in the plane of the benzene molecule is no longer present in the benzene-Ne and benzene-Ar complex, lowering the symmetry in the complex from D_{6h} to C_{6v} . The most important consequence of this is that all modes of vibronic A and E symmetry in D_{6h} , both gerade and ungerade, in principle become IR allowed in the complex cation. Interestingly, this clearly manifests itself in the spectrum of the benzene-Ar cation as shown by the appearance of the two peaks indicated with an arrow in Figure 2.6. The relatively strong resonance at 678 cm^{-1} is assigned to the high-frequency mode of the Jahn-Teller active ν_6 vibration (see Figure 2.1). In the bare benzene cation, this mode has E_{1g} vibronic symmetry and is not IR allowed. This mode has, however, unambiguously been assigned in other experimental studies on bare benzene and its various complexes [11–14]. The second manifestation of the symmetry breaking in the benzene-Ar complex is the shoulder on the high-energy side of the strong resonance at 632 cm^{-1} . One could suspect this to be the predicted Van der Waals band at 1.7 cm^{-1} , but as it is only observed as a shoulder on this particular resonance, and as it is shifted by $\sim 6\text{ cm}^{-1}$ this possibility is unlikely [36]. From Figure 2.1 it can be seen, however, that in this region the ν_{16} overtone modes, obviously of gerade character in D_{6h} , are expected. The shoulder is assigned to the highest frequency, doubly degenerate, ν_{16} overtone mode, which is thus found at 635 cm^{-1} . In the ZEKE spectrum shown by Lindner *et al.* [11], three small features are discernible at 586 , 611 and 638 cm^{-1} , which have not been assigned thus far. It is here proposed to assign these three features to the ν_{16} overtone modes, as indicated in Table 2.1.

Both resonances that appear due to symmetry breaking in the benzene-Ar complex, are almost absent in the case of benzene-Ne, even though the formal breaking of symmetry is, of course, the

same. The effect of the symmetry breaking on the IR intensity of lines that only become allowed in the complex is expected to be significantly less for the neon complex, however, due to its lower atomic mass and in particular due to its substantially lower polarizability (0.3956 \AA^3 for Ne versus 1.6411 \AA^3 for Ar [41]). Therefore, the clear difference in the spectrum of benzene-Ar compared to benzene-Ne with respect to these two lines is the best evidence for their assignments.

To study these symmetry breaking effects somewhat further, measurements are also performed on the benzene-Kr complex (not shown). Here one would expect an even more pronounced appearance of the two E_g modes of the benzene cation in the IR spectrum of the Van der Waals complex. The interpretation of relative line-intensities in the spectrum of the benzene-Kr complex in the $600\text{--}700 \text{ cm}^{-1}$ spectral region is complicated, however, as the vibrational levels in this region are very close to the dissociation limit of the benzene-Kr cation [17].

It is now also interesting to study a benzene-Ar_n Van der Waals complex in which the original D_{6h} symmetry is retained. The obvious candidate for such a study is the benzene-Ar₂ complex, for which two different conformers exist [35, 42]. In one conformer, denoted as the (1|1) complex, the argon atoms are centered on the axis above and below the benzene plane. In the other conformer, denoted as the (2|0) complex, both argon atoms are located on the same side of the benzene plane. The (1|1) complex has D_{6h} symmetry, and it is expected that modes of gerade symmetry are rigorously absent from its IR absorption spectrum. To selectively prepare the (1|1) complex cation, the excitation laser is tuned to 38564.2 cm^{-1} , which is the center of the $S_1(6^1) \leftarrow S_0$ transition in the neutral benzene-Ar₂ complex [35]. From the rotationally resolved spectrum as recorded and analyzed by Weber *et al.* it has been concluded that this transition is that of a symmetric top molecule, and that the rotational constants obtained are consistent with the (1|1) structure of the complex [35]. Moreover, this transition is red-shifted by some 20 cm^{-1} with respect to the corresponding transition in benzene-Ar, a shift that is almost identical to the 21 cm^{-1} red-shift observed in going from the benzene monomer to the benzene-Ar complex. The latter is strong evidence that both argon atoms are in identical positions relative to the benzene plane, and that there is relatively little interaction between the two argon atoms. Therefore, it is believed that the (1|1) complex is selectively excited in this transition. For completeness it should be mentioned that there is another transition of the benzene-Ar₂ complex that is found to be blue-shifted by 4 cm^{-1} with respect to the same transition in benzene-Ar, which has consequently been assigned to the $S_1(6^1) \leftarrow S_0$ transition in the (2|0) conformer [42].

After preparing the (1|1) complex in the electronically excited state, ionization is performed by tuning the second UV laser just slightly above the ionization threshold, which is some 160 cm^{-1} lower than that of the benzene-Ar complex [43]; an almost identical lowering of the ionization threshold is found in going from the benzene monomer to the benzene-Ar complex, again supporting the selective preparation of the (1|1) complex cation.

The IR absorption spectrum of the benzene-Ar₂ (1|1) complex cation throughout the $600\text{--}750 \text{ cm}^{-1}$ region is depicted in Figure 2.7, together with the spectrum of the benzene-Ar cation already shown earlier. The IR spectrum of the benzene-Ar₂ cation is deduced through recording the appearance of the benzene-Ar ionic dissociation product as a function of IR wavelength; single photon dissociation of the benzene-Ar₂ cation into a bare benzene ion and two argon atoms is energetically not possible, and indeed not observed, in this frequency range.

In the spectrum of the benzene-Ar₂ complex the Fermi-resonance structure of the ν_{11} and $\nu_6 + \nu_{16}$ modes discussed earlier can still be recognized. The two gerade modes of the benzene cation, indicated by arrows in the spectrum of the benzene-Ar cation, appear to be absent in the higher

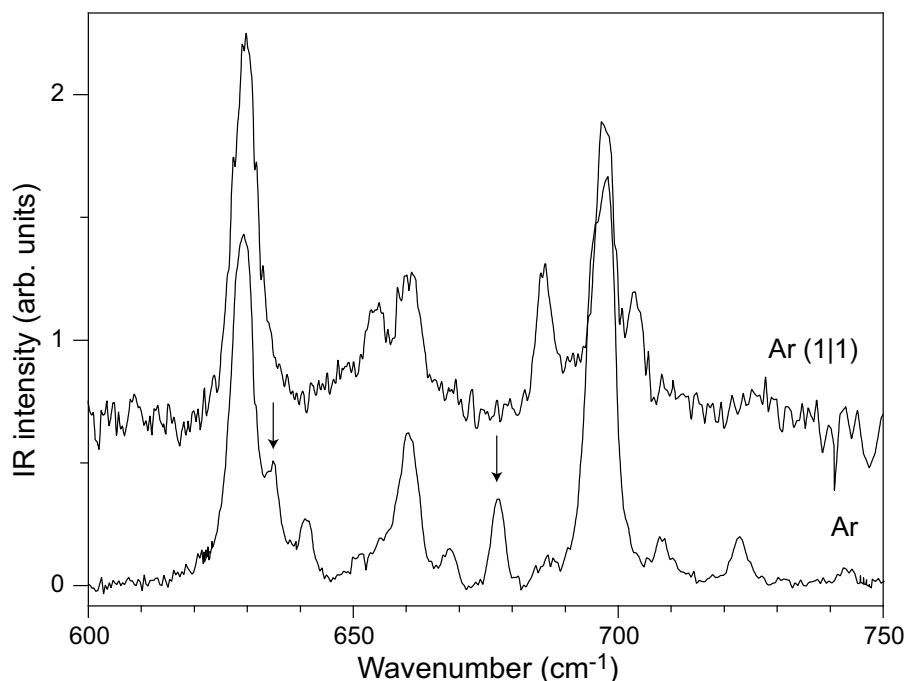


Figure 2.7: Part of the IR absorption spectrum of the benzene-Ar₂ complex cation in the symmetric (1|1) configuration (upper trace), compared to the spectrum of the benzene-Ar complex cation (lower trace) already shown in Figure 2.6.

symmetry benzene-Ar₂ ionic complex. Due to the lower signal-to-noise ratio in the spectrum of the benzene-Ar₂ complex, Van der Waals sidebands cannot be recognized as such in the spectrum. However, there is rather strong additional structure in the spectrum of the benzene-Ar₂ cation; the central peak of the Fermi-triad appears to be split in the benzene-Ar₂ complex, whereas the highest frequency peak of the triad has distinct additional structure on either side. It is clear that as long as this additional structure is not understood, no firm conclusions on the absence of gerade modes in this spectrum can be drawn.

The additional structure observed in the spectrum of the benzene-Ar₂ cation is quite intriguing. From the experimental preparation procedure detailed above, one can be quite confident to originally have had the (1|1) complex ions in their vibrational ground state with possibly only one low-frequency Van der Waals modes excited; Van der Waals sidebands would not be expected to occur anyway with significant intensity. The apparent absence of the gerade modes in the spectrum of the benzene-Ar₂ cations seems to confirm that there is indeed inversion symmetry in the complex ion. Nevertheless, there is no straightforward explanation for the occurrence of the three distinct additional lines in the spectrum if the symmetry of the complex ion is indeed D_{6h}. One could speculate on possible other, lower symmetry, arrangements of the Ar atoms in the ionic complex. An interesting structure is one in which the Ar atoms are positioned away from the symmetry axis, but in such a way as to retain inversion symmetry of the complex. Such a structure, which would have C_{2h} symmetry, would formally not even be Jahn-Teller unstable. It might therefore be energetically favorable for the system to partially lift the Jahn-Teller instability by displacement of the Ar atoms, instead of by distortion of the benzene nuclear framework. In reducing the symmetry from D_{6h} to C_{2h} the degeneracy of the E_{1u} modes is lifted, yielding a total of six modes of B_u symmetry in this spectral region which would

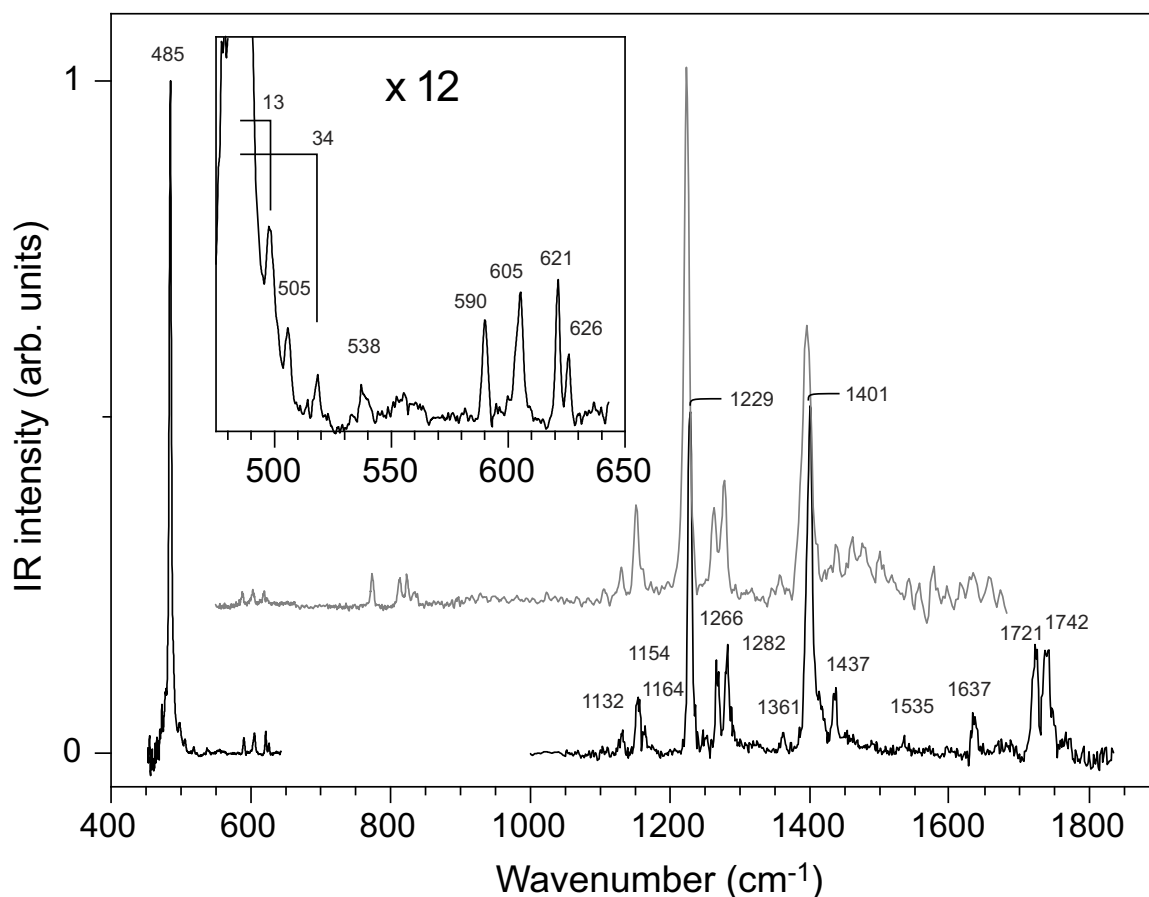


Figure 2.8: Parts of the IR absorption spectrum of the C_6D_6 -Ar cation. For reference, the spectrum that was measured by Satink *et al.* [19] is added in gray. In the inset, weak additional resonances on the high frequency side of the strong IR active ν_{11} mode at 485 cm^{-1} are shown, and the frequencies of two Van der Waals modes are indicated.

couple in an, IR active, Fermi-multiplet, and which might explain the observed spectra.

2.3.4 Deuterated benzene

To get more insight into the vibrational structure of the benzene cation and to confirm some of the vibrational assignments made, IR photodissociation studies on complexes of fully deuterated benzene (C_6D_6) with Ar have been performed as well. Ground state C_6D_6 -Ar cations are produced after laser excitation (38765 cm^{-1}) and subsequent ionization (35650 cm^{-1}) of the jet-cooled neutral complexes [34, 44]. A preliminary version of the IR spectrum covering the $450\text{--}1500\text{ cm}^{-1}$ range has been published before [19]. In the present study, a particular focus is laid on the low frequency range from $450\text{--}650\text{ cm}^{-1}$, (which is investigated with an improved spectral resolution) and on the high frequency range, between 1000 cm^{-1} and 1850 cm^{-1} . It would also have been interesting to study the C–D stretching vibrations, but unfortunately, at the time of the experiment the region around 2200 cm^{-1} was not yet accessible with the IR source.

The resulting IR absorption spectrum is shown in Figure 2.8. To present a complete overview of the deuterated benzene-Ar spectrum, the spectrum that is recorded by Satink *et al.* [19] is included in

gray. In the low-frequency range of the spectrum, the dominant IR absorption peak observed at 485 cm^{-1} can unambiguously be assigned to the ν_{11} [out-of-plane C–H bending] mode, found in neutral C_6D_6 at 496 cm^{-1} [25]. The peak positions of four resonances in the 600 cm^{-1} region are indicated in the figure as well. The resonances at 621 cm^{-1} and 626 cm^{-1} could not be resolved as separate ones in an earlier study [19]. In addition, the line shape of the 605 cm^{-1} resonance suggests that it might be composed of more than one mode. In trying to assign all these observed modes, it has to be realized that the two lowest $\nu_6 + \nu_{16}$ combination modes are expected in this region, borrowing intensity from the ν_{11} mode via a Fermi-resonance, just as in the protonated benzene cation. Apart from these modes, the three $\nu_4 + \nu_{16}$ combination modes fall in this region. A consistent picture is obtained when the modes at 605 cm^{-1} and 621 cm^{-1} are assigned as $\nu_6 + \nu_{16}$ combination modes. In the Fermi-resonance model described earlier, now with a slightly increased coupling parameter α of 23 cm^{-1} , unperturbed values of 494 cm^{-1} for the ν_{11} mode and 601 cm^{-1} and 616 cm^{-1} for the $\nu_6 + \nu_{16}$ combination modes are obtained. The latter values are in good agreement with the values expected from a two-mode Jahn-Teller simulation [13]. The absorption at 590 cm^{-1} , the (blended) absorption at 605 cm^{-1} and the absorption at 626 cm^{-1} are then assigned to the $\nu_4 + \nu_{16}$ combination modes, having A_{2u} , E_{2u} and A_{1u} symmetry, respectively. All these assignments are indicated in Table 2.2.

On the high-frequency side of the 485 cm^{-1} resonance, additional structure is observed as shown on an expanded scale in the inset to Figure 2.8. This structure could be the Van der Waals sidebands of the strong ν_{11} mode. However, the resonances at 506 cm^{-1} and 538 cm^{-1} have also been reported in ZEKE studies on the bare deuterated benzene cation [30]. There, the only vibrational modes that can occur in this spectral region are the ν_{16} overtone modes. Although these modes are of gerade symmetry in the bare benzene cation, we already know from our work on protonated benzene-Ar complex cations, that such modes can appear in the IR spectrum due to symmetry breaking in the complex. We therefore attribute these two absorptions to the two lowest ν_{16} overtone modes; an additional mode observed by Lindner *et al.* at 562 cm^{-1} is most likely the highest frequency ν_{16} overtone mode (see Table 2.2). The remaining two resonances in the low-frequency part of the spectrum are attributed to intermolecular Van der Waals vibrations, and their frequency offset relative to the 485 cm^{-1} peak is given in the figure, indicating Van der Waals modes at 13 cm^{-1} and at 34 cm^{-1} . These values are higher than those of protonated benzene, which is contrary to the expectations as the reduced mass is increased [36]. It is noted, however, that the character of the intra-molecular mode (pure out-of-plane C–D bending) to which the Van der Waals modes appear as sidebands is rather different than the character of the intra-molecular modes for which sidebands are observed in protonated benzene (the $\nu_6 + \nu_{16} - \nu_{11}$ Fermi triad). This difference may lead to the appearance of different Van der Waals modes as sidebands. It may prove necessary to perform a similar experiment on deuterated benzene-Ne to ascertain the present (conflicting) assignment.

The high frequency range is dominated by two strong resonances at 1229 cm^{-1} and 1401 cm^{-1} . It is interesting to note that, although they are also the strongest observed resonances in the work of Satink *et al.*, the relative intensities are different. One reason for this could be that the settings of FELIX in the present study are optimized for a higher frequency range than in the previous work; the bandwidth in the high-frequency range is then narrower and the peak intensities observed in that range are higher. It can be seen in Figure 2.8 that the integrated intensities for the two recorded spectra are similar, supporting this hypothesis.

For the assignment some major changes are proposed to the previous work by Applegate and

Miller. First, it seems somewhat awkward that in the protonated species both ν_{14} and ν_{19} are assigned to strong resonances, whereas for C_6D_6 ν_{14} has not been identified. Second, there are two reasonably alike pairs of resonances, one at 1266 and 1282 cm^{-1} , and one at 1721 and 1742 cm^{-1} , respectively. The spacings and relative intensities in these sets are quite similar and are reminiscent of the quadratic splittings that are observed for the linearly Jahn-Teller active modes. Indeed, Applegate and Miller assign two sets of ZEKE resonances, (338,357 cm^{-1}) and (786,797 cm^{-1}) to quadratically split Jahn-Teller modes. In combination with an IR active modes at 485 cm^{-1} (ν_{11}) the latter set yields 1271 and 1282 cm^{-1} ; the former set gives rise to the high-frequency resonances in combination with a strong IR active mode at 1385 cm^{-1} . Taking into account a slight anharmonicity in the combination mode frequency, the resonance at 1401 cm^{-1} is a perfectly reasonable partner. It is, however, unlikely that a combination band (as this is what Applegate and Miller assigned the 1401 cm^{-1} resonance to) is the source of yet another combination. It is therefore proposed to assign the resonance at 1401 cm^{-1} to ν_{19} and that at 1229 cm^{-1} to ν_{14} .

2.3.5 Hot band spectroscopy of benzene-Ar

The combined experimental work on the C_6H_6 cation has resulted in the assignment of all modes below 800 cm^{-1} , as well as in the assignment of some additional strong resonances like the ν_1 mode of E_{1g} symmetry at 969 cm^{-1} (see Table 2.1). Many more resonances have been observed, but a further unambiguous identification has proven to be difficult. IR absorption spectroscopy has the obvious advantage that it has rigorous selection rules, as opposed to ZEKE and MATI spectroscopy, where the appearance of lines in the spectra is governed by Franck-Condon overlap of the wave functions of the corresponding vibronic levels.

To further exploit the possibilities offered by IR photodissociation spectroscopy, vibronic levels of different symmetry can be used as initial states in the IR absorption process. Obviously, the initially excited vibrational state for such an experiment should lie below the dissociation limit of the complex to prevent dissociation before the actual IR transition can be induced. The preparation of a pure sample of ions in one selected vibrationally excited state, *i.e.*, without any population in the vibrational ground state of the ion, is experimentally difficult. It is relatively straightforward, however, to produce a sample of ions with a known distribution over a selected set of vibrational levels. By measuring the IR absorption spectrum of this sample, a type of ‘hot-band’ spectroscopy is performed.

In this experiment, neutral benzene-Ar complexes are resonantly excited as described earlier, but now the ionization laser is tuned to a frequency several hundred cm^{-1} above the ionization threshold. Specifically, the frequency of the ionization laser is tuned slightly above that required to produce ionic complexes in a selected vibrationally excited state. In this way, ions are produced in a mixture of vibrational states; ground state ions are produced when the electron carries away the maximum possible excess energy, whereas vibrationally excited ions in the targeted state are prepared when electrons with near-zero kinetic energy are produced. The vibrational population distribution that is thus created is completely governed by Franck-Condon factors, which are well known from, e.g., ZEKE spectroscopy measurements [11].

In the first experiment of this type, the ionization laser is tuned some 350 cm^{-1} above the ionization threshold for the benzene-Ar complex. As can be seen from Table 2.1, ions can then be prepared in the lowest energy ν_6 mode of B_{1g} symmetry. Obviously, it is energetically also possible to produce ions in any of the lower lying vibrational levels, e.g., in the vibrational ground state as well as in the three ν_{16} modes around 300 cm^{-1} . Based on the results of ZEKE-measurements [11] it is

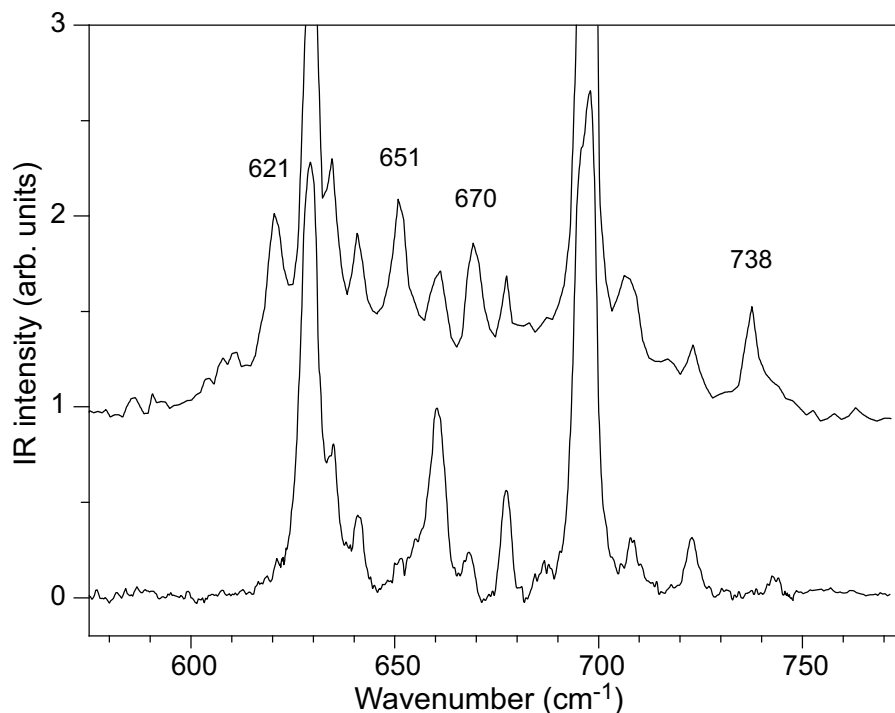


Figure 2.9: IR absorption spectrum of benzene-Ar complex cations recorded with the ionization laser tuned to some 350 cm^{-1} above the ionization threshold (upper trace). IR absorption occurs both from the ground vibrational state as well as from the ν_6 vibrationally excited state of the cation. For comparison the IR spectrum of the benzene-Ar complex cation recorded when only the vibrational ground state is initially populated, and which has already been shown in Figure 2.6, is included as well (lower trace). The frequencies of the four distinct new resonances originating from the ν_6 mode of B_{1g} symmetry at 347 cm^{-1} are indicated.

expected that both the vibrational ground state and the lowest energy ν_6 mode will be almost equally populated with only a few percent of the total population residing in the ν_{16} modes in this case. The IR photodissociation spectrum of this sample of ions in which a mixture of vibrational states is populated is thus expected to show all the resonances observed before for the vibrational ground state of the benzene-Ar cation together with additional resonances. These additional resonances then most likely originate from the ν_6 mode of B_{1g} symmetry, obeying the corresponding selection rules.

The $580\text{--}770\text{ cm}^{-1}$ range of the IR absorption spectrum of benzene-Ar cations prepared in this mixture of vibrational states is shown as the upper trace in Figure 2.9. For comparison, a (saturated) IR absorption spectrum of the vibrationally cold benzene-Ar cations is displayed in the lower trace of the figure. As expected, all vibrational structure present in the lower trace is also discernible in the upper spectrum. In addition, however, four distinct new resonances appear in the so-called hot-band spectrum at photon energies of 621 cm^{-1} , 651 cm^{-1} , 670 cm^{-1} and 738 cm^{-1} . These four resonances disappear if the ionization laser is even only slightly red-detuned (on the order of only 10 cm^{-1}), confirming that these four transitions indeed originate from the vibrationally excited ν_6 mode at 347 cm^{-1} in the ion.

One has to realize that it is not *a priori* expected that clearly separated, distinct additional resonances appear in our hot-band spectrum. In the typical hot-band spectra of molecules of the size of the benzene molecule, most often only a gradual broadening and red-shift of IR absorption lines

compared to the spectra of the vibrationally cold molecules is observed [25]. This is due to the fact that modes that are IR active from the vibrational ground state are always IR active from the vibrationally excited levels as well; the cross-anharmonicities between the vibrationally excited modes and the IR active modes in general lead to a gradual red-shift of the IR transitions with increasing vibrational excitation. Of course, transitions to other fundamental modes might become IR allowed from the vibrationally excited levels as well, but these then necessarily appear as combination modes, e.g., decreasing one quantum in the originally vibrationally excited mode and increasing one quantum in another mode, and are therefore expected to be rather weak. In this case it is the Fermi-resonance of the IR active ν_{11} mode with all other nearby modes of the same vibronic symmetry, widely shifting lines in position and distributing IR intensity over many lines, which leads to the appearance of distinct new lines in the hot-band spectrum.

Selection rules dictate that only states of vibronic B_{2u} and E_{2u} symmetry can be reached via IR allowed transitions originating from a state of vibronic B_{1g} symmetry. Although population with excited Van der Waals modes could result in resonances from modes with a different symmetry, its abundance is assumed to be marginal and its possible influence on the spectrum is therefore neglected. Starting from the lowest frequency ν_6 mode, the IR active transition to the $\nu_6 + \nu_{11}$ combination mode of vibronic B_{2u} symmetry is expected to be dominant in the spectral region shown in Figure 2.9. It therefore appears likely that all four modes are of B_{2u} symmetry, and are observable due to coupling to the $\nu_6 + \nu_{11}$ combination mode. The $\nu_6 + \nu_{11}$ combination mode will again have a Fermi-resonance with the (single) B_{2u} $\nu_6^2 + \nu_{16}$ combination mode as well as with the (single) $\nu_6 + \nu_{16}$ combination mode of the same symmetry (see Figure 1). The only other mode of vibronic B_{2u} symmetry that is expected in this region is the ν_{17} [C–H out-of-plane bending] mode. This mode is quadratically Jahn-Teller active and has (tentatively) been assigned to a resonance at 990 cm^{-1} . It should therefore be observed at $990 - 347 = 643\text{ cm}^{-1}$. One could assign the resonance at 651 cm^{-1} to the ν_{17} component, but the shift of 7 cm^{-1} seems too large. The four extra modes observed are therefore interpreted as the above discussed Fermi-quartet.

In a second measurement of a hot-band spectrum, the ionization laser is tuned some 370 cm^{-1} above the ionization threshold for the benzene-Ar complex. In this case vibrationally excited ions are prepared in both low frequency ν_6 modes as well as in the vibrational ground state with almost equal probability [11]. The resulting hot-band spectrum is shown in the upper trace of Figure 2.10, where it is compared to the hot-band spectrum that we already discussed above (lower trace). It is evident from these spectra that three new resonances, originating from the ν_6 mode of B_{2g} symmetry at 367 cm^{-1} , now appear in the spectrum. Again, the IR active transition to the $\nu_6 + \nu_{11}$ combination mode, which now is of vibronic B_{1u} symmetry, is expected to give IR intensity to the three modes observed in the spectrum, which consequently all have to be of B_{1u} symmetry. The absolute frequencies of the additional resonances observed in the hot-band spectra as well as their symmetry assignments are listed in Table 2.1. As all these modes are most likely mixtures of the $\nu_6 + \nu_{11}$, $\nu_6^2 + \nu_{16}$, $\nu_6 + \nu_{16}$ modes, no more definite assignment has been made.

2.4 Conclusions

The infrared (IR) absorption spectra of the jet-cooled benzene cation complexed with Ne and Ar have been recorded throughout the $275\text{--}1900\text{ cm}^{-1}$ and the $2800\text{--}3200\text{ cm}^{-1}$ range via IR-laser induced vibrational dissociation spectroscopy. By starting the IR photodissociation process from vibrationally

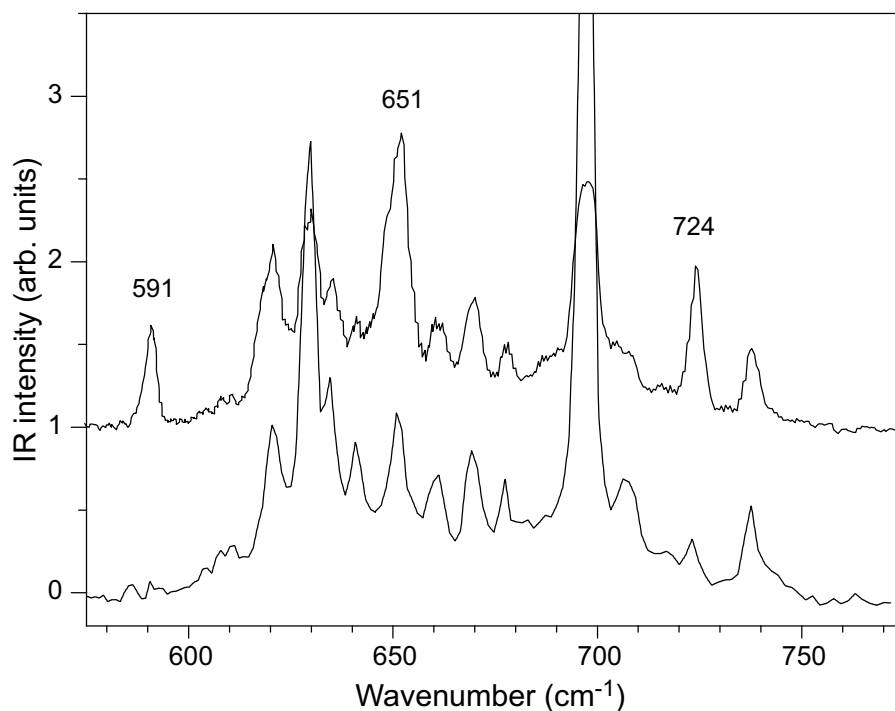


Figure 2.10: IR absorption spectrum of benzene-Ar complex cations recorded with the ionization laser tuned to some 370 cm^{-1} above the ionization threshold (upper trace). IR absorption occurs both from the ground vibrational state as well as from the two ν_6 vibrationally excited states of the cation. For comparison the IR spectrum of the benzene-Ar complex cation recorded when only the vibrational ground state and the lowest vibrationally excited ν_6 state are initially populated (see Figure 2.9), is included as well (lower trace). The frequencies of the three distinct new resonances originating from the ν_6 mode of B_{2g} symmetry at 367 cm^{-1} are indicated.

excited complex cations, additional information on the vibrational structure has been obtained. The combined results from the work presented here and previous ZEKE and MATI studies on benzene cations have made a complete assignment of all observed vibrational modes below 800 cm^{-1} possible. It has also enabled a tentative first assignment of the benzene cation spectrum up to 1900 cm^{-1} . A detailed comparison between the IR absorption spectra of benzene-Ne and benzene-Ar in selected spectral regions convincingly demonstrates that the spectrum of the benzene-Ne cation indeed represents the IR absorption spectrum of the bare benzene cation. In using Ne as a messenger atom in the IR photodissociation technique, Van der Waals sidebands can appear in the spectrum, but no effects of the formal symmetry breaking in the complex due to the presence of the messenger atom have been observed. We therefore conclude that, to within our present spectral resolution, the spectrum of the benzene-Ne cation as shown in Figure 2.3 is the *true* and complete IR spectrum of the benzene cation, and should serve as a benchmark for future analyses of the vibrational properties of this important species.

References

- [1] H. Jahn and E. Teller, Proc. Royal Soc. London A **161**, 220 (1937).
- [2] K. Raghavachari, R. Haddon, T. A. Miller, and V. Bondybey, J. Chem. Phys. **79**, 1387 (1983).
- [3] J. Cernicharo, A. M. Heras, A. G. G. M. Tielens, J. R. Pardo, F. Herpin, M. Guélin, and L. B. F. M. Waters, Ap. J. **546**, L123 (2001).
- [4] A. Leger and J. L. Puget, Astron. Astrophys. **137**, L5 (1984).
- [5] L. J. Allamandola, A. G. G. M. Tielens, and J. R. Barker, Ap. J. **290**, L25 (1985).
- [6] O. Braltbart, E. Castellucci, G. Dujardin, and S. Leach, J. Phys. Chem. **87**, 4799 (1983).
- [7] T. A. Miller and V. Bondybey, *Molecular Ions: Spectroscopy, Structure and Chemistry* (North-Holland Publishing Company, 1983), chap. The Jahn-Teller Effect in Benzenoid Cations: Theory and Experiment, p. 201.
- [8] S. R. Long, J. T. Meek, and J. P. Reilly, J. Chem. Phys. **79**, 3206 (1983).
- [9] G. Müller, J. Y. Fan, J. L. Lyman, W. E. Schmidt, and K. L. Kompa, J. Chem. Phys. **90**, 3490 (1989).
- [10] J. Le Calvé, M. Schmidt, and M. Mons, J. Phys. Chem. **96**, 4131 (1992).
- [11] R. Lindner, K. Müller-Dethlefs, E. Wedum, K. Haber, and E. Grant, Science **271**, 1698 (1996).
- [12] H. Krause and H. J. Neusser, J. Chem. Phys. **97**, 5923 (1992).
- [13] J. G. Goode, J. D. Hofstein, and P. M. Johnson, J. Chem. Phys. **107**, 1703 (1997).
- [14] K. Siglow and H. J. Neusser, J. El. Spect. Relat. Phenom. **112**, 199 (2000).
- [15] C. H. Kwon, H. L. Kim, and M. S. Kim, J. Chem. Phys. **119**, 215 (2003).
- [16] A. B. Burrill, J. T. Zhou, and P. M. Johnson, J. Phys. Chem. A **107**, 4601 (2003).
- [17] H. Krause and H. J. Neusser, J. Chem. Phys. **99**, 6278 (1993).
- [18] O. Dopfer, R. V. Olkhov, and J. P. Maier, J. Chem. Phys. **111**, 10754 (1999).
- [19] R. G. Satink, H. Piest, G. von Helden, and G. Meijer, J. Chem. Phys. **111**, 10750 (1999).
- [20] T. A. Barckholtz and T. A. Miller, Int. Rev. of Phys. Chem. **17**, 435 (1998).
- [21] B. E. Applegate, T. A. Barckholtz, and T. A. Miller, Chem. Soc. Rev. **32**, 38 (2003).
- [22] B. E. Applegate and T. A. Miller, J. Chem. Phys. **117**, 10654 (2002).
- [23] P. M. Johnson, J. Chem. Phys. **117**, 9991 (2002).
- [24] E. B. Wilson, Jr., Phys. Rev. **45**, 706 (1934).
- [25] G. Herzberg, *Molecular Spectra and Molecular Structure* (Krieger Publishing company, Malabar, FLA, 1991), 2nd ed.

- [26] K. Müller-Dethlefs and J. B. Peel, J. Chem. Phys. **111**, 10550 (1999).
- [27] M. Ford, R. Lindner, and K. Müller-Dethlefs, Mol. Phys. **101**, 705 (2003).
- [28] H. Longuet-Higgins, Adv. Spectrosc. **2**, 429 (1961).
- [29] H. Krause, Ph.D. thesis, Technische Universität München (1993).
- [30] R. Lindner, Ph.D. thesis, Technische Universität München (1996).
- [31] K. Siglow, Ph.D. thesis, Technische Universität München (2000).
- [32] T. Weber, E. Riedle, H. J. Neusser, and E. Schlag, J. Mol. Struct. **249**, 69 (1991).
- [33] K. Siglow, R. Neuhauser, and H. J. Neusser, Chem. Phys. Lett. **293**, 19 (1998).
- [34] T. Weber, A. V. Bargaen, E. Riedle, and H. J. Neusser, J. Chem. Phys. **92**, 90 (1990).
- [35] T. Weber and H. J. Neusser, J. Chem. Phys. **94**, 7689 (1991).
- [36] A. van der Avoird and V. F. Lotrich, J. Chem. Phys. **120**, 10069 (2004).
- [37] P. Hobza, O. Bludsky, K. Selzle, and E. Schlag, J. Chem. Phys. **97**, 335 (1992).
- [38] M. J. Frisch, G. W. Trucks, H. B. Schlegel, G. E. Scuseria, M. A. Robb, J. R. Cheeseman, V. G. Zakrzewski, J. J. A. Montgomery, R. E. Stratmann, J. C. Burant, et al., *Gaussian 98, Revision A.7*, Pittsburgh, PA (1998).
- [39] R. Neuhauser, J. Braun, H. J. Neusser, and A. van der Avoird, J. Chem. Phys. **108**, 8408 (1998).
- [40] R. Neuhauser, K. Siglow, and H. J. Neusser, Phys. Rev. Lett. **80**, 5089 (1998).
- [41] *Handbook of Chemistry and Physics* (CRC press, Boca Raton, FL, 1993-1994), 74th ed.
- [42] M. Schmidt, M. Mons, and J. L. Calvé, Chem. Phys. Lett. **177**, 371 (1991).
- [43] H. J. Neusser and H. Krause, Chem. Rev. **94**, 1829 (1994).
- [44] K. Siglow, R. Neuhauser, and H. J. Neusser, J. Chem. Phys. **110**, 5589 (1999).

Assignment	Symmetry	Krause [12, 29]	Lindner [11, 30]	Goode [13]	Siglow [14, 31]	This work & Satink [19]	Kwon [15]
ν_{16}	B _{1u}	285	289	292			296
ν_{16}	E _{1u}	303	306	306		305	305
ν_{16}	B _{2u}		328				327
$ 3/2, 1 >$	B _{1g}	343	347	350			350
$ 3/2, 2 >$	B _{2g}	363	367	370			363
ν_4	E _{2g}	416	418	422			420
ν_{16}^2			586				596
ν_{16}^2			608				
$\nu_{16} + 3/2, 1 >, 3/2, 2 > / \nu_{11}^\dagger$	E _{1u}	626	630	632		632	
ν_{16}^2						638	
$\nu_{16} + 3/2, 1 >, 3/2, 2 > / \nu_{11}^\dagger$	E _{1u}	659	660	663		661	
$ 1/2, 1 >$	E _{1g}	674	677	677	678		
$\nu_{16} + 3/2, 1 >, 3/2, 2 > / \nu_{11}^\dagger$	E _{1u}		696	700		697	697
ν_{10}	A _{1g}		724	727			724
$ 1/2, 3 >$	E _{1g}		763				761
ν_{10}	E _{2g}		843				843
ν_4^2	E _{2g}		847				
			853				
ν_{12}	E _{2u}		883				878
ν_5	E _{2g}		934				
ν^*	A _{1u} , A _{2u} , E _{1u}					948	
	B _{1u}					958 [†]	
ν_1	E _{1g}	967	969		969		967
	B _{2u}					968 [†]	
ν_{10}	A _{2g}		983				986
ν^*			994			990	
	B _{2u}					998 [†]	
	B _{2u}					1017 [†]	
	B _{1u}					1018 [†]	
$ 3/2, 3 >$			1018				
$ 3/2, 4 >$			1031				
ν^*						1067	
$ 1/2, 4 >$		1069	1073		1073		1072
	B _{2u}		1089			1085 [†]	
	B _{1u}					1091 [†]	
ν^*						1180	1183
$ 3/2, 5 >$		1228	1230				
$ 3/2, 6 >$			1245				
$ 1/2, 6 >$		1242	1257				1255
$\nu_{16} + \nu_{17}$	B _{1g} , B _{2g} , E _{1g}		1286				1283
$\nu_{18} + 3/2, 1 >$	E _{2u}		1297			1295	
$\nu_1 + 3/2, 1 >$	B _{1g}	1303	1305				
$\nu_1 + 3/2, 2 >$	B _{2g}	1326	1328				1322
$\nu_{14}, \nu_4 + \nu_{18}$	E _{2u} , E _{1u}		1356			1361	1357
$\nu_4 + \nu_{17}$	A _{1u} , A _{2u} , E _{2u}					1399	1393
$ 3/2, 7 >$			1408				
$\nu_{11} + 1/2, 3 >$						1433	1420
$ 3/2, 8 >$			1435				
			1440				
ν_{19}	A _{1u} , A _{2u} , E _{2u}					1481	1475
$\nu_{10} + \nu_{11}$	A _{1u} , A _{2u} , E _{2u}					1501	
$\nu_4 + \nu_{11}$	E _{2u}		1522			1529	
$\nu_1 + \nu_{11}$	E _{1u}					1629	
							1648
$\nu_{11} + 3/2, 3 > \text{ or } \nu_{14} + 3/2, 1 >$						1704	
$\nu_{11} + 3/2, 4 > \text{ or } \nu_{14} + 3/2, 2 >$						1721	
						1797	1786
$\nu_{17} + \nu_{18}^2$						1815	1825
ν_{20}	A _{2u}					3089	
ν_{13}	E _{2u}					3098	

Table 2.1: Assignment of observed vibrational frequencies (in cm^{-1}) for the benzene cation in different experiments. The resonances labeled with ν^* are assigned to unspecified fundamental modes (cf. section 2.3.1). Frequencies labeled with † are deduced from the hot-band spectroscopy described in section 2.3.5.

Assignment	Symmetry	Krause	Lindner	Goode	This work & Satink	Kwon
		[12, 29]	[11, 30]	[13]	[19]	[15]
ν_{16}	B _{1u}	245	249	245		252
ν_{16}	E _{1u}	262	265	262		263
ν_{16}	B _{2u}	286	289	285		289
$ 3/2, 1 >$	B _{1g}	336	338	335		334
ν_4	E _{2g}	340	344			343
$ 3/2, 2 >$	B _{2g}	353	357			
ν_{11}	E _{1u}				485	491
ν_{16}^2	E _g		505		506	509
ν_{16}^2	A _g		540		538	550
ν_{16}^2	E _g		562			
ν_{10}	A _{1g}		562			550
$\nu_4 + \nu_{16}$	A _{2u}	588			590	
$\nu_4 + \nu_{16}, \nu_{16} + 3/2, 1 >$	E _{2u} , E _{1u}	601	604	603	605	
$\nu_{16} + 3/2, 1 >$	E _{1u}		622	620	621	
$\nu_4 + \nu_{16}$	A _{1u}				626	
$ 1/2, 2 >$	A _{2u}	633	636	634		
ν_{10}	E _{2g}		673	673		658
ν_4^2	E _{1g}		697			680
$ 1/2, 3 >$			739			
ν_5	E _{2g}		754			750
ν_{18}	E _{2u}				773	766
$ 3/2, 3 >$			786			
$ 3/2, 4 >$			797			
ν_{17}	E _{1u}				813	
$\nu_4 + \nu_{11}$	E _{2u}				823	
ν_{15}	E _{2u}				835	840
$ 1/2, 4 >$			868			
ν_{12}	E _{2u}		877			
$\nu_{16} + 1/2, 2 >$			887			
$\nu_{16} + 1/2, 2 >$			900			
$\nu_{16} + 1/2, 2 >$		922	924			
ν_1	E _{1g}		926			926
$ 1/2, 5 >$			1058			
$ 3/2, 5 >$			1119			
$\nu_{18} + 3/2, 1 >$	E _{2u}				1132	
$ 3/2, 6 >$			1143			
$\nu_{18} + 3/2, 2 >$	E _{2u}				1154	
$\nu_4 + \nu_{17}$	A _{1u} , A _{2u} , E _{2u}				1164	
$\nu_{14}, \nu_{11} + 1/2, 3 >$	E _{2u}				1229	
$\nu_{11} + 3/2, 3 >$					1266	
$ 1/2, 8 >$					1266	
$\nu_{11} + 3/2, 4 >$					1282	
$ 3/2, 7 >$			1297			
$ 3/2, 8 >$			1316			
$\nu_{19}, \nu_{18} + 1/2, 2 >$	A _{1u} , A _{2u} , E _{2u}				1401	
$\nu_{17} + 1/2, 2 >$					1437	
$ 3/2, 11 >$			1545			
$ 3/2, 12 >$			1563			
$\nu_5 + \nu_{12}, \nu_4 + \nu_{14}, \nu_{18} + 1/2, 4 >$					1637	
$\nu_{19} + 3/2, 1 >$	E _{2u}				1722	
$\nu_{19} + 3/2, 2 >$	E _{2u}				1738	

Table 2.2: Assignment of observed vibrational frequencies for the deuterated benzene cation in different experiments.

CHAPTER 3

THE IR ABSORPTION SPECTRUM OF THE GAS PHASE NEUTRAL BENZENE DIMER

The infrared (IR) absorption spectrum of the jet-cooled benzene dimer has been recorded throughout the 300–1700 cm^{-1} range via ion-dip spectroscopy. The spectrum for $(\text{C}_6\text{H}_6)_2$ closely resembles that of the neutral benzene molecule and that of $\text{C}_6\text{H}_6\text{--C}_6\text{D}_6$ can be described as a combination of two monomer spectra. On close inspection several resonances appear in spectra for both species that are IR forbidden in the monomer. The spectra can be favorably compared to calculated spectra for a distorted T-shaped geometry. Evidence has been found for one intermolecular vibration for the fully protonated dimer with an energy of 51 cm^{-1} .

3.1 Introduction

The benzene dimer serves as a prototype system for the study of dispersive intermolecular forces. There exist two types of interaction that could stabilize the cluster: first, a hydrogen-bond type interaction between the π -cloud of one moiety and a C–H group of the other, and second, a purely dispersive interaction between two π -clouds. As these two interactions could lead to two different stable geometries, it has been a subject of study for long time to find out what the equilibrium structure of the gas-phase benzene dimer is. This question has drawn considerable experimental [1–11] and theoretical attention [12–16].

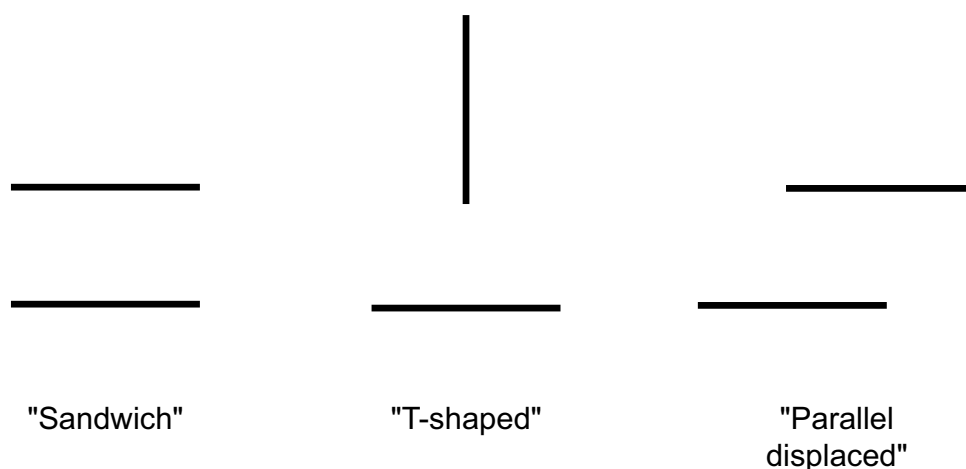


Figure 3.1: Schematic overview of proposed structures of the benzene dimer

Figure 3.1 schematically shows three possible geometries which have been proposed for the gas phase benzene dimer. There exists general agreement that the highly symmetric sandwich structure is not the lowest energy structure. There are two other proposed geometries for which it is not yet clear which is the most stable one. First, a T-shaped dimer is proposed, where one of the hydrogens is pointed into the π -cloud of the aromatic ring. A second proposed structure is the so-called parallel-displaced geometry, where there is a pair of somewhat less strong hydrogen atom– π -cloud interactions. In both cases, dispersive interactions between the π -clouds stabilize the system.

Early on, Klemperer and co-workers observed the existence of a permanent dipole for benzene dimers in the gas phase, a finding which cannot be brought in agreement with the presence of a highly symmetric sandwich-like structure [1]. The result did, however, agree with findings in X-ray spectroscopic experiments on crystalline phase benzene, where the benzene molecules were found to be stacked in a fashion where the two molecular planes are perpendicular to each other, roughly in a T-shaped geometry [17]. Mass-resolved spectroscopic experiments have yielded the observation that the UV $S_16^1 \leftarrow S_0$ transition is split into two resonance peaks, leading to a conclusion that there in fact exist two non-equivalent excitation centers [2–8]. Felker and co-workers employed Raman spectroscopy and confirmed the presence of two, inequivalent sites of the monomer moieties [10]. Furthermore, their data suggested that one of these sites had a higher symmetry than the other. This could be explained by a T-shaped structure which exhibits an internal rotation along the stem of the T. This conclusion was enforced in a microwave spectroscopic experiment, where a symmetric-top-like structure was found, but where the individual lines were split up into four components, which suggests

two interconversion tunneling pathways between different dimer geometries [9]. This last suggestion of a very floppy system could well explain the failure so far to produce rotationally resolved UV spectroscopic data. Finally, Raman spectroscopic experiments have also yielded some information about the intermolecular potential of the cluster [11].

In this chapter, direct Infrared (IR) absorption measurements of the benzene dimer in a double-resonance IR-UV experiment are presented. The IR absorption spectrum provides detailed information about the intra- and – possibly – intermolecular potential. From a comparison with ab-initio calculations it is observed that the IR absorption spectra for the perprotonated benzene dimer and for C_6H_6 - C_6D_6 are best described as that of distorted T-shaped structures.

3.2 Experiment

In the experiment, a mixture of $\sim 1\%$ benzene vapor, consisting of a near 1:1 ratio of perprotonated (C_6H_6) and perdeuterated (C_6D_6) benzene, in argon at a backing pressure of 2 atm. is expanded through a 0.5 mm diameter pulsed nozzle into vacuum. In the adiabatic expansion, the molecules are vibrationally and rotationally cooled to about 5 K. The expansion conditions enable the formation of weakly bonded Van der Waals complexes of benzene that are internally cooled as well.

For the measurement of the IR absorption spectra of the jet-cooled neutral benzene dimer, IR ion-dip spectroscopy is employed. Ions are produced from ground state molecules using a one-color ionization scheme. For this, the molecules are excited to the ν_6 excited vibrational state in the first electronically excited singlet state S_1 using a frequency-doubled dye laser (Coumarin 500). The molecules are then ionized by a second photon from the same UV laser source. This second photon gives the complex a considerable excess energy over the ionization potential. Still, dissociation of the clusters is observed to be only marginal, yielding typically a ratio monomer:dimer of 1:5 in the number of detected cations.

It was shown by several groups that the $S_1 6^1 \leftarrow S_0$ transition is split into two components [2–8]. In Figure 3.2 a small part of the UV spectrum is shown for $(C_6H_6)_2$ (solid line) and $C_6H_6 - C_6D_6$ (dashed line). One can observe a splitting of $\sim 4\text{ cm}^{-1}$, which is associated with a site-specific excitation, but it has thus far not been possible to relate either of the components to one specific site. In the present work on $(C_6H_6)_2$, all spectra were recorded with the UV probe laser tuned to the high-frequency component of the doublets at 38569 cm^{-1} . The spectrum of C_6H_6 - C_6D_6 exhibits four

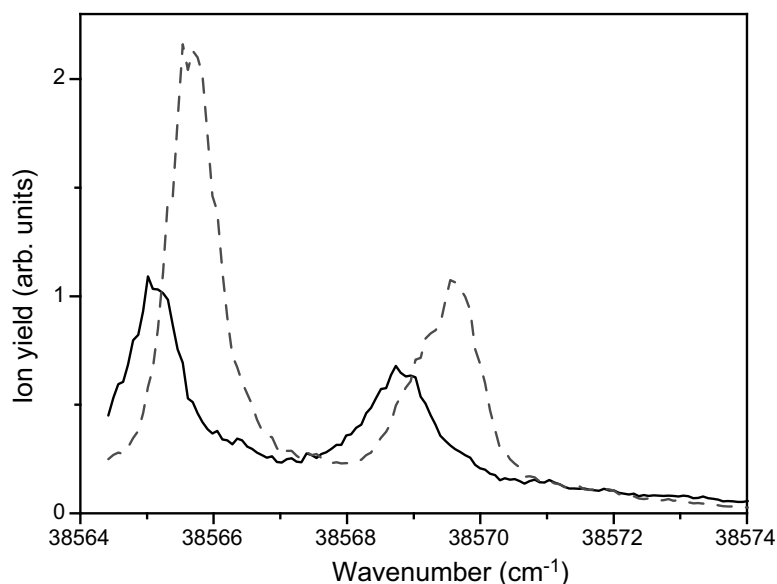


Figure 3.2: Part of the UV spectrum of the benzene dimer showing $(C_6H_6)_2$ (solid line) and $C_6H_6 - C_6D_6$ (dashed line). The UV spectrum is not corrected for UV laser power.

resonances: two near 38565 cm^{-1} for excitation of the C_6H_6 moiety that are split by $\sim 4\text{ cm}^{-1}$ (also shown in Figure 3.2, and two near 38746 cm^{-1} for excitation of C_6D_6 . For the current work, the UV probe laser is tuned to the resonance near 38569 cm^{-1} .

3.3 Results

In the present experiment two isotopic species of the benzene dimer are studied: the fully protonated benzene dimer, $(\text{C}_6\text{H}_6)_2$, (or the *homodimer*) and the mixed dimer, $\text{C}_6\text{H}_6\text{--C}_6\text{D}_6$ (or *heterodimer*). The IR-IDS spectra of both isotopomers of the benzene dimer exhibit sharp resonances with line widths that are determined by the FELIX spectral properties. To be able to directly convert the IR-IDS spectra into IR absorption spectra it is checked for a limited number of resonances that these are the result of a single-photon absorption process. For these resonances this has been verified by measuring the number of detected benzene dimer ions as a function of IR fluence, using a set of fixed-value attenuators. To convert the obtained ion signal into IR absorption intensities the ion signal is normalized to a constant background ion signal to correct for source fluctuations and long-term drifts in the probe laser power. The spectra are corrected for IR laser fluence and are then converted making use of the following formula: $\sigma(\nu) = -\log(s(\nu))$, where $s(\nu)$ is the ion signal as a function of frequency ν and $\sigma(\nu)$ the (relative) IR absorption cross-section. In the following, only the IR absorption spectra obtained this way are presented.

The IR absorption spectrum of the fully protonated benzene dimer is displayed in the top panel of Figure 3.3. The spectrum exhibits one very strong resonance at 674 cm^{-1} and two weaker ones at 1036 cm^{-1} and at 1480 cm^{-1} . The resonance observed at 674 cm^{-1} is so strong that it can still be observed when the FELIX intensity is attenuated by a factor of 100. Consequently, the other resonances are hardly discernible at full-scale, and an enlarged representation with a magnification factor of 60 is shown in the figure. To avoid obscuring the unenlarged spectrum, the strongest mode at 674 cm^{-1} has been omitted from the enlargement. At least 12 clearly discernible resonances can be observed in the experimental spectrum, whose bandwidths are determined by the FELIX spectral profile. The line positions of all observed resonances are given in the figure and can be found in Table 3.2.

To be able to describe the observed IR absorption spectrum and, possibly, to assign it to either the T-shaped or to the parallel-displaced geometry, theoretical calculations are performed on these two structures. For the calculations, geometries for the two structures are taken from Refs. [14, 18]. They are then optimized at the MP2 level of theory, using a 6-311G(d,p) basis set. The parallel-displaced structure is found to be more stable than the T-shaped by $\sim 303\text{ cm}^{-1}$. For the two structures vibrational frequencies are then calculated in the harmonic approximation. The T-shaped structure exhibits low-frequency imaginary frequencies hinting at the presence of a similar structure of lower symmetry that is more stable. Upon submitting a distorted T-shaped structure with C_s symmetry to

Structure	Electronic energy	
	kJ/mole	cm^{-1}
Parallel displaced	0	0
T-shaped	3.6	303
distorted T-shaped	3.3	277

Table 3.1: Relative electronic energies for the various structures of the benzene dimer, calculated at the MP2/6-311G(d,p) level

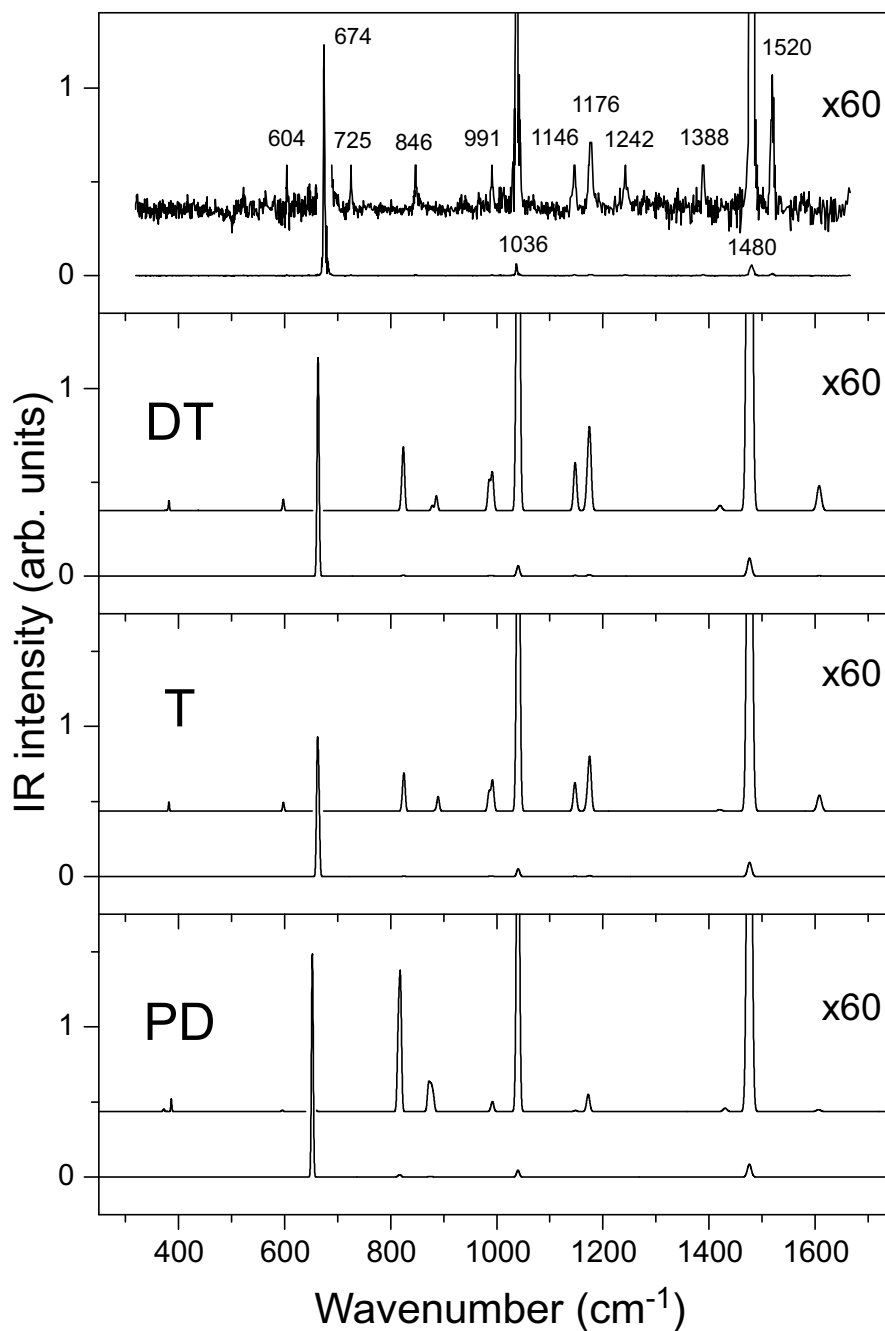


Figure 3.3: Observed IR absorption spectra of the perprotonated benzene dimer (C_6H_6)₂. In the three lower panels, theoretical spectra, calculated at the MP2/6-311G(d,p) level are shown for the distorted T-shaped (second panel, labeled “DT”), the T-shaped (third panel, “T”) and the parallel-displaced (lower panel, “PD”) geometries. The calculated intensities are convoluted with a Gaussian function representing the FELIX spectral profile. Frequencies are scaled by a factor of 0.986.

full geometry optimization at MP2/6-311G(d,p) level a third structure is found to be 0.3 kJ/mole (25 cm^{-1}) more stable than the T-shaped structure. For this geometry the IR fundamental modes are also calculated and no imaginary frequencies are found. All calculations are performed using the

(C ₆ H ₆) ₂		C ₆ H ₆		Assignment
Observed	Theory	Observed	Theory	
604	601	606	601	ν_6
674	667	671	666	ν_{11}
725				
846	829	849	827	ν_{10}
991	997	992	999	ν_1
1036	1047	1037	1047	ν_{18}
1146	1154		1156	ν_{15}
1176	1182	1178	1182	ν_9
1242		1242		$\nu_{10} + \nu_{16}$
1388		1388		$\nu_5 + \nu_{16}$
1480	1484	1485	1487	ν_{19}
1520		1522		$\nu_{10} + \nu_{11}$

Table 3.2: Observed and theoretical values for the IR active modes of the benzene dimer (C₆H₆)₂ (in cm⁻¹). For reference, observed and calculated frequencies for the monomer are also given. The assignments are given in the Wilson notation for the monomer modes.

Gaussian98 package [19].

The resulting theoretical vibrations can best be described by vibrations of the monomer units that are mostly localized in one subunit. The vibrations that are associated with the same modes in different monomers are found at frequencies that are spaced apart by typically less than 1 cm⁻¹, which agrees with previous experimental findings [10]. The bandwidth of FELIX precludes detection of any such small shifts and therefore, in all assignments that are made, modes will be referred to as if they are strictly monomeric vibrations. Furthermore, throughout this chapter, the Wilson notation will be used to identify the vibrations [20].

To compare the obtained theoretical spectra to the experimental spectrum, the IR spectrum of the benzene monomer is also calculated and its theoretical line positions are scaled by a factor of 0.986 to match observed frequencies best [21]. The dimer frequencies are then scaled with the same factor and the stick spectra are convoluted by a Gaussian function representing the FELIX spectral profile. The width of the Gaussian function was chosen to be 0.5 % of the FELIX central frequency. The theoretical spectra are displayed in Figure 3.3 for the distorted T-shaped dimer, the T-shaped dimer and the parallel-displaced dimer in the second, third and lowest panel, respectively. As in the panel with the experimental spectrum, both panels with calculated spectra include a 60x zoom-in of the spectrum. It can immediately be observed that in all theoretical spectra the three strongest resonances that can be discerned are equally well reproduced. This is not too surprising as these are the three IR active modes that are also observed in the benzene monomer, ν_{11} , ν_{18} , and ν_{19} , respectively. The main differences lie in the intensities that are found in the dimer for the modes that are symmetry-forbidden in the monomer. Here one can see that the theoretical spectra of the distorted T-shaped and symmetrical T-shaped geometries match the experimental spectrum much better than that of the parallel displaced geometry. Specifically, five out of the remaining nine observed resonances, observed at 604, 846, 991, 1146 and 1176 cm⁻¹, are predicted with an excellent agreement between experiment and theory for the (distorted) T-shaped geometries. Most experimental resonances can directly be assigned to monomer vibrations, both by their close match to monomer line position, but also from inspection using visualization software of the motions associated with theoretical resonances [22]. The resonance at 604 cm⁻¹ for instance is easily attributed to ν_6 , an in-plane ring deformation mode, and the strongest resonance, at 674 cm⁻¹, can easily be assigned to the ν_{11} benzene umbrella mode. For all experimental resonances, the line positions can be found in Table 3.2, together with theoretical line positions found for the distorted T-shaped geometry and the assigned benzene fundamental modes.

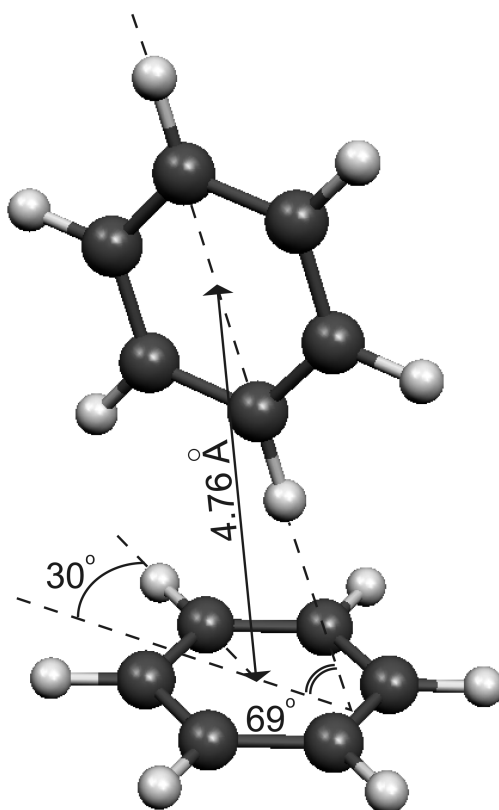


Figure 3.4: Structure of the assigned, distorted T-shaped benzene dimer.

For reference, calculated and observed vibrational modes for the benzene monomer are also included.

Not all observed resonances are predicted by the calculations. The resonances found at 725 cm^{-1} , 1242 cm^{-1} , 1388 cm^{-1} and 1520 cm^{-1} cannot be attributed to benzene fundamental modes. They are therefore most probably the result of combination modes, *i.e.*, two normal modes that are excited simultaneously. The resonance observed at 1520 cm^{-1} , for instance, is most likely a combination mode between the intense ν_{11} mode and the ν_{10} mode, as fundamental modes, both observed in benzene and calculated for the dimer, are too far away. The other two resonances that are assigned to combination bands are found at 1242 cm^{-1} and 1388 cm^{-1} and are attributed to the combination bands $\nu_5 + \nu_{10}$ and $\nu_5 + \nu_{16}$, respectively. All these combination modes have also been observed in the neutral monomer, making their assignment much safer [21]. The resonance at 725 cm^{-1} cannot be assigned to a combination band or to a benzene fundamental mode. The most likely origin of this resonance is a combination of an *intramolecular* vibration, ν_{11} , and an *intermolecular* vibration. Low energy vibrations have been observed for the benzene dimer in Raman experiments around 50 cm^{-1} [11]. The separation between ν_{11} and the combination band of 51 cm^{-1} found here would be in perfect agreement with the earlier observations. It is unclear, however, what the nature of this intermolecular mode is. The present calculations yield intermolecular vibrational frequencies of 9 cm^{-1} , 15 cm^{-1} , 30 cm^{-1} , 66 cm^{-1} , 78 cm^{-1} and 79 cm^{-1} . However, it is not clear whether harmonic frequencies are meaningful for these modes. From parametrized force field calculations Hobza and co-workers predict stretching vibrations at 41 cm^{-1} [14].

The calculated geometry of the distorted T-shaped benzene dimer is depicted in Figure 3.4. The

distance between the centers of mass is ca. 4.76 Å, which agrees fairly well with the experimental value of 4.96 Å[9]. The angle over which the monomer forming the stem of the T is rotated from the symmetric T position is $\sim 21^\circ$. The C–H bond of the stem monomer’s hydrogen atom pointing into the second monomer’s π -cloud is 1.081 Å, only slightly shorter than the bond lengths of the other C–H groups, roughly 1.083 Å. This C–H bond shortening has in a recent paper been labeled ‘anti-hydrogen bond’, a somewhat misleading term, since the shortening is most likely explained by a profitable larger overlap for the π clouds that is achieved by a steric compression of the C–H bond [18]. Unfortunately, the signature of this shortening, a blue-shifted C–H stretching vibration, lies out of the frequency range that is probed in the present experiment.

The spectrum of the isotopically mixed dimer, *i.e.*, the dimer of C_6H_6 and C_6D_6 , is recorded with the UV probe laser tuned to the 38569 cm^{-1} transition that is associated with the excitation of the C_6H_6 moiety. The mixed dimer exhibits an even richer IR absorption spectrum than the perprotonated dimer and it is depicted in Figure 3.5. As in the case of the perprotonated dimer, theoretical spectra for all three calculated geometries for the benzene dimer are displayed below the experimental spectrum. They are scaled with the same factor as for the homodimer, 0.986. For the two T-shaped structures, the spectra are shown for the system in which the cross-bar of the T is deuterated and the stem is protonated. The experimental spectrum is dominated by two resonances at 498 cm^{-1} and at 674 cm^{-1} . A similar enlargement as in Figure 3.3 reveals a wealth of other resonances. One resonance is observed very close to the 674 cm^{-1} resonance and is only seen unobscured in the inset in the experimental spectrum. As in the case of the perprotonated dimer, the assignment of most modes is rather straightforward, and can be done to vibrations that are localized in a single monomer. The strong resonances in the spectrum, found at 674 cm^{-1} , 1037 cm^{-1} , and at 1481 cm^{-1} can again be attributed to dipole allowed fundamental modes in perprotonated benzene. The equivalent fundamental normal modes ν_{11} , ν_{18} , and ν_{19} in perdeuterated benzene are observed at 498 cm^{-1} , 816 cm^{-1} and 1334 cm^{-1} , respectively. Most other resonances can easily be assigned to benzene fundamental modes and all but one resonance observed for the perprotonated dimer are observed here. It is interesting to note that no combination mode is observed where the two component vibrations are localized in different monomer units: the characters of all observed combination modes are either purely C_6H_6 or purely C_6D_6 . The most interesting resonance found in the perprotonated dimer, the suspected combination band of ν_{11} and the intermolecular vibration, observed at 725 cm^{-1} , is not observed. Although one can argue that there is some structure around the same frequency for the isotopically mixed dimer, it is certainly not as prominent as in the perprotonated dimer.

All 22 observed resonances, their assignments and calculated frequencies have been included in Table 3.3. One, albeit weak, resonance at 966 cm^{-1} could unfortunately not be assigned.

All IR absorption spectra for the benzene heterodimer are recorded with the UV probe laser tuned to the high-frequency component of the $\text{S}_16^1 \leftarrow \text{S}_0$ transition doublet at 38569 cm^{-1} . From the calculated spectra it has been inferred that this is a transition associated with a (distorted) T-shaped geometry. It would be of interest to also study the IR absorption properties of the benzene dimer when the UV probe laser is tuned to the low-frequency component. Calculations show that the IR spectra for distorted T-shaped structures are different when the monomer units on different sites are perdeuterated. This is clearly observed in Figure 3.6, where the calculated spectra are shown for the distorted T-shaped structure where either the cross-bar (top trace) or the stem of the T (bottom trace) are deuterated. One can see that several low-intensity modes have substantially different IR intensities when different monomer sites are deuterated. Specifically the absence of the modes around

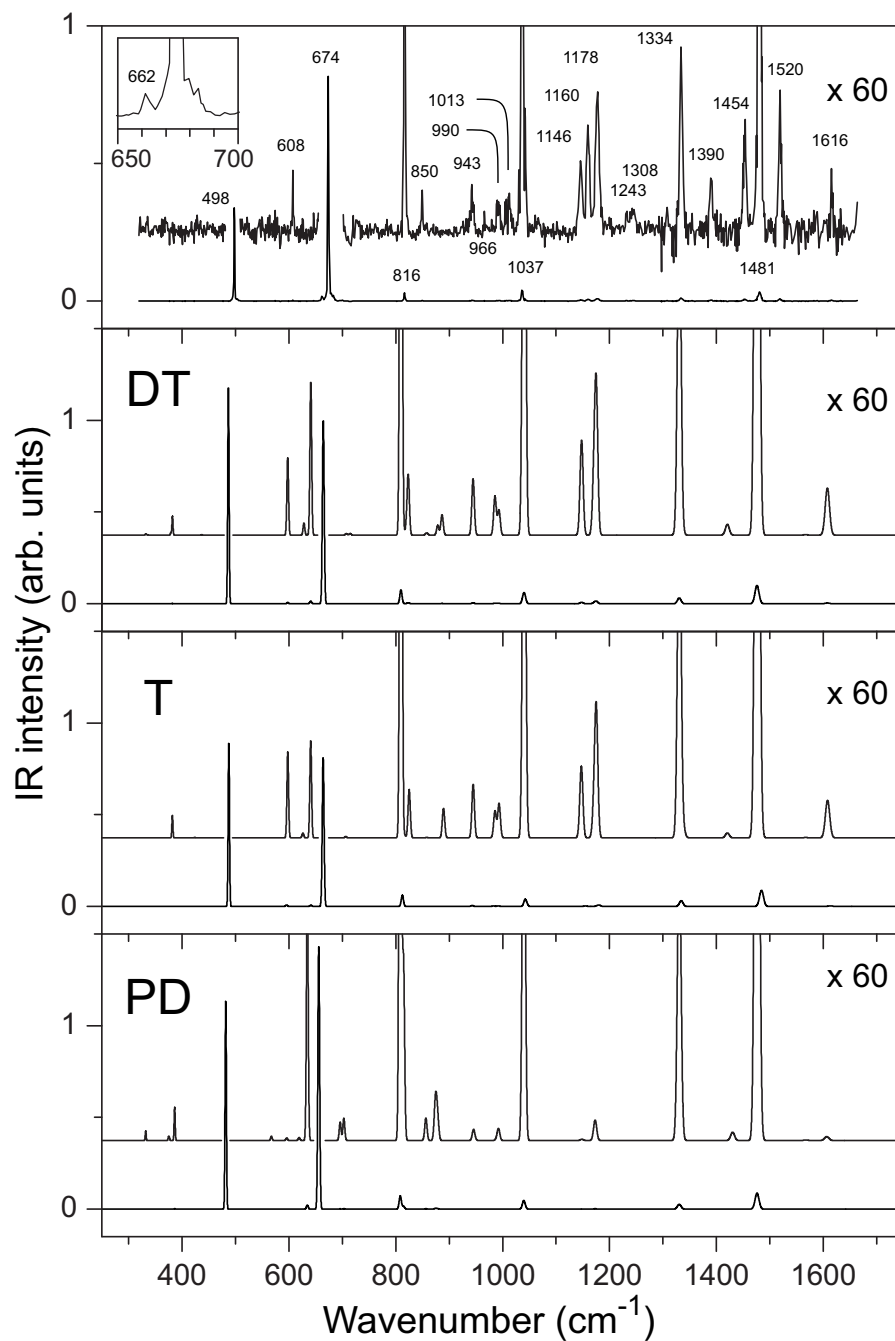


Figure 3.5: Observed IR absorption spectra of the benzene dimer $C_6H_6-C_6D_6$. In the two lower panels, theoretical spectra, calculated at the MP2/6-311G(d,p) level are shown for the distorted T-shaped (second panel), T-shaped (third panel) and the parallel-displaced (lower panel) geometries. For both T-shaped structures the cross-bar of the T is deuterated. The calculated intensities are convoluted with a Gaussian function representing the FELIX spectral profile. Frequencies are scaled by a factor of 0.986.

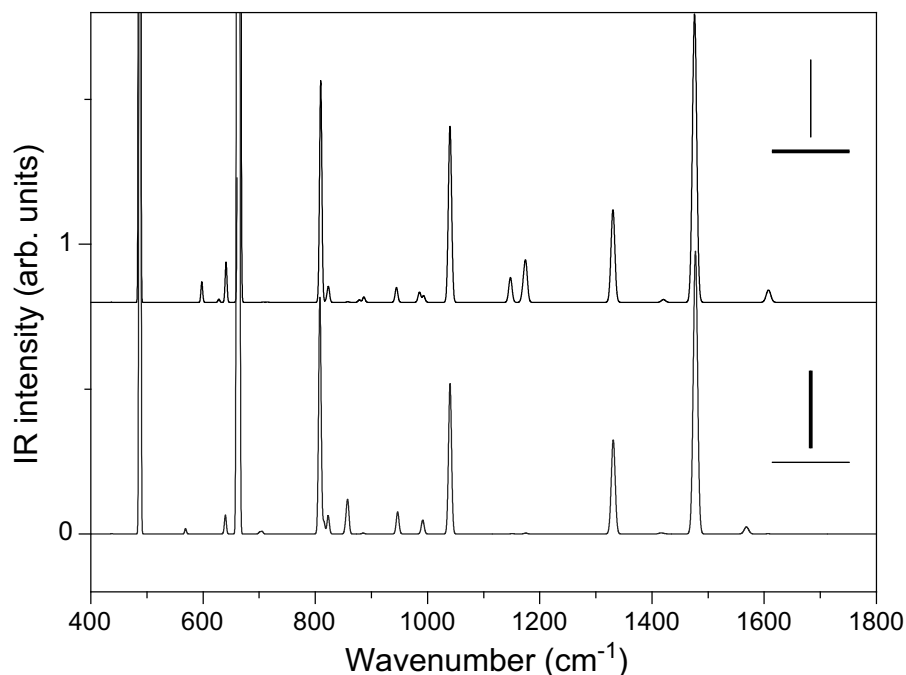


Figure 3.6: *Calculated IR absorption spectra for distorted T-shaped structures that are deuterated in two different sites: in the top spectrum the cross bar of the T is perdeuterated, while in the bottom spectrum the stem of the T is perdeuterated.*

1170 cm^{-1} in the stem-deuterated species suggests that a different spectrum may be obtained when probing the other $S_16^1 \leftarrow S_0$ transition.

The distorted T-shaped structure shown in Figure 3.4 is a very floppy structure. The stem molecule can occupy one of six symmetry equivalent positions above the cross-bar molecule. The barriers separating those minima are expected to be low. There are two principal pathways that connect those minima. One is a precession around the sixfold symmetry axis of the cross-bar molecule. The other one is a pathway that connects two opposite sides via the symmetric transition state. The relative height of this transition state is rather low: the present calculations indicate an energy difference of 25 cm^{-1} between minimum and transition state. Exchange between the minima might be responsible for the observed splitting in the microwave spectra. This data indicates the presence of two exchange pathways, which might be the ones described above. The floppiness of the benzene dimer system is similar to that what has been found earlier for the ammonia dimer: initially several experimental findings seemed to contradict each other but they could be brought into accordance with each other and with theoretical calculations by assuming a very dynamical system [23]. For the benzene dimer the last word, obviously, has not been said and still more theoretical work may be needed. The present observations can then serve as useful additional experimental information for further theoretical calculations.

3.4 Conclusions

For the fully protonated benzene dimer and for a dimer of one fully protonated and one fully deuterated benzene the IR absorption spectra have been measured in the range of 400 cm^{-1} to 1700 cm^{-1} .

$C_6H_6-C_6D_6$		C_6H_6, C_6D_6		Assignment
Observed	Theory	Observed	Theory	
498	490	503	489	D6- ν_{11}
608	601	606	601	H6- ν_6
662	645	661	644	D6- ν_{10}
674	668	671	666	H6- ν_{11}
816	814	813	814	D6- ν_{18}
850	828	849	827	H6- ν_{10}
943	950	945	952	D6- ν_1
966				
990	999	991	999	H6- ν_1
1013			993	H6- ν_{12} [†]
1037	1046	1037	1047	H6- ν_{18}
1146	1154		1156	H6- ν_{15}
1160				D6- $\nu_{10} + \nu_{11}$
1178	1182	1178	1182	H6- ν_9
1243		1240		H6- $\nu_{10} + \nu_{16}$
1308				D6- $\nu_{11} + \nu_{18}$
1334	1338	1333	1340	D6- ν_{19}
1390		1388		H6- $\nu_5 + \nu_{16}$
1454		1450		D6- $\nu_1 + \nu_{11}$
1481	1485	1485	1487	H6- ν_{19}
1520		1522		H6- $\nu_{10} + \nu_{11}$
1616		1616		D6- $\nu_6 + \nu_{17}$

Table 3.3: Observed and theoretical values for the IR active modes of the benzene dimer, $C_6H_6-C_6D_6$ (in cm^{-1}). For reference observed and calculated frequencies for the benzene monomer are included. The mode indicated with [†] could alternatively be assigned to the resonance at 966 cm^{-1} .

The spectra exhibit a rich vibrational structure that can easily be assigned to benzene monomer modes. Ab-initio calculations confirm that most vibrational modes are localized to the individual monomer units. Upon comparison of the experimental spectra with calculated spectra for three different geometries it is concluded that the IR spectrum resembles that of a T-shaped geometry. The lowest energy structure found is a distorted T shaped geometry and its IR absorption spectrum matches the present observations well. For the fully protonated benzene dimer one intermolecular vibration is observed in the form of a combination band with the strong IR fundamental mode ν_{11} . The associated frequency of the intermolecular vibration was found to be 51 cm^{-1} , in close agreement with earlier observations [11].

References

- [1] K. C. Janda, J. C. Hemminger, J. S. Winn, S. E. Novick, S. J. Harris, and W. Klemperer, *J. Chem. Phys.* **63**, 1419 (1975).
- [2] J. Hopkins, D. Powers, and R. Smalley, *J. Phys. Chem.* **85**, 3739 (1981).
- [3] P. R. Langridge-Smith, D. V. Brumbaugh, C. A. Haynam, and D. H. Levy, *J. Phys. Chem.* **85**, 3742 (1981).
- [4] K. Fung, H. L. Selzle, and E. W. Schlag, *J. Phys. Chem.* **87**, 5113 (1983).
- [5] K. Börnsen, H. L. Selzle, and E. W. Schlag, *J. Chem. Phys.* **85**, 1726 (1986).
- [6] K. Börnsen, H. L. Selzle, and E. W. Schlag, *Z. Naturforsch.* **39a**, 1255 (1984).
- [7] O. Krätzschar, H. L. Selzle, and E. W. Schlag, *J. Phys. Chem.* **98**, 3501 (1994).
- [8] K. Law, M. Schauer, and E. Bernstein, *J. Chem. Phys.* **81**, 4871 (1984).
- [9] E. Arunan and H. Gutowsky, *J. Chem. Phys.* **98**, 4294 (1993).
- [10] B. F. Henson, G. V. Hartland, V. A. Ventura, and P. M. Felker, *J. Chem. Phys.* **97**, 2189 (1992).
- [11] V. Ventura and P. Felker, *J. Chem. Phys.* **99**, 748 (1993).
- [12] S. Tsuzuki, T. Uchimaru, K. Matsumura, and M. Mikami, *Chem. Phys. Lett.* **319**, 547 (2000).
- [13] P. Hobza, H. L. Selzle, and E. W. Schlag, *J. Phys. Chem.* **100**, 18790 (1996).
- [14] V. Špirko, O. Engkvist, P. Soldán, H. L. Selzle, E. W. Schlag, and P. Hobza, *J. Chem. Phys.* **111**, 572 (1999).
- [15] C. Gonzalez, T. C. Allison, and E. C. Lim, *J. Phys. Chem. A* **104**, 2953 (2000).
- [16] C. Gonzalez, T. C. Allison, and E. C. Lim, *J. Phys. Chem. A* **105**, 10583 (2001).
- [17] E. Cox, D. Cruickshank, and J. Smith, *Proc. Royal Soc. London A* **247**, 1 (1958).
- [18] P. Hobza, V. Špirko, H. L. Selzle, and E. W. Schlag, *J. Phys. Chem. A* **102**, 2501 (1998).
- [19] M. J. Frisch, G. W. Trucks, H. B. Schlegel, G. E. Scuseria, M. A. Robb, J. R. Cheeseman, V. G. Zakrzewski, J. J. A. Montgomery, R. E. Stratmann, J. C. Burant, et al., *Gaussian 98, Revision A.7*, Pittsburgh, PA (1998).
- [20] E. B. Wilson, Jr., *Phys. Rev.* **45**, 706 (1934).
- [21] G. Di Lonardo, L. Fusina, G. Masciarelli, and F. Tullini, *Spectrochim. Acta, Part A* **55**, 1535 (1999), and references therein.
- [22] J.-R. Hill, *Program Viewmol, version 2.4* (2003).
- [23] G. Cotti, H. Linnartz, W. L. Meerts, A. van der Avoird, and E. H. T. Olthof, *J. Chem. Phys.* **104**, 3898 (1996).

CHAPTER 4

THE IR ABSORPTION SPECTRUM OF THE GAS PHASE NEUTRAL BENZOIC ACID MONOMER AND DIMER

The infrared (IR) absorption spectrum of the jet-cooled benzoic acid monomer and dimer have been recorded throughout the 500–1900 cm⁻¹ range via ion-dip spectroscopy. Both spectra show a wealth of vibrational modes and the monomer spectrum is remarkably different from that of the dimer. Density functional theory calculations show quantitative agreement with the experimental data. The C–O–H out-of-plane bending vibration in the dimer is poorly reproduced in the theoretical calculations and a more accurate description of the doubly hydrogen bonded structure is therefore still needed.

4.1 Introduction

Over the last decade a substantial number of experiments have been performed to investigate the structure of isolated molecules of biological interest. These studies include the pioneering spectroscopic work of the Levy and Simons groups on, among others, amino acids in the gas phase [1–4] and of De Vries on gas phase nucleobases [5]. Although these studies are highly relevant, they only address isolated molecules. In nature, most biologically relevant molecules are attached to other species by hydrogen and/or Van der Waals bonding. The most notable example of this is the double stranded helix of DNA. This structure is bonded through numerous hydrogen bonds and it is of interest to study the effects of bonding on the structure of individual sub-units. It has been concluded that bonding solely by dispersive forces can result in almost no structural changes to the different constituents [6]. For hydrogen bonded molecular systems, however, the structure of the individual monomer units might be significantly altered.

Studies involving (doubly) hydrogen bonded systems include investigations of the pairing configurations of nucleic acid base pairs [7–10], of their analogues [11–14], small acid dimer systems [15–18] and hydrated amino-acids and their analogues [19–23].

Some of these involve IR spectroscopy in the spectral region where the X–H (X=C,O,N,...) stretching fundamentals are found. A remarkable observation is the, commonly found, broad, structured absorption around 3000 cm^{-1} , which is attributed to strong mixing between the X–H stretching fundamental and bending overtone modes [11, 15, 16]. Finally, Gerhards *et al.* probed the C=O stretching vibrations of a protected amino acid dimer system [24].

To study other vibrational modes a tunable source of IR radiation that allows one to probe the lower vibrational energy region is required. Here, the IR absorption spectroscopy of the smallest aromatic acid, benzoic acid (BA), and its dimer are presented using FELIX as an IR source. The BA dimer is doubly hydrogen bonded through the carboxylic acid group; it has a double minimum potential in the O–H stretching coordinate in which the hydrogen atoms of the OH group can switch synchronously between monomer units. Its high symmetry makes the BA dimer a very interesting system that can serve as a prototype for doubly hydrogen bonding, and it has been studied quite extensively using various techniques [25–28]. From a direct measurement of the IR spectra, one can conclude on possible changes in the vibrational structure upon dimerization of individual BA monomer units. In an earlier study, Stepanian *et al.* recorded the matrix isolation spectrum of BA and found substantial differences between the IR spectra of the monomer and dimer [29]. It is unclear, however, what the influence of the argon matrix is in such studies and gas phase experiments are highly desirable.

4.2 Experiment

A sample of benzoic acid is heated to a temperature of $75\text{ }^{\circ}\text{C}$ and seeded into argon (stagnation pressure approx. 1 bar). This mixture is then expanded through a 0.5 mm diameter nozzle into vacuum. In the adiabatic expansion the internal degrees of freedom in the molecules are cooled and rotational temperatures of about 5 K are reached. The expansion conditions enable the formation of benzoic acid dimer clusters, which are internally cooled as well.

For the measurement of the IR absorption spectra of the jet-cooled neutral benzoic acid monomer and dimer, IR ion-dip spectroscopy (IR-IDS) is employed. Ions are produced from ground state mo-

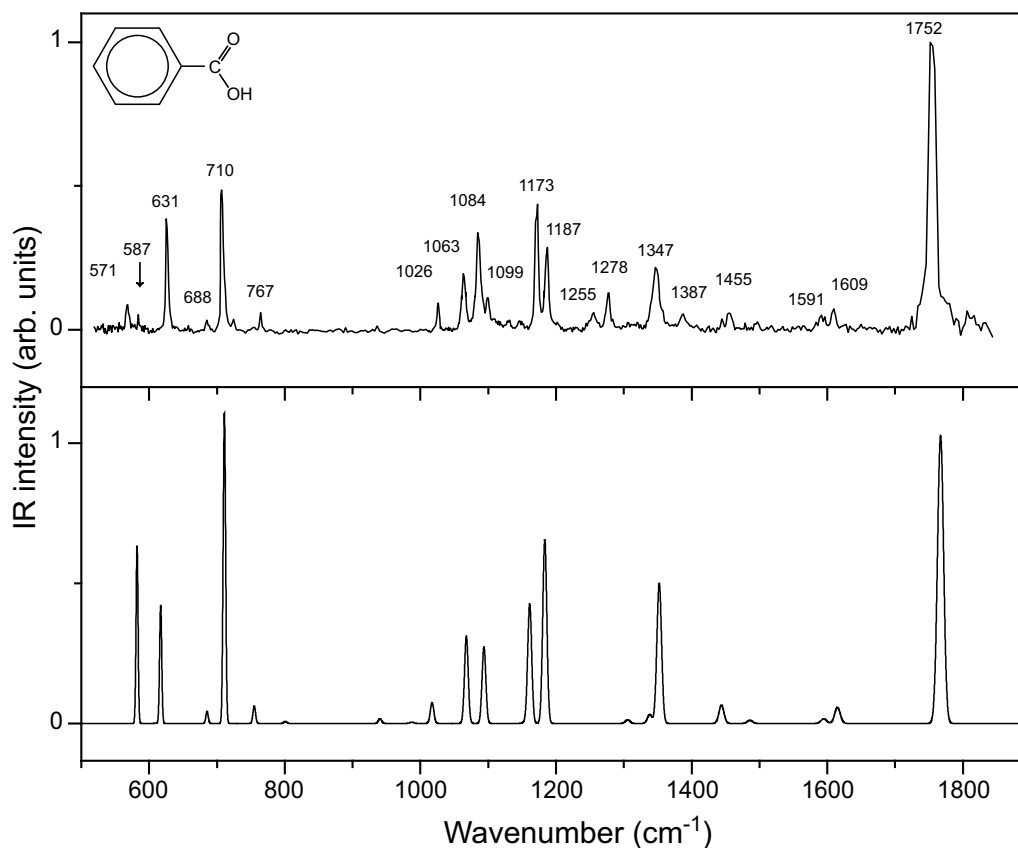


Figure 4.1: Observed IR absorption spectrum of the benzoic acid monomer, compared to the calculated IR spectrum (lower curve). Theoretical frequencies are scaled by a factor 0.98.

lecules using a two-color ionization scheme. For this, the molecules are first excited to the vibrational ground state in the first electronically excited singlet state S_1 using a frequency doubled dye laser (Rhodamine 6G). The molecules are then ionized by the light from an ArF excimer laser (193 nm).

For the monomer, the transition to the S_1 state has been reported at 35955 cm^{-1} . The BA monomer undergoes a fast intersystem crossing from the S_1 state into the lowest electronically excited triplet state, T_1 , a process that takes place on a sub-ps timescale [27]. The lifetime of the triplet state is rather long, presumably many μs . The ArF laser is fired some 100 ns after the excitation laser and thus ionizes all molecules from T_1 . For the benzoic acid dimer, the $S_1 \leftarrow S_0$ transition is red-shifted by 200 cm^{-1} . Interestingly, the benzoic acid dimer does therefore not exhibit the fast intersystem crossing to the triplet state that is so characteristic for the monomer and the benzoic acid dimers can be directly ionized out of the S_1 state. As the lifetime of the S_1 state of the BA dimer is only 9 ns, the ionizing laser is now fired almost simultaneously with the excitation laser.

4.3 Results

4.3.1 The benzoic acid monomer

In Figure 4.1 the IR absorption spectrum of the BA monomer is shown. To obtain this from the ion-dip spectrum, the ion signal is corrected for source and UV laser fluctuations to get a (nearly) constant

Observed	Theory Freq.	Intens.	Ref. [29]	Mode description
571	583	71	568	out-of-plane C–O–H bend
587				
631	617	50	628	in-plane ring C–C–C bend
688	685	6	687	out-of-plane ring C–C–H bend
710	711	152	711	out-of-plane ring C–C–H bend (umbrella)
767	755	9	767	in-plane C–O–H bend, ring deformation
1026	1018	15	1027	in-plane ring C–C–H bend
1063	1068	63	1066	in-plane ring C–C–H bend
1084	1094	60	1086	in-plane ring C–C–H bend
1099			1100	
1173	1162	94	1169	C–C–H bend, C–O–H bend, both in-plane
1187	1183	147	1185	C–C–H bend, C–O–H bend, both in-plane
1255			1251	
1278			1275	
1347	1353	131	1347	C–C–H bend, C–O–H bend, both in-plane
1387			1383	
1455	1444	18	1456	C–C stretch, ring deformation
1591	1595	5	1590	C–C stretch, ring deformation
1609	1615	18	1606	C–C stretch, ring deformation
1752	1767	350	1752	C=O stretch, C–O–H bend

Table 4.1: Observed and theoretical frequencies (in cm^{-1}) and theoretical intensities (in km/mole) for the IR active modes of the benzoic acid monomer. Frequencies of modes observed and attributed to the benzoic acid monomer from matrix isolation studies (Ref. [29]) are listed as well.

baseline ion signal, and subsequently the natural logarithm from these data is taken, and normalized to the (relative) FELIX fluence. The observed frequencies of a total of twenty spectral lines are indicated in the figure and are also listed in Table 4.1. The absolute frequency accuracy is about 3 cm^{-1} at the low frequency end of the spectrum, gradually deteriorating to 12 cm^{-1} at the high frequency end. The line width observed in the spectrum is almost exclusively determined by the bandwidth of the laser, and is some 0.5 % of the FELIX frequency.

In the lower part of Figure 4.1 a calculated IR spectrum is shown. Frequencies and intensities of IR active modes are determined from density functional calculations using the B3LYP functional with Dunning’s D95(d,p) basis set, as implemented in Gaussian 98 [30]. The frequencies in the calculated spectra are scaled by a factor of 0.98 to show best agreement with experimental data. Frequencies and intensities are then convoluted with a Gaussian function representing the FELIX spectral profile, where a bandwidth of 0.5 % of the FELIX central frequency is used. The calculated vibrational modes are inspected using visualization software. Both (scaled) theoretical line positions and a short description (where possible) of the fundamental IR active vibrations are given in Table 4.1.

The theoretical and experimental spectra agree very well, both in line positions and intensities. The dominant mode in both spectra is the one experimentally found at 1752 cm^{-1} which is readily assigned to the C=O stretching vibration. Most of the other resonances are also unambiguously assigned to fundamental vibrations. There are still two spectral regions where the agreement between theory and experiment is less than perfect. The first region is that between 550 and 650 cm^{-1} , where three distinct resonances are found whereas only two fundamentals are expected. It is interesting to note that the two strongest observed modes have line positions that are considerably further apart than predicted. Such behavior could be the signature of a Fermi resonance, however, the two strong theoretical modes are of different symmetry, which rules out a Fermi coupling between the two of them [31]. The weak but clearly observable resonance at 587 cm^{-1} could nevertheless still be the

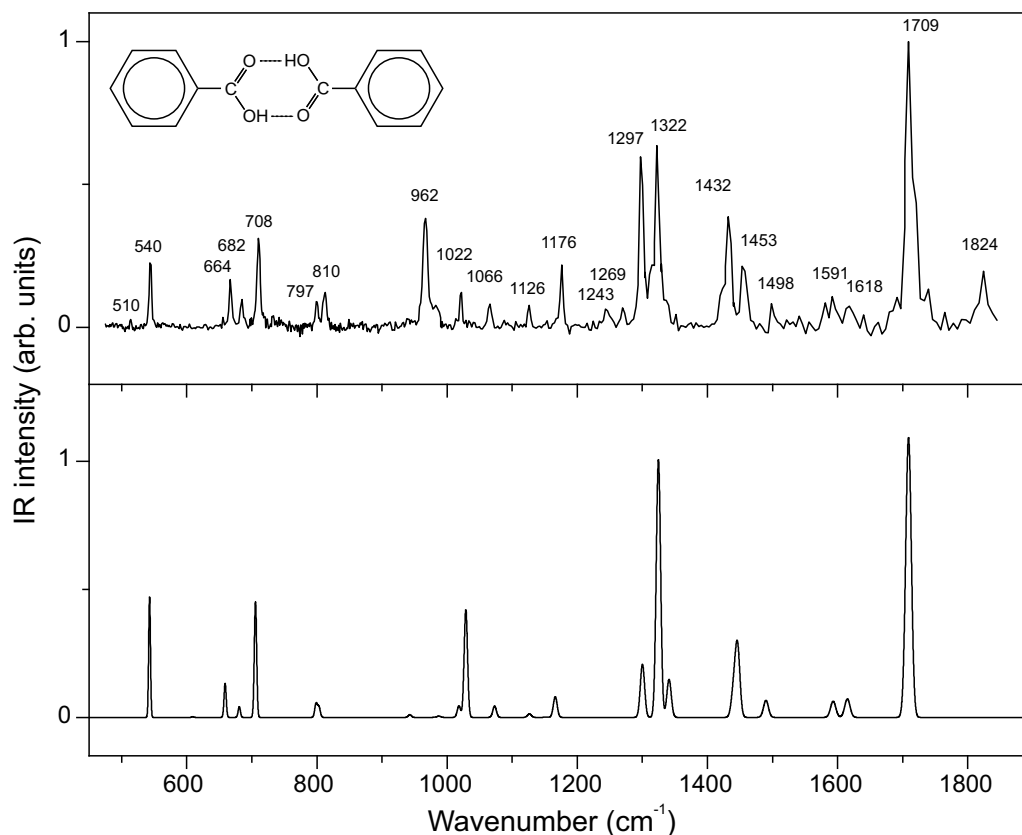


Figure 4.2: Observed IR absorption spectrum of the benzoic acid dimer, together with the calculated IR spectrum (lower curve). Theoretical frequencies are scaled by a factor 0.98.

result of a Fermi resonance with one of the fundamentals. A possible set of fundamentals that may combine to serve as a partner in the Fermi interaction are calculated fundamentals at 157 and 424 cm^{-1} . The second discrepancy between theory and experiment is found between 1200 and 1300 cm^{-1} . As no fundamentals are expected in this region it is very likely that the resonances observed here are combination modes. A possible assignment for the resonance at 1278 cm^{-1} is the combination between the fundamental at 710 cm^{-1} and one of the modes participating in the (possible) Fermi resonance around 600 cm^{-1} . For the resonance at 1255 cm^{-1} various combinations between strong IR active modes and calculated low-lying vibrations could be responsible. As the latter have never been observed, a definite assignment is not possible.

It is noted that most resonances that are found in this work, have been identified by Stepanian *et al.* in a matrix isolation (MI) spectroscopy experiment as well [29]. The MI intensities differ somewhat from the present data, but in general good agreement is found. For completeness, the values determined via MI spectroscopy have been included in Table 4.1.

4.3.2 The benzoic acid dimer

In Figure 4.2 the IR absorption spectrum of the BA dimer is displayed. It is clear from looking at the experimental data that the signal-to-noise ratio for the dimer spectrum is somewhat worse than for the monomer spectrum, which is solely due to the lower abundance of the dimer in the

beam ($\sim 10\%$ relative to the monomer abundance). Below the experimental data, the corresponding theoretical spectrum is shown. The line positions are scaled with the scaling factor that gave the best match between theoretical and experimental spectra for the monomer, *i.e.*, a factor of 0.98. Like for the monomer, calculated frequencies and intensities are then convoluted with a Gaussian function representing the FELIX spectral profile.

The agreement between experimental and theoretical spectra is rather good. From a visual inspection of the modes, it is clear that most vibrations in the dimer are best described as either a symmetric or an anti-symmetric combination of two monomer vibrations. Of these, only the latter have any significant IR intensity. As in the IR absorption spectrum of the BA monomer, most resonances are readily assigned to fundamental vibrations. The spectrum is dominated by a strong mode at 1709 cm^{-1} which very well matches the theoretical calculations, and which is assigned to the asymmetric C=O stretching vibration. Here, it is interesting to note that Gerhards *et al.* observed a considerably smaller shift of a C=O stretching vibration frequency upon dimerization, in an experiment involving a protected amino acid dimer system [24]. In the low energy region the agreement between theory and experiment is striking: with a single exception – the resonance at 962 cm^{-1} – all resonances between 500 and 1200 cm^{-1} are very well predicted, both in line positions and intensities. At higher energies, in the region between 1200 and 1700 cm^{-1} , line positions still match quite well, but intensities seem somewhat off. In the whole spectrum, two modes show clear discrepancies. One of these is the fairly strong resonance at 962 cm^{-1} . It seems quite likely that this resonance has to be assigned to the strong mode in the theoretical spectrum at 1028 cm^{-1} . This mode is the asymmetric out-of-plane bending vibration of the O–H groups. The hydrogen atoms are directly involved in the double hydrogen bond, and this thus forms a test for the description of out-of-plane vibrations hindered by a hydrogen bond.

The mismatch between theory and experiment could result from either a deficient theoretical description of the interaction or from a breakdown in the harmonic approach to calculate the vibrational frequency. To check the last hypothesis the potential energy surface was evaluated along the normal coordinate involved in the out-of-plane bending vibration*. Over a range between -0.5 \AA and $+0.5\text{ \AA}$ (total displacement) single-point energies are calculated every 0.01 \AA . In Figure 4.3, this intersection of the potential energy surface is shown where the calculated values are depicted with solid circles. In the inset, a close-up is shown of the equilibrium position of the molecule. Included in the graphs are two fits of quadratic functions to calculated values: the first fit takes into account all calculated values (dashed line), whereas the second only takes into account the calculated values in the range of -0.1 \AA and 0.1 \AA (solid line). It can be observed in the inset that the full-range fit deviates slightly from the calculated values in the equilibrium region, where the calculated potential is somewhat shallower. Also note the slightly higher energy ($< 1\text{ cm}^{-1}$) for the equilibrium position, an offset which is well within the error margins for DFT calculations. For both fitted quadratic functions the vibrational eigenstates are analytically evaluated using the harmonic formula $\omega = \sqrt{k/\mu}$ where k is the force constant from the potential function $V(x) = \frac{1}{2}kx^2$, and μ the reduced mass of the atoms involved in the normal mode. For the full-range fit a (scaled) vibrational energy of 1117 cm^{-1} is found, and for the equilibrium position range fit a value of 1024 cm^{-1} . The latter value is rather close to the (scaled) value of 1028 cm^{-1} found in the initial frequency calculation, for which only the second derivative of the potential energy in the equilibrium position is evaluated. Since the potential is

*A word of care is in its place right here as the evaluation of the potential here is *stricto sensu* not correct: The potential is evaluated along a Cartesian vector describing the normal mode. A more rigorous test can be done when the actual internal coordinate is scanned. The evaluation along the Cartesian vector is expected to yield a good indication of the shape of the potential, though.

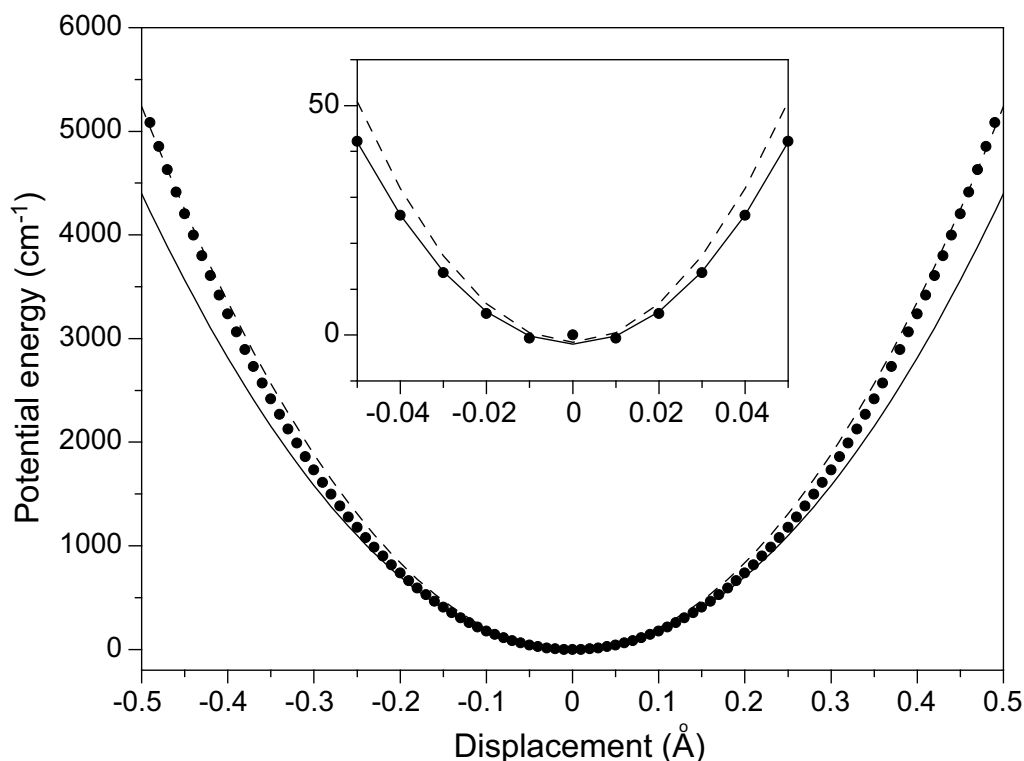


Figure 4.3: Intersection of the potential energy surface of the benzoic acid dimer along the asymmetric out-of-plane C–O–H bending mode coordinate. Calculated single-point energies (solid circles) are fitted to a quadratic function taking into account the full displacement range (dashed line) and the range between -0.1 Å and 0.1 Å. The inset is a close-up of the equilibrium region. In the inset the full-range fit is shifted vertically to fall within the vertical limits.

rather shallow in this point, the full-range fit value is blue-shifted from both, which is the contrary to the experimental finding. From this it seems most likely that the mismatch between experimental and calculated values is not due to the harmonic approximation to evaluate vibrational frequencies, but from an imperfect description of the hydrogen bonding in the theoretical method used. Therefore, it would be desirable for the theoretical model to be refined if one wants to reproduce hydrogen bonding interactions correctly.

The second discrepancy between theoretical and experimental spectra in Figure 4.2 lies in the resonance observed at 1824 cm^{-1} . This resonance might result from a combination band of the C=O stretching vibration at 1709 cm^{-1} with a low frequency intermolecular stretching vibration, e.g. the one predicted at 120 cm^{-1} . Another possibility is that this resonance is due to the overtone mode of the C–O–H out-of-plane bending vibration. The associated anharmonicity deduced then for this mode of $2 \times 962 - 1824 = 100\text{ cm}^{-1}$ is quite reasonable.

One can compare the here presented data to the ones obtained by Stepanian *et al.* in absorption spectroscopy of matrix-isolated BA [29]. In general, good agreement is found although more lines are found and unambiguously identified in the present study than in the MI experiment. In cases where BA monomer and BA dimer vibrational modes overlap, the dimer modes often escape observation in the MI experiments. This is avoided in the present mass-selective gas-phase technique. The observed line positions are tabulated in Table 4.2 and a description of the modes is given. The MI data of

Observed	Theory Freq.	Intens.	Ref. [29]	Mode description
510				
540	543	130	547	acid groups asymmetric rocking
664	659	45	670	acid groups asymmetric scissor
682	681	15		out-of-plane ring C–C–H bend
708	706	163		out-of-plane ring C–C–H bend
797	799	22		acid groups scissor, ring deformation
810	803	17		out-of-plane ring C–C–H bend
962	1028	221	960	out-of-plane acid group C–O–H bend
1022	1018	24		in-plane ring C–C–H bend
1066	1073	24		in-plane ring C–C–H bend
1126	1126	8		in-plane ring C–C–H bend
1176	1166	48		in-plane ring C–C–H bend
1243				
1269				
1297	1300	140	1297	C–C–H bend, C–O–H bend, both in-plane
1322	1324	687	1322	C–C–H bend, C–O–H bend, both in-plane
1432	1440	76	1430	C–C–H bend, C–O–H bend, both in-plane
1453	1446	199		C–C–H bend, C–O–H bend, both in-plane
1498	1490	50		C–C–H bend, C–O–H bend, both in-plane
1591	1593	51		C–C stretch, ring deformation
1618	1615	60		C–C stretch, ring deformation
1709	1710	956	1699	C=O stretch, in-plane C–O–H bend
1824				

Table 4.2: Observed and theoretical frequencies (in cm^{-1}) and theoretical intensities (in km/mole) for the IR active modes of the benzoic acid dimer. Frequencies of modes observed and attributed to the benzoic acid dimer from matrix isolation studies (Ref. [29]) are listed as well.

Stepanian *et al.* are added for completeness [29].

4.4 Conclusions

The IR absorption spectra of the jet-cooled benzoic acid monomer and dimer have been recorded in the $500\text{--}1900\text{ cm}^{-1}$ region. Due to the mass-selected detection scheme, one can directly compare the vibrational structure of the monomer to that of the dimer, and it is seen that dimerization leads to a dramatic change in the vibrational structure. The theoretical methods used to calculate the IR absorption spectrum proved to be very accurate in this mid-IR spectral region, in contrast to earlier studies in the O–H stretching region. The fact that theoretical calculations clearly fail in the prediction of hydrogen bond affected vibrations, in this study demonstrated for the O–H out-of-plane bending vibration in the dimer, leads to conclude that some fine-tuning in the methods to describe hydrogen-bonded systems is imperative.

References

- [1] T. R. Rizzo, Y. D. Park, L. A. Peteanu, and D. H. Levy, *J. Chem. Phys.* **84**, 2534 (1986).
- [2] T. R. Rizzo, Y. D. Park, and D. H. Levy, *J. Chem. Phys.* **85**, 6945 (1986).
- [3] L. C. Snoek, E. G. Robertson, R. T. Kroemer, and J. P. Simons, *Chem. Phys. Lett.* **321**, 49 (2000).
- [4] L. C. Snoek, R. T. Kroemer, M. Hockridge, and J. P. Simons, *Phys. Chem. Chem. Phys.* **3**, 1819 (2001).
- [5] E. Nir, L. Grace, B. Brauer, and M. S. de Vries, *J. Am. Chem. Soc.* **121**, 4896 (1999).
- [6] B. F. Henson, G. V. Hartland, V. A. Venturo, and P. M. Felker, *J. Chem. Phys.* **97**, 2189 (1992).
- [7] E. Nir, K. Kleinermmanns, and M. S. de Vries, *Nature (London)* **408**, 949 (2000).
- [8] E. Nir, C. Janzen, P. Imhof, K. Kleinermmanns, and M. S. de Vries, *Phys. Chem. Chem. Phys.* **4**, 740 (2002).
- [9] E. Nir, C. Janzen, P. Imhof, K. Kleinermmanns, and M. S. de Vries, *Phys. Chem. Chem. Phys.* **4**, 732 (2002).
- [10] C. Plützer, I. Hüning, and K. Kleinermmanns, *Phys. Chem. Chem. Phys.* **5**, 1158 (2003).
- [11] Y. Matsuda, T. Ebata, and N. Mikami, *J. Chem. Phys.* **110**, 8397 (1999).
- [12] A. Müller, F. Talbot, and S. Leutwyler, *J. Chem. Phys.* **112**, 3717 (2000).
- [13] A. Müller, F. Talbot, and S. Leutwyler, *J. Chem. Phys.* **115**, 5192 (2001).
- [14] A. Müller, F. Talbot, and S. Leutwyler, *J. Am. Chem. Soc.* **124**, 14486 (2002).
- [15] G. M. Florio, E. L. Sibert, and T. S. Zwier, *Faraday Discuss.* **118**, 315 (2001).
- [16] T. Yahagi, A. Fujii, T. Ebata, and N. Mikami, *J. Phys. Chem. A* **105**, 10673 (2001).
- [17] F. Madeja and M. Havenith, *J. Chem. Phys.* **117**, 7162 (2002).
- [18] C. A. Southern, D. H. Levy, G. M. Florio, A. Longarte, and T. S. Zwier, *J. Phys. Chem. A* **107**, 4032 (2003).
- [19] J. A. Dickinson, P. W. Joireman, R. W. Randall, E. G. Robertson, and J. P. Simons, *J. Phys. Chem. A* **101**, 513 (1997).
- [20] J. A. Dickinson, M. R. Hockridge, E. G. Robertson, and J. P. Simons, *J. Phys. Chem. A* **103**, 6938 (1999).
- [21] E. G. Robertson, *Chem. Phys. Lett.* **325**, 299 (2000).
- [22] E. G. Robertson, M. R. Hockridge, P. D. Jelfs, and J. P. Simons, *Phys. Chem. Chem. Phys.* **3**, 786 (2001).
- [23] M. Mons, I. Dimicoli, B. Tardivel, F. Piuuzzi, E. G. Robertson, and J. P. Simons, *J. Phys. Chem. A* **105**, 969 (2001).
- [24] M. Gerhards, C. Unterberg, and A. Gerlach, *Phys. Chem. Chem. Phys.* **4**, 5563 (2002).

- [25] D. E. Poeltl and J. K. McVey, J. Chem. Phys. **78**, 4349 (1983).
- [26] S. Kamei, H. Abe, N. Mikami, and M. Ito, J. Phys. Chem. **89**, 3636 (1985).
- [27] G. Meijer, M. S. de Vries, H. E. Hunziker, and H. R. Wendt, J. Phys. Chem. **94**, 4394 (1990).
- [28] K. Remmers, W. L. Meerts, and I. Ozier, J. Chem. Phys. **112**, 10890 (2000).
- [29] S. Stepanian, I. Reva, E. Radchenko, and G. Sheina, Vib. Spectrosc. **11**, 123 (1996).
- [30] M. J. Frisch, G. W. Trucks, H. B. Schlegel, G. E. Scuseria, M. A. Robb, J. R. Cheeseman, V. G. Zakrzewski, J. J. A. Montgomery, R. E. Stratmann, J. C. Burant, et al., *Gaussian 98, Revision A.7*, Pittsburgh, PA (1998).
- [31] G. Herzberg, *Molecular Spectra and Molecular Structure* (Krieger Publishing company, Malabar, FLA, 1991), 2nd ed.

CHAPTER 5

FINGERPRINT IR SPECTROSCOPY TO PROBE AMINO ACID CONFORMATIONS IN THE GAS PHASE

The infrared (IR) absorption spectra of different conformational isomers of gas phase amino acid molecules are measured in the molecular fingerprint region of 330–1500 cm⁻¹. The IR absorption spectra for three conformers of the amino acid tryptophan show absorption bands that uniquely identify the conformational structure of the molecule and that are well matched by Density Functional Theory (DFT) calculations. The present observations hold great promise for future identification of conformational folding of larger molecules by means of their IR absorption characteristics.

5.1 Introduction

Over the last twenty years sophisticated techniques have been developed to bring intact large biomolecules into the gas phase. The techniques most widely used today are Matrix-Assisted Laser Desorption Ionization (MALDI) [1] and ElectroSpray Ionization (ESI) [2]. Due to their ability to provide mass and sequence information of biological samples, both techniques have revolutionized analytical biochemistry. However, inferring structural information on gas phase ions and molecules is often a difficult task. The knowledge of the gas phase structure can provide important insight into fundamental intramolecular interactions and can serve as calibration point for theoretical models. While elaborate tools for solid and liquid samples exist, most of them cannot be applied to gas phase samples. One of the few techniques that can provide direct structural information on gas phase species is ion mobility, in which large ionized molecules are mass-selected and pass through a drift cell filled with a buffer gas [3, 4]. The molecular ions will arrive at the end of the drift cell after a period of time which depends on their collisional cross-section. Information can also be obtained using spectroscopic methods, either in the Ultraviolet (UV) [5] or in the Infrared (IR)[6, 7]. Especially the IR absorption spectrum is a unique identifier for the structure: line intensities and frequencies give direct information on the forces that hold the molecule together. Additional information can be obtained by the direct measurement of the direction of the vibrational transition dipole moment of isolated species [8]. Selective IR induced isomerization in the gas phase is another interesting technique that provides structural and dynamical information [9]. Recently, conformational isomerization has been demonstrated for a flexible molecule using UV-UV stimulated emission pumping spectroscopy. This method not only allows for the determination of lower and upper values for isomerization barriers between different conformers, it also enables a determination of relative energies of the zero-point levels of the various conformers [10].

IR absorption spectra of gas phase species can be obtained by ion- or fluorescence-dip spectroscopy [6, 7, 11], a technique that has been applied to various interesting systems, such as isolated [12] or paired nucleobases [13], to the amino acids phenylalanine and tryptophan [14, 15] and to β -sheet model systems [16, 17]. These experiments have all been performed using laser systems that cover the near- and mid-IR and are limited to wavelengths shorter than about $7\text{ }\mu\text{m}$. In this range X–H (X=C,O,N) and C=O stretching vibrations are probed and the experiments provide insight into the conformational arrangement, as transitions exhibit shifts in absorption frequency and changes in intensity in the presence of, for instance, intra-molecular hydrogen bonds or solvating molecules. However, most vibrational modes have characteristic frequencies that lie further in the IR and are not accessible using standard laser systems.

The amino acid tryptophan has been studied extensively by various groups as it absorbs strongly in the near-UV and as it is an important probe in fluorescence spectroscopy [18]. Even though tryptophan is a relatively simple molecule, in the gas phase it is observed to fold into several different conformers. The various conformers have different electronic transitions and can be selectively excited using UV lasers [19]. A detailed structural assignment, however, requires more information. IR spectra in the X–H spectral region have recently been obtained for different conformers and, combined with Density Functional Theory (DFT), a first assignment to specific geometries is obtained [15].

Here the IR absorption spectra are presented for three conformers of tryptophan in the gas phase over a wide frequency range, from 330 cm^{-1} to 1500 cm^{-1} . It is observed that the conformation has a strong influence on the spectra. The experimental results are combined with DFT calculations, and

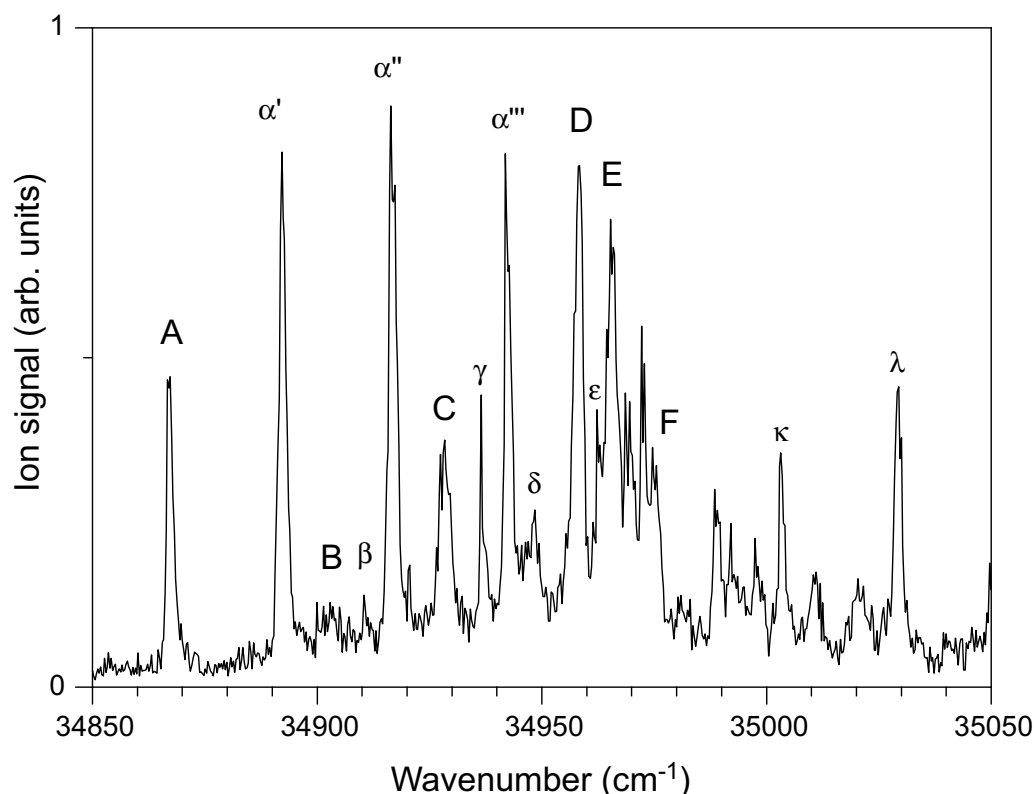


Figure 5.1: REMPI spectrum of tryptophan. The 0–0 transitions for each conformer (A–F) are labeled with a capital. The other resonances labeled by Greek letters are all excited vibrations of conformer A. Labeling has been adopted from Refs. [15, 19].

unique information on the structures of the individual conformers is obtained.

5.2 Experiment

The present IR absorption spectra of tryptophan conformers in the region of 330–1500 cm^{-1} are measured in a pulsed molecular beam experiment with mass and conformer specific detection. Gas phase tryptophan molecules are evaporated in a custom-made oven that is placed behind the nozzle of a pulsed valve (General Valve). Gas-phase tryptophan molecules are entrained by an argon gas pulse of typically 200 μs duration and in a supersonic expansion into vacuum the molecules are internally cooled. After passing through a skimmer, they interact with pulsed UV and IR laser beams.

The IR absorption spectra are measured making use of IR Ion-Dip Spectroscopy (IR-IDS). In this technique the internally cooled molecules are resonantly ionized by a pulsed UV laser to produce a constant ion signal. A few μs before the UV laser fires, the IR laser interacts with the molecules. If a vibrational transition in the molecules is induced by the IR light, population is transferred into an excited vibrational state, yielding a depletion of ground state molecules. This results in a reduction of the number of ions produced. By measuring the ion signal while tuning the IR wavelength, an ion-dip spectrum is recorded.

Conformer specificity is achieved by selecting the frequency of the UV laser. In Figure 5.1 the

REMPI spectrum of tryptophan in the region from 34850 cm^{-1} to 35050 cm^{-1} is shown. In this spectrum, which is very similar to the ones obtained by other groups, a considerable number of resonances can be observed [15, 19]. By evaluating the saturation behavior of the resonances it has been established that the peaks in this spectrum are due to a total of six different conformers, for which the 0–0 transitions have been labeled by the capitals A–F [19]. Most of the other resonances in the spectrum, labeled by Greek letters, are due to vibrationally excited states of conformer A. These observations were later confirmed when the system was studied using UV-UV hole burning spectroscopy [15].

5.3 Results and Discussion

5.3.1 Calculations

To analyze the observed spectra, DFT calculations are performed to find the most stable geometries for tryptophan. Starting geometries are obtained by performing a systematic scan over 4 dihedral angles describing the orientation of the amino acid group, using the AM1 semi-empirical method. The fifth dihedral angle, associated with the bond between the indole and amino acid groups, is kept at 90° and 270° , respectively. A total of 32 starting geometries are submitted to a full geometry optimization using the B3LYP functional with the 6-31+G(d) basis set. For these 32 low-energy geometries also the IR absorption spectra are calculated in the harmonic approximation. All calculations are performed using the Gaussian 98 package [20].

The structures obtained in the calculations can be classified by their various intra-molecular hydrogen bonds. Three main types of hydrogen bonding between the acid and amino groups are possible. First, the hydroxyl hydrogen can hydrogen bond to the amino-nitrogen atom (type I hydrogen bonding). In this structure added stabilization is found in interactions between the amino-hydrogens and the π -electrons of the indole group. Second, the amino-hydrogen atoms can hydrogen bond to the hydroxyl O–H oxygen atom (type II) or, in the third case, they can hydrogen bond to the carboxylic C=O oxygen atom (type III). Similar results have been obtained by others [15]. The 12 structures with the lowest calculated energies are depicted in 5.2, where their relative energies are indicated (in kJ/mole; calculated at the B3LYP/6-31+G(d) level). Also indicated are the internal hydrogen bonds (dashed lines) and the hydrogen bonding classification. One can observe that the four lowest energy structures all exhibit type I hydrogen bonding. It thus appears to be favorable for the system to form only one internal 'classical' hydrogen bond and orient the NH_2 hydrogens toward the π -cloud.

5.3.2 IR spectra

In Figure 5.3, the IR absorption spectra in the range between 330 cm^{-1} and 1500 cm^{-1} are displayed for three conformers, labeled A, D and E, where the notation introduced by Rizzo *et al.* is used [19]. The ion-dip signal is normalized to the constant ion current produced by the UV laser. The relative IR absorption cross sections are then obtained as the natural logarithm of this normalized signal. The absolute frequency accuracy is about 3 cm^{-1} at the low frequency end of the spectrum, gradually deteriorating to 15 cm^{-1} at the high frequency end. The line width observed in the spectrum is almost exclusively determined by the bandwidth of the laser, and is about 1 % of the FELIX frequency.

One can immediately observe that the three spectra are different and that the conformation has a large effect on the vibrational structure. The strong resonance near 1400 cm^{-1} in conformer A, for

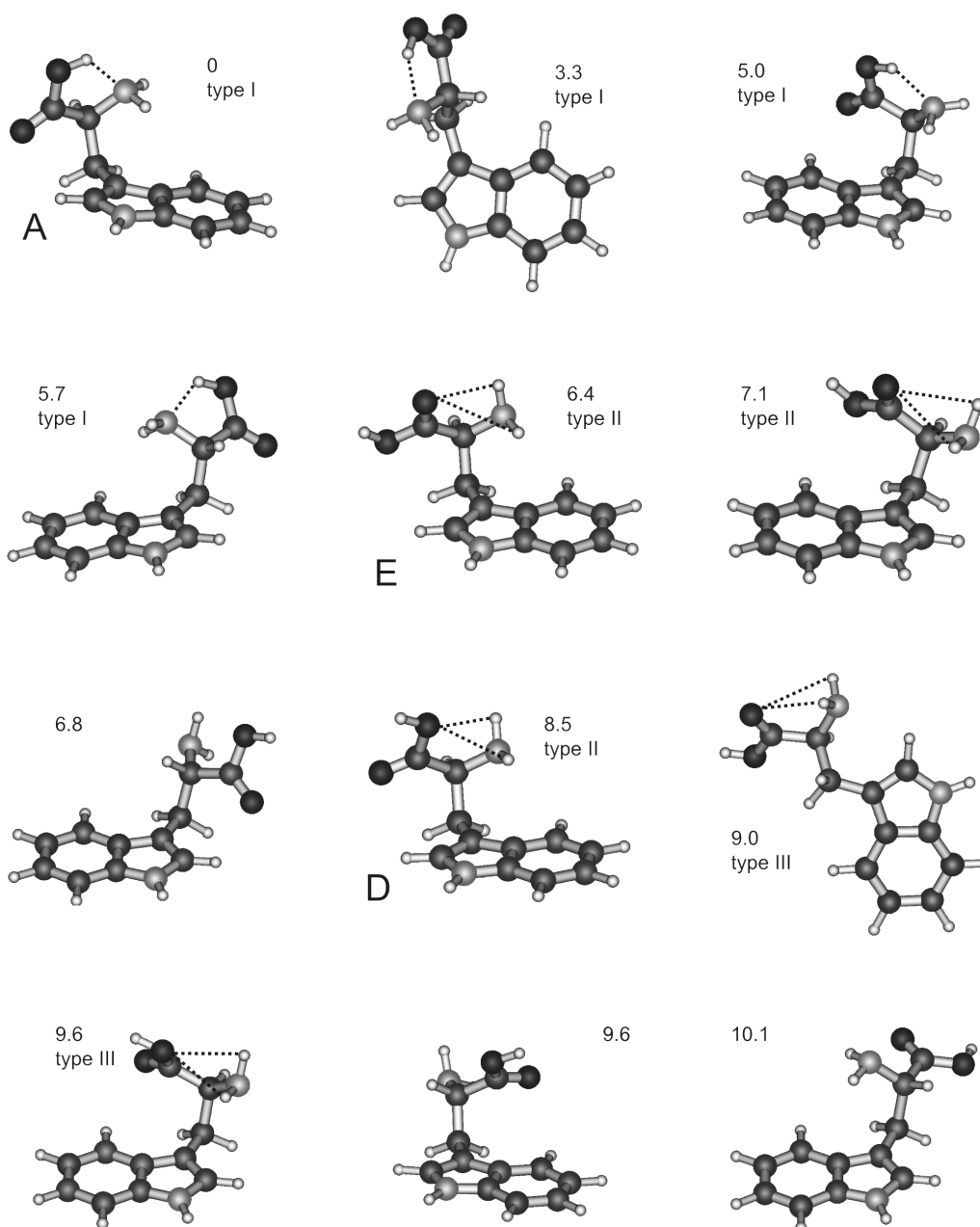


Figure 5.2: Geometries of the 12 lowest calculated energy structures for tryptophan. Included are the relative energies (in kJ/mole) calculated at the B3LYP/6-31G(d,p) level, with the inclusion of zero-point energies. When clearly identifiable, the type of hydrogen bonding that gives the structure stability is also indicated.

instance, is not present in the spectra of the other two conformers. The region below 700 cm^{-1} appears to show the most pronounced differences. As this is the region where vibrations that involve floppy, large-amplitude motions are expected, this low frequency range should be especially sensitive to the conformation of the molecule.

The calculated spectra of the 32 low-energy geometries can be compared to the experimental spectra. In Figure 5.3, the IR spectra of the three low energy conformers that show the best match with

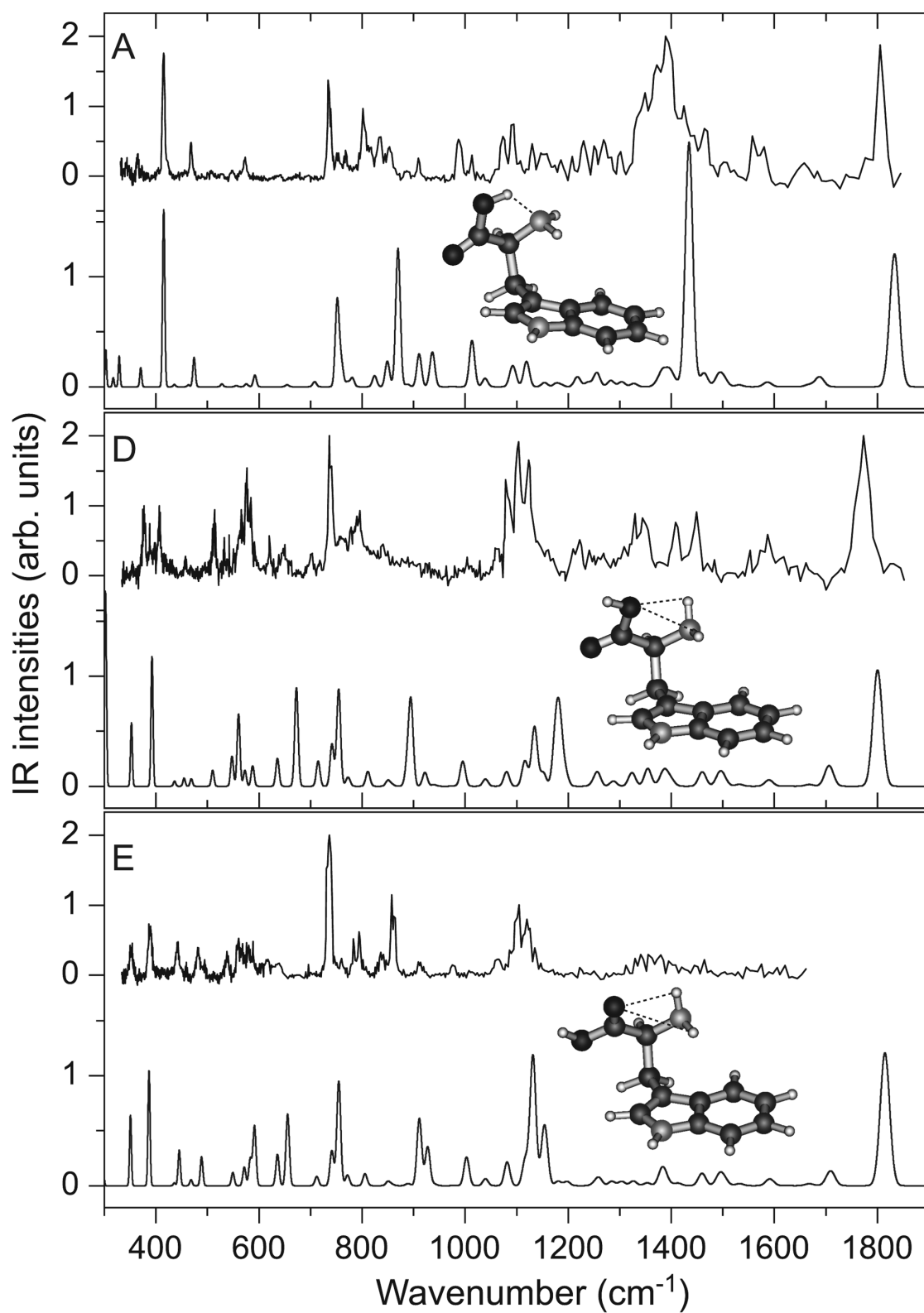


Figure 5.3: Infrared absorption spectra of three conformers of tryptophan. Below each experimental spectrum a theoretical spectrum is displayed. The corresponding geometries are displayed in the figure as well.

the experiment are presented as simulated spectra where the theoretical IR intensities are convoluted with the (frequency dependent) spectral profile of FELIX. No scaling of the calculated frequencies is performed.

The experimental spectrum of conformer A (top trace) matches best with the calculated spectrum of the lowest energy conformer, in which a hydrogen bond between the hydroxyl hydrogen and the amino-nitrogen is present. Computer animation of the calculated normal modes reveals that the strongest mode in the spectrum, at 1434 cm^{-1} is the carboxylic C–O–H bend which is perturbed by the hydrogen bond. The second strongest mode is the free C=O stretch at 1806 cm^{-1} . Other unique features are the four lowest energy modes below 600 cm^{-1} , of which the strongest, around 400 cm^{-1} , results from the (very much local-mode) out-of-plane motion of the N–H in the indole group. The strong resonance at 738 cm^{-1} , which is observed for all conformers close to this frequency, is associated with the indole “umbrella mode”. The largest difference between theoretical and experimental spectra is the predicted strength of a fundamental mode at 869 cm^{-1} . The motion associated with this calculated normal mode is essentially an inversion of the amino hydrogens through the (amino acid group) N–C–H plane. This mode is predicted around 900 cm^{-1} for all calculated structures, but is experimentally not found for any of the three conformers investigated. From earlier experiments, for instance on aniline, it is known, however, that such an inversion mode is rather poorly described in the harmonic approximation [21].

The strong mode around 1400 cm^{-1} , observed for conformer A and assigned to result from hindered C–O–H bending, is not observed in the spectra of conformer D and E. This suggests that the C–O–H groups in these two conformers are not involved in hydrogen bonding. IR active modes that involve bending of the C–O–H group are calculated for those conformers as well, but the intensities are predicted to be substantially lower.

A definite assignment of conformer D (middle trace) is more difficult than for conformer A. The resulting assignment is based on a good overall agreement between the experimental and the calculated spectra shown in the figure. A key feature in this calculated geometry is the presence of the hydrogen bonds between the amino-hydrogens and the hydroxyl oxygen. In addition, the geometry shown is the lowest energy structure of type III hydrogen bonding.

The spectrum of conformer E (bottom trace) allows for a more solid assignment. The experimental spectrum is observed to have four sharp resonances in the spectral range between 300 cm^{-1} and 500 cm^{-1} . These modes are extremely well reproduced in the calculated spectrum. The three lowest-frequency modes represent the indole N–H out-of-plane bending vibration, but in this structure they are rather strongly coupled to concerted deformations of the amino-acid group. This coupling leads to a distribution of IR intensity over all three modes, which explains the lower intensity relative to that of the localized N–H out-of-plane bending vibration in conformer A. In the proposed structure for conformer E, hydrogen bonds are present between the amino-hydrogens and the carbonyl C=O oxygen. A unique feature in the experimental and calculated spectra, that is not found in the spectra of the other calculated structures, is a resonance at 480 cm^{-1} . Although the agreement between calculated and experimental spectra is remarkable and warrants the present assignment, it is unfortunate that there is no data in the spectral region of the C=O stretch. The hydrogen bond could shift this frequency substantially (cf. Chapter 4 or the work by Gerhards *et al.* [16]).

5.3.3 Discussion

The structures that are here assigned to conformers A, D and E are the lowest energy structures calculated for each of the above mentioned types of hydrogen bonding. For A and E, this assignment is the same as that obtained previously from IR experiments in the hydrogen stretching region [15]. For D, a slightly different structure, having the same type of hydrogen bonding, is found to be lower in energy. The differences in energy, structure and IR spectrum between the conformer D proposed here and the one proposed previously [15] are small, however. Since neither of the two spectra calculated for D agree very well with the experiment, we cannot exclude that this conformer has another not yet considered structure.

It can be seen from the present data that for a molecule of the size of tryptophan many local minima in the Potential Energy Surface (PES) can be found in ab-initio calculations. For the assignment of IR spectra of larger molecules, such as di-, tri- and higher order peptides, the computational efforts for a full geometry optimization become more and more expensive. It is thus of the utmost importance to find a method to generate good starting structures where the full PES is sampled. The use of low-level approximative techniques to obtain starting structures does reduce the computational effort, but can by no means guarantee obtaining all minima. In the present method the semi-empirical AM1 method is used to optimize structures that were generated in a systematic scan over the dihedral angles that determine the orientation of the amino acid group with respect to the indole residue. In an alternative method, structures were generated in a simulated-annealing procedure using Allinger's MM3 force field [22]. A full geometry optimization of these structures at the B3LYP/6-31+G(d) level yielded again the lowest energy structure that conformer A is assigned to, together with some, but not all of the low-energy structures obtained with AM1. Interesting is the comparison with the previous calculations of Snoek *et al.*: in their calculations the first evaluation of a structure was not done at the AM1 level, but using the Hartree-Fock method. Snoek and co-workers obtained several low-energy structures that were not found in this work, which would suggest that their method is a better one [15]. On the other hand, in the present work several other stable structures are obtained that were not found by Snoek and co-workers. [23]. As the Hartree-Fock optimization is, in comparison with AM1, still rather time-consuming it might not be feasible to use this procedure for much larger systems. On the bright side, most low energy structures that were 'missing' in the present calculations could be guessed from visually inspecting the obtained geometries and making small changes in the orientations of the amino acid side group using chemical intuition, which makes the semi-empirical or force field approach a useful instrument.

5.4 Conclusions

The data presented here constitute the first IR measurement of a gas phase biomolecule in the molecular fingerprint region. The combination of a widely tunable IR laser with the ion-dip technique makes it possible to obtain IR spectra that are both mass and conformer specific over a broad spectral range, thereby dramatically increasing the number of vibrations that can be probed. The technique can be extended to larger species as well as toward longer wavelength. However, when the molecules become very large, difficulties arise in bringing them into the gas phase, as well as in selectively ionizing them. For large species, complementary IR spectral information could be obtained from experiments performed on ionic species in the gas phase, generated by MALDI or ESI. In such experiments, a mass change after resonant multi-photon dissociation could be monitored using mass spectrometry or

an IR induced conformational change could be detected by ion mobility measurements.

References

- [1] F. Hillenkamp, M. Karas, R. Beavis, and B. Chait, *Anal. Chem.* **63**, A1193 (1991).
- [2] J. Fenn, M. Mann, C. Meng, S. Wong, and C. Whitehouse, *Science* **246**, 64 (1989).
- [3] G. von Helden, T. Wyttenbach, and M. T. Bowers, *Science* **267**, 1483 (1995).
- [4] D. E. Clemmer, R. Hudgins, and M. F. Jarrold, *J. Am. Chem. Soc.* **117**, 10141 (1995).
- [5] D. W. Pratt, *Annu. Rev. Phys. Chem.* **49**, 481 (1998).
- [6] T. S. Zwier, *Annu. Rev. Phys. Chem.* **47**, 205 (1996).
- [7] T. Ebata, A. Fujii, and N. Mikami, *Int. Rev. Phys. Chem* **17**, 331 (1998).
- [8] F. Dong and R. E. Miller, *Science* **298**, 1227 (2002).
- [9] B. C. Dian, A. Longarte, and T. S. Zwier, *Science* **296**, 2369 (2002).
- [10] B. C. Dian, J. R. Clarkson, and T. S. Zwier, *Science* **303**, 1169 (2004).
- [11] R. H. Page, Y. Shen, and Y. T. Lee, *J. Chem. Phys.* **88**, 4621 (1988).
- [12] E. Nir, C. Janzen, P. Imhof, K. Kleinermanns, and M. S. de Vries, *J. Chem. Phys.* **115**, 4604 (2001).
- [13] E. Nir, C. Janzen, P. Imhof, K. Kleinermanns, and M. S. de Vries, *Phys. Chem. Chem. Phys.* **4**, 732 (2002).
- [14] L. C. Snoek, E. G. Robertson, R. T. Kroemer, and J. P. Simons, *Chem. Phys. Lett.* **321**, 49 (2000).
- [15] L. C. Snoek, R. T. Kroemer, M. Hockridge, and J. P. Simons, *Phys. Chem. Chem. Phys.* **3**, 1819 (2001).
- [16] M. Gerhards, C. Unterberg, and A. Gerlach, *Phys. Chem. Chem. Phys.* **4**, 5563 (2002).
- [17] C. Unterberg, A. Gerlach, T. Schrader, and M. Gerhards, *J. Chem. Phys.* **118**, 8296 (2003).
- [18] J. M. Beechem and L. Brand, *Ann. Rev. Biochem.* **54**, 43 (1985).
- [19] T. R. Rizzo, Y. D. Park, L. A. Peteanu, and D. H. Levy, *J. Chem. Phys.* **84**, 2534 (1986).
- [20] M. J. Frisch, G. W. Trucks, H. B. Schlegel, G. E. Scuseria, M. A. Robb, J. R. Cheeseman, V. G. Zakrzewski, J. J. A. Montgomery, R. E. Stratmann, J. C. Burant, et al., *Gaussian 98, Revision A.7*, Pittsburgh, PA (1998).
- [21] H. Piest, G. von Helden, and G. Meijer, *J. Chem. Phys.* **110**, 2010 (1999).
- [22] N. L. Allinger, Y. H. Yuh, and J.-H. Lii, *J. Am. Chem. Soc.* **111**, 8551 (1989).
- [23] R. T. Kroemer, private communication.

CHAPTER 6

THE MID-IR ABSORPTION SPECTRUM OF GAS-PHASE COMPLEXES OF THE NUCLEOBASES GUANINE AND CYTOSINE

The mid-infrared (IR) absorption spectrum of jet-cooled complexes of the nucleobases guanine and cytosine has been recorded in the 500-1800 cm⁻¹ range by ion-dip spectroscopy. Some 20 clearly separated and sharp resonances are observed. The combination of the experimental data with new high-level ab-initio calculations is consistent with a previous structural assignment and a tentative refined assignment is made. These data can serve as a test of the method in the mid-IR regime.

Adapted from: J. M. Bakker, I. Compagnon, G. Meijer, G. von Helden, M. Kabeláč, P. Hobza, and M. S. de Vries, *Phys. Chem. Chem. Phys.* **6**, 2810-2815 (2004)

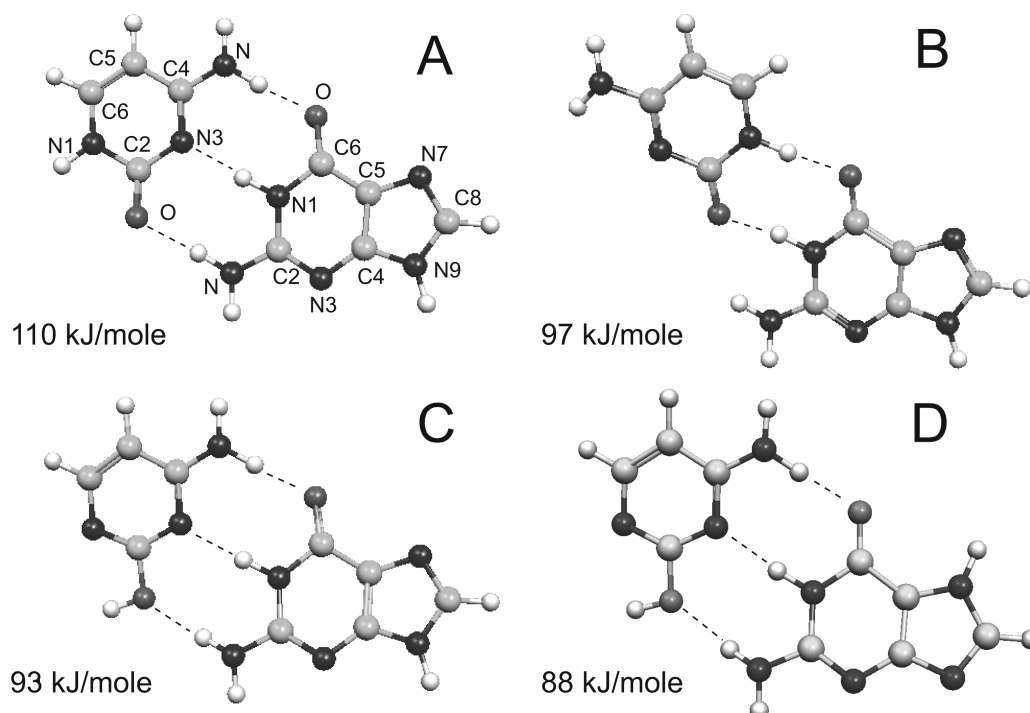


Figure 6.1: Structures of the four lowest-energy G-C pairs. The stabilization energies calculated at RI-MP2/TZVPP level are given for each structure. Also included is the atom labeling convention which is used throughout this chapter.

6.1 Introduction

One of the questions yet to be answered for the DNA system is what determines the ultimate stabilization of the classical Watson-Crick structure [1]. Several factors play a role and it is unclear what part in the total stabilization they play: (i) the multiple hydrogen bonds between the base pairs that cross-link the two strands, (ii) the interaction between the nucleobases on one strand, the so-called stacking mechanism, and (iii) the stabilization by the deoxyribose backbone and other environmental effects. This question has caused a considerable theoretical effort to evaluate the various factors [2–4]. To investigate this matter experimentally one can adopt the approach of trying to separate the factors that play a role, which can be achieved by studying isolated molecules in the gas phase. Spectroscopic studies of gas phase biological molecules have enabled the elucidation of fundamental interactions governing biological processes unobscured by such effects as the broadening of spectral lines by sample-solvent interactions [5, 6]. The obvious start of gas phase studies involving the biological heredity system lies in interrogating the fundamental building blocks, the isolated purine and pyrimidine molecules. By extending the study to complexes of these building blocks, one can extract valuable information on the multiple hydrogen-bonded interactions, stabilizing the two strands.

Considerable spectroscopic knowledge on individual gas-phase nucleobases has been obtained in recent years [7–12]. One of the striking findings is the presence of many tautomers that are different from the form in which they are found in DNA in living matter. Using spectroscopic techniques, also complexes of nucleobases have been investigated [13–15]. In those studies the Watson-Crick geometries of the paired nucleobases have not been observed so-far.

Figure 6.1 shows the four lowest energy structures of the guanine-cytosine (G-C) complex, out of more than 23 possible hydrogen bonded structures [16]. Structure A represents the triply hydrogen bonded Watson-Crick structure. Structure C is very similar, but it has the cytosine as an enol rather than a keto tautomer. Structure D is again very similar: it is another Watson-Crick type bonded structure, now with an enol cytosine tautomer and a guanine tautomer where one hydrogen is attached at the N7 position (as opposed to N9 for structure C). Finally, in structure B the tautomers as found in DNA are hydrogen bonded in a way which would be impossible if the sugar backbone were present. To discern the structures, a nomenclature was introduced by Nir et al. [14]. In this notation, structure C is called K9-1E, indicating that guanine is found in the keto form, with a hydrogen attached to N9; cytosine is in its enol form, and the OH group is oriented toward N1 (cf. Figure 6.1). Using REMPI spectroscopy and UV-UV hole burning so far two structures of G-C complexes have been distinguished [14]. With the help of IR-UV hole burning in the near IR between 3300 cm^{-1} and 3700 cm^{-1} one of these could tentatively be identified as structure C [14] and the other one as structure B [17]. The identification of structure C is not unambiguous: the X-H (X=N,C) stretching vibrations of structures C and D are very similar, and assignment was done based on the relative energies of the structures. Both tautomers of guanine have been observed in a jet experiment, and assignment of the spectrum to structure D can not be ruled out [12]. No spectrum is observed that can be assigned to structure A, however. This could be caused by a considerable difference in the UV spectral properties or by a dramatically reduced lifetime of the G-C complex in structure A. Broad REMPI spectra have been observed for complexes of 1-methyl cytosine with 9-methyl guanine and of cytidine with guanine that can tentatively be assigned to structure A [18].

The general strategy to elucidate the structure of a molecular system in the gas phase is to combine UV spectroscopy and UV-UV / IR-UV hole-burning spectroscopy with high-level theoretical calculations. The UV-UV hole burning spectroscopy ascertains that a specific UV transition is resulting from one single structure, whereas the IR-UV hole burning spectroscopy is used to identify this structure.

Here, the IR absorption spectrum of the gas-phase complex of guanine and cytosine, recorded in the $500\text{--}1800\text{ cm}^{-1}$ region, is presented. At the same time, a set of new high-level calculations to interpret the recorded data are presented. These data serve the dual purpose of testing the original assignment of this complex and testing the comparison of the highest level of the high-level computations with the experiment in this region of the IR spectrum.

The calculations represent a new step in theoretical studies of DNA bases [16]. All calculations on DNA bases and base pairs should be performed at a single, common level that accurately describes all interactions in the system. Hartree-Fock (HF) and Density Functional Theory (DFT) calculations, for instance, only correctly describe hydrogen bonded interactions but are not able to describe the equally important stacking interactions. Surprisingly, up to now no DFT functional exists that describes the stacking of DNA bases. The first acceptable level for a correct description of both hydrogen bonding and stacking interactions is the MP2 level using at least a DZ+P basis set. This level provides accurate characteristics (structure, stabilization energies, and vibrational frequencies) of hydrogen bonded pairs but underestimates stabilization energies for stacking. Reliable values for all characteristics of any type of DNA base pair are generated, however, if the MP2 calculations are performed with the TZ+P basis set, i.e. a triple-zeta basis set with two sets of first polarization functions and one set of second polarization functions on all the atoms [19]. Such a treatment is feasible for obtaining structure and stabilization energy of a pair but computationally too costly for generating vibrational frequencies. Therefore the following computational strategy is adopted: structure and stabilization

energy are calculated at the MP2/TZ+P level, allowing for a comparison between the stabilization energies of the studied hydrogen bonded complexes with those of stacked complexes. The vibrational frequencies are then determined at a cheaper MP2/DZ+P level.

6.2 Experimental

Since the vapor pressure of the nucleobases is very low at room temperature and they are thermally labile the experiment is performed using the laser-desorption source. For the measurement of the IR absorption spectra of the jet-cooled guanine-cytosine (GC) complexes IR ion-dip spectroscopy is employed. Ions are produced from ground state molecules using a two-photon ionization scheme. For this, the molecules are first excited to the lowest vibrational level in the first electronically excited singlet state (S_1) using the frequency doubled dye laser (Rhodamine 640). A second photon from the excitation laser pulse ionizes the molecules. In the present experiment, the UV detection laser is running at a 10 Hz repetition rate, while FELIX is set to run at 5 Hz. By independently recording both the IR-*on* signal and the IR-*off* signal a normalized ion-dip spectrum can be obtained, that is insensitive to long-term drifts in UV laser power or source conditions.

The IR ion-dip spectrum for GC is recorded with the UV probe laser at 33314 cm^{-1} . This frequency corresponds to the $S_1 \leftarrow S_0(0-0)$ transition of the complex structure that was earlier assigned to structure C, based on IR-UV hole burning spectroscopy in the near IR region between 3300 and 3700 cm^{-1} [14]. That earlier spectrum contained the frequency of the OH stretching vibration of the enol-cytosine as a distinctive feature. As the OH stretching vibration of structure D was calculated to be almost identical, no definite assignment was made. The present data in the mid-IR may assist in accomplishing a final assignment as the current spectral range contains the CO stretching vibrational frequency as well as a large number of skeletal vibrational frequencies that can serve for further structural identification.

6.3 Theoretical methods

The use of DZ+P or even TZ+P basis sets in a combination with the exact MP2 treatment for DNA base pairs is difficult if not impractical. Recently the applicability of the approximative resolution of identity (RI) MP2 methods [20, 21] for nucleic acid base pairs and larger DNA fragments [22] has been explored and it has been shown that this method is capable of an accurate description of both hydrogen bonded and stacked DNA base interactions. The results obtained with the RI-MP2 method differ only marginally from those evaluated with the exact MP2 method, while the efficiency is larger by up to one order of magnitude.

The potential energy surface (PES) of the GC pair is investigated using the molecular dynamics/quenching (MD/Q) method with the Cornell *et al.* empirical force field [23]. MD/Q simulations are performed in the NVE microcanonical ensemble (N, V and E refer to the number of particles, volume and energy, respectively) within the quaternion formalism. The MD simulations are carried out at a constant total energy corresponding to an average temperature of 298 K which is high enough to allow crossing over relatively high energy barriers and thus to sample the whole potential energy surface. Every 1 ps the MD run is interrupted, the kinetic energy is removed and the structure of the complex of guanine and cytosine is optimized using the conjugate gradient method. The geometry

and the corresponding energy are then stored, while the MD run is restarted from the point where it has been interrupted. The total simulation time is 250 ns.

The investigation of the GC PES is limited to 16 different pairings of nucleobases, obtained by combining the four most stable tautomers of guanine and cytosine [24]. The three most stable structures of the complex, which are the same as found earlier and shown in Figure 6.1, are further optimized by gradient optimizations at the RI-MP2 level using DZ+P (cc-pVDZ [3s2p1d/2s1p]) and TZ+P (TZVPP [5s3p2d1f/3s2p1d]) basis sets with a standard (default) auxiliary basis set. Harmonic vibration frequencies are determined numerically using the smaller basis set while stabilization energies are evaluated with the larger one. The stabilization energy is corrected for the basis set superposition error using the function counterpoise procedure [25] and also the deformation energy is included. Although the *a posteriori* inclusion of the BSSE can be a source of error, this error is certainly much smaller than when the counterpoise-corrected procedure is not used. Performing a counterpoise-corrected gradient optimization would solve the problem, but that type of optimization for the complexes presented is much more time consuming and is not feasible for routine calculations. All the calculations are carried out using the TURBOMOLE 5.6 program suite [26].

6.4 Results and discussion

The IR ion-dip spectrum of GC is converted into an IR absorption spectrum after it is checked that the depletions due to each resonance are the result of a one-photon absorption process. For a limited number of resonances this has been verified by performing measurements of the depletion as a function of IR laser intensity. The normalized ion-dip signal $s(\nu)$ is therefore converted into relative IR absorption cross-sections $\sigma(\nu)$ using the conversion $\sigma(\nu) = -\log(s(\nu))$ and by correcting for the FELIX output power.

Figure 6.2 shows the IR absorption spectrum thus obtained for the GC complex in the 500-1800 cm^{-1} region. The spectrum shows a large number of clear resonances, the line widths of which are mainly determined by the FELIX spectral profile. Below the experimental spectrum four traces are shown that represent the theoretical spectra of the four lowest-energy configurations. The IR intensities obtained from the calculations are convoluted with a Gaussian function representing the FELIX spectral profile. The bandwidth used in the convolution is 0.5 % of the FELIX frequency. Furthermore, the frequencies of the theoretical modes are scaled by a factor of 0.956 to obtain the best agreement with the observed spectrum and the vertical axis scaling for the three theoretical curves is the same.

From a comparison between the experimental spectrum and the theoretical curves one can observe that the spectra of structures C and D resemble the data the best. Particularly in the region of 1000 cm^{-1} to 1800 cm^{-1} the experimental spectrum is rather well predicted, as in this region for both structures all observed lines can directly be attributed to calculated modes and only minor differences in the spectra calculated for structures C and D are observed. In the lower energy region, below 1000 cm^{-1} , the agreement is less convincing but equal to or better than that for the calculated spectra of either structure A or B. The only serious disagreement between theory and experiment lies in the abnormally large intensity of the resonance calculated at 578 cm^{-1} (scaled value) for structure C. One could be tempted to assign the spectrum to structure D, based upon this discrepancy. It is necessary, however, to have information about the structures and the nature of the vibrational modes before such a decision can be made.

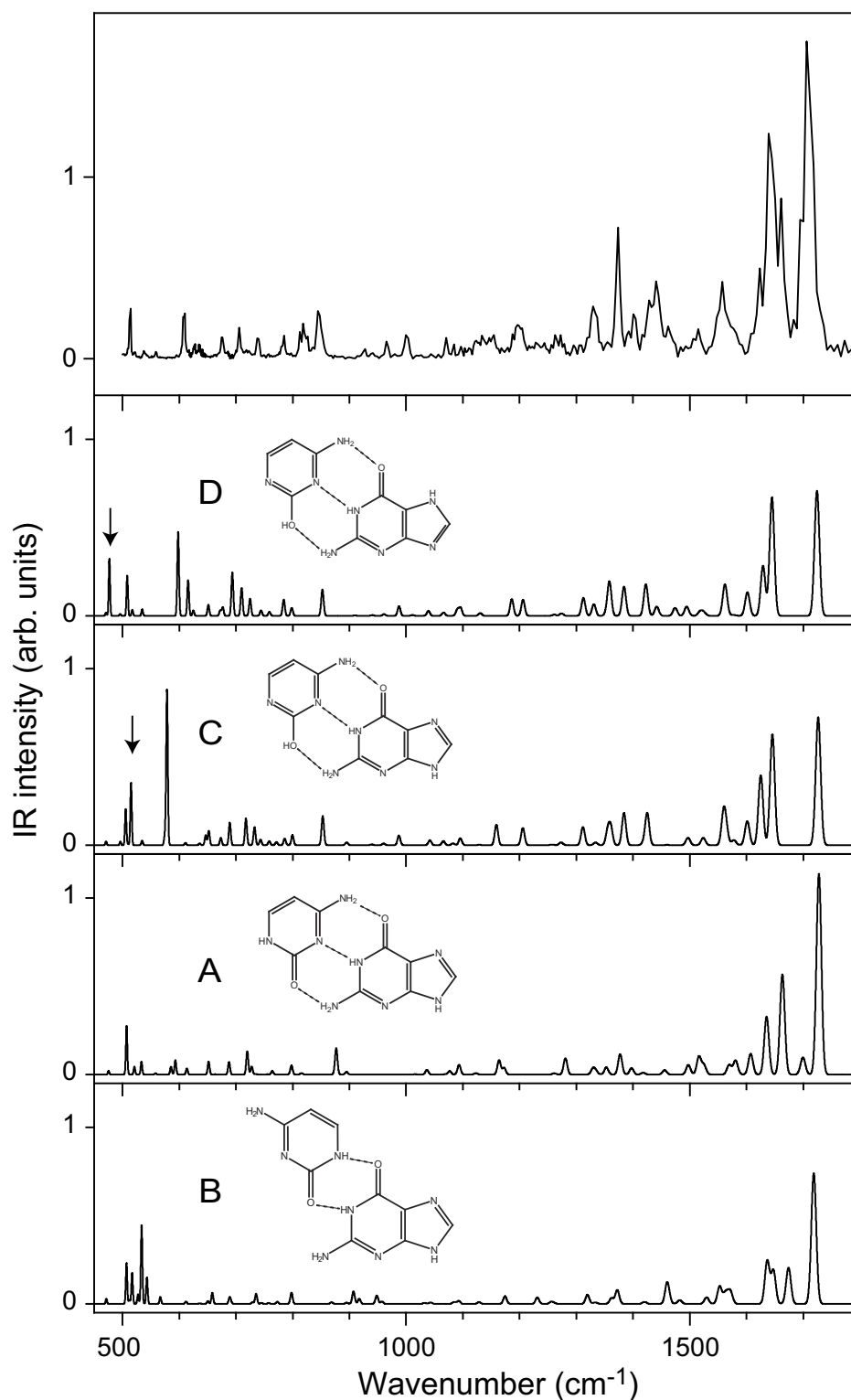


Figure 6.2: IR absorption spectrum of the guanine-cytosine complex. Below the experimental spectrum are theoretical spectra of the four lowest-energy configurations of guanine-cytosine complexes. Theoretical frequencies for all structures are scaled by a factor of 0.956 and convoluted with a Gaussian function representing the FELIX spectral profile.

Structure C is a slightly non-planar (deviation of planes of the bases is about 20°), Watson-Crick-type structure of canonical guanine and a tautomer of cytosine in which a hydrogen atom is detached from the N1-H group and attached to the C2=O group, forming an enol side group. The presence of the OH group as well as the change of the cytosine electronic structure leads to a weaker interaction between G and C than in structure A. The distances between the heavy atoms in the hydrogen bonds (cyt N-H-gua O), (cyt N3-gua H-N1) and (cyt O-gua H-N) in structure C are 2.84, 2.97 and 3.07 Å, respectively (cf. Figure 6.1). Here, all geometric parameters refer to the calculations done at the RI-MP2/cc-pVDZ level. Both amino groups in structure C are non-planar with respect to the base plane (deviation in both subsystems is approximately 20°). Structure D is very similar to structure C but a hydrogen atom is detached from the N9-H group and attached to the N7. The base planes are tilted with respect to each other by about 23° , the hydrogen bond distances are 2.85, 2.95 and 3.10 Å and the amino hydrogens are oriented out-of-plane by about 25° .

Structures C and D correspond to the second and third local minima at the G-C potential energy surface (PES). Their (absolute) stabilization energies (including deformation energy and difference in tautomerization energies, a sum of relative energies of isolated tautomers with respect to the canonical form) are 93 kJ/mole and 88 kJ/mole, respectively. This is about 17 kJ/mole and 23 kJ/mole less stable than the global minimum structure, the canonical Watson-Crick structure A. Structure A is perfectly planar with only negligible deviation (less than 1°) of amino hydrogens from the plane of the base. The distances between the heavy atoms participating in the hydrogen bonds are 2.78, 2.92 and 2.92 Å, respectively and they are slightly shorter than in the cases of structures C and D.

Structure B, possessing a different hydrogen bond pattern between canonical forms of guanine and cytosine, is about 4 kJ/mole more stable than structure C (97 kJ/mole) and this structure thus corresponds to the first local minimum at the PES. Structure B is slightly non-planar and it contains only 2 hydrogen bonds with the following distances between heavy atoms : O(G)... N1H(cyt)=2.77 Å, and N1H(gua)...O(cyt)=2.71 Å.

The present RI-MP2/TZVPP stabilization energies are systematically larger than the respective RI-MP2/cc-pVDZ ones by about 6-8 kJ/mole. More detailed information on all 50 complexes obtained at the G-C PES by considering the four most stable tautomers of guanine and of cytosine will be published later [24].

To discuss the nature of the resonances in the experimental spectrum the calculated vibrational modes are inspected using visualization software to identify the associated motions of the atoms. Line positions of all observed resonances and (scaled) frequencies of the assigned theoretical vibrations, including short descriptions of the modes, can be found in Table 6.1. Most of the assigned modes are identical for both structure C and D; only when they differ an explicit mode description is given for structure D. Throughout the rest of the discussion scaled values will be given for theoretical frequencies to facilitate comparison to Figure 6.1. The dominating feature in the experimental spectrum, the highest frequency resonance found at 1706 cm^{-1} , is associated with the guanine C=O stretching mode, with a slight coupling to a bending motion of the guanine N1-H group. As this is the only C=O group in structures C and D, its assignment is unambiguous. For structure A the two C=O stretching modes are coupled, and result in one symmetric and one asymmetric stretching mode of which the latter (calculated at 1727 cm^{-1}) has large IR intensity, and the former (1699 cm^{-1}) only little. The two C=O stretching vibrations in structure B are not coupled to each other, but to an N-H in-plane bending mode. This interaction is less favorable for the cytosine stretching mode (1674 cm^{-1}), which has considerably less IR intensity than its guanine counterpart (1718 cm^{-1}). The

modes lying at somewhat lower energy, between 1000 cm^{-1} and 1700 cm^{-1} are all associated with skeletal motions in the plane of the molecules, coupled in varying strength with in-plane NH_2 or NH bending vibrations. Most of the modes here are rather well reproduced, except for a somewhat strong IR intensity for the resonance experimentally found at 1374 cm^{-1} , which might be due to overlapping resonances. The region below 1000 cm^{-1} contains a number of clear resonances that cannot so easily be assigned to a specific theoretical mode. Most vibrations here are out-of-plane bending motions of the various hydrogen atoms.

There is one mode with appreciable IR activity that could make an assignment to either structure C or D possible. The N9-H and N7-H out-of-plane bending vibrations are calculated to be very localized in structures C and D, respectively, and should be sensitive to its environment: in structure C the N9-H group is rather isolated, whereas in structure D the N7-H group could be influenced by the presence of the C6=O group. For both structures the respective N-H out-of-plane bending vibration is indicated with an arrow in the calculated spectrum. In structure C, around 500 cm^{-1} two vibrational modes are expected: the C-O-H in-plane bending mode at 506 cm^{-1} and the N9-H out-of-plane bending mode at 515 cm^{-1} . In structure D, only the C-O-H in-plane bending mode is expected here, at 508 cm^{-1} while the N7-H out-of-plane bending mode is calculated to lie at 477 cm^{-1} . From the fact that there is only one observed resonance, at 514 cm^{-1} , we are tempted to assign the experimental spectrum to structure D. Unfortunately, the data do not cover the range where the N7-H bending mode is expected in structure D, and a definite assignment can still not be made.

It must be pointed out that the calculated vibration at 578 cm^{-1} in the spectrum of structure C, which is predicted with a larger IR intensity than what is observed cannot be invoked to finalize the assignment: the motions associated with this mode are those of the two hydrogens of the guanine amino group moving in-phase through the plane of the molecule. It has been observed earlier that such inversion-like modes that have a double minimum in the PES are poorly reproduced in the harmonic approximation [27, 28]. It therefore is better not to use this resonance to assign the structure based on the comparison between calculated and experimental spectra. The cytosine NH_2 group does not exhibit a simultaneous bending vibration or tunneling mode in this structure nor in the three others; in structure C one localized N-H out-of-plane bending mode is predicted at 401 cm^{-1} .

Structure D shows the same pattern: one tunneling-like mode is found at 598 cm^{-1} (although with substantially less IR intensity than its equivalent in structure C) and a localized N-H out-of-plane bending mode at 392 cm^{-1} . The guanine NH_2 group in structure A does not exhibit the tunneling mode. Rather, its out-of-plane bending vibration is symmetric and yields almost no IR intensity. This different behavior is most likely caused by the fact that in this structure the cytosine is found as a keto tautomer, and the hydrogen bonding is substantially different.

Although the guanine tautomer in structure D is energetically not favored, it has been observed in a jet-experiment [12]. Moreover, the GC origin is found to be much closer to the 7H keto form of guanine than the 9H keto tautomer [12]. Differently phrased: GC complexes with G in the K9 form might have resonances that are found at higher frequencies in the UV spectrum, and hence may be too difficult to observe, because they could be hidden by spectral congestion due to resonances of the K7-C complex. Alternatively, their higher-lying excited state could favor fast dynamical processes that reduce the efficiency of the R2PI process.

6.5 Conclusions

The IR absorption spectrum is measured for the complex of the nucleobases guanine and cytosine isolated in the gas phase in the mid-IR fingerprint region, between 500 cm^{-1} and 1800 cm^{-1} . The IR spectrum contains a large number of sharp resonances that can be used to assign the spectrum. A comparison with theoretical spectra of a set of possible geometries is consistent with a previous assignment to a Watson-Crick type hydrogen bonded structure that contains an enol cytosine tautomer. A tentative assignment is made to a structure with a guanine tautomer in which a hydrogen atom is detached from the N9-H group and attached to N7, but a final assignment can only be made when further experimental work in the frequency regime below 500 cm^{-1} is done.

The comparison between experimental and calculated spectra for the benzoic acid dimer in Chapter 4 appears more favorable than the present one, but one has to keep in mind that the IR absorption spectrum of the benzoic acid dimer is much simpler than that of the guanine-cytosine basepair. Not only does the benzoic acid dimer have a substantially smaller number of degrees of freedom, but its higher symmetry rules out IR transitions to a large fraction of its vibrational modes. Given the higher complexity of the basepair system it can be concluded that the presently used MP2 method gives an altogether fairly accurate description of the vibrational structure of the basepair, allowing for an almost unique assignment. The MP2 method does not exhibit errors in the description of hydrogen bonded bending modes, as seen for the B3LYP treatment of the benzoic acid dimer. From these observations it is concluded that the MP2 method can be used with confidence for the theoretical treatment of larger hydrogen bonded systems and for structural identification based on IR spectroscopic measurements.

References

- [1] J. Watson and F. Crick, *Nature (London)* **171**, 737 (1953).
- [2] C. F. Guerra, F. M. Bickelhaupt, J. G. Snijders, and E. J. Baerends, *J. Am. Chem. Soc.* **122**, 4117 (2000).
- [3] P. Hobza and J. Sponer, *J. Am. Chem. Soc.* **124**, 11802 (2002).
- [4] D. Sivanesan, I. Sumathi, and W. J. Welsh, *Chem. Phys. Lett.* **367**, 351 (2003).
- [5] T. S. Zwier, *J. Phys. Chem. A* **105**, 8827 (2001).
- [6] E. G. Robertson and J. P. Simons, *Phys. Chem. Chem. Phys.* **3**, 1 (2001).
- [7] E. Nir, L. Grace, B. Brauer, and M. S. de Vries, *J. Am. Chem. Soc.* **121**, 4896 (1999).
- [8] E. Nir, M. Muller, L. I. Grace, and M. S. de Vries, *Chem. Phys. Lett.* **355**, 59 (2002).
- [9] N. J. Kim, G. Jeong, Y. S. Kim, J. Sung, S. K. Kim, and Y. D. Park, *J. Chem. Phys.* **113**, 10051 (2000).
- [10] C. Plützer, E. Nir, M. de Vries, and K. Kleinermanns, *Phys. Chem. Chem. Phys.* **3**, 5466 (2001).
- [11] D. Luhrs, V. J., and I. Fischer, *Phys. Chem. Chem. Phys.* **3**, 1827 (2001).
- [12] W. Chin, M. Mons, I. Dimicoli, F. Piuze, B. Tardivel, and M. Elhanine, *Eur. J. Phys. D* **20**, 347 (2002).
- [13] E. Nir, K. Kleinermanns, and M. S. de Vries, *Nature (London)* **408**, 949 (2000).
- [14] E. Nir, C. Janzen, P. Imhof, K. Kleinermanns, and M. S. de Vries, *Phys. Chem. Chem. Phys.* **4**, 732 (2002).
- [15] C. Plützer and K. Kleinermanns, *Phys. Chem. Chem. Phys.* **4**, 4877 (2002).
- [16] Theoretical calculations for this work are performed by Pavel Hobza and Martin Kabeláč.
- [17] M. S. de Vries, private communication.
- [18] A. Abu-Riziq, L. S. Grace, and M. S. de Vries, to be published.
- [19] P. Jurecka and P. Hobza, *J. Am. Chem. Soc.* **125**, 15608 (2003).
- [20] M. Feyereisen, G. Fitzgerald, and A. Komornicki, *Chem. Phys. Lett.* **208**, 359 (1993).
- [21] F. Weigend and M. Häser, *Theor. Chem. Acc.* **97**, 331 (1997).
- [22] P. Jurecka, P. Nachtigall, and P. Hobza, *Phys. Chem. Chem. Phys.* **3**, 4578 (2001).
- [23] W. D. Cornell, P. Cieplak, C. I. Bayly, I. R. Gould, K. M. Merz, D. M. Ferguson, D. C. Spellmeyer, T. Fox, J. W. Caldwell, and P. A. Kollman, *J. Am. Chem. Soc.* **117**, 5179 (1995).
- [24] M. Kabeláč, K. Kleinermanns, M. de Vries, and P. Hobza, to be published.
- [25] S. Boys and F. Bernardi, *Mol. Phys.* **19**, 553 (1970).
- [26] R. Ahlrichs, M. Bar, M. Haser, H. Horn, and C. Kolmel, *Chem. Phys. Lett.* **162**, 165 (1989).

- [27] J. M. Bakker, L. Mac Aleese, G. Meijer, and G. von Helden, Phys. Rev. Lett. **91**, 203003 (2003).
- [28] H. Piest, G. von Helden, and G. Meijer, J. Chem. Phys. **110**, 2010 (1999).

Observed	Calculated structure C	Mode description structure D	structure D (if different)
514	515 or 506	508	
538	534	535	cyt CO o.o.p. bending
559	-	-	
628	578	598	
636	611	616	
675	652	651	gua i.p. skeletal
705	689	694	
740	717	710	
785	-	-	
818	-	-	
845	853	852	
928	895	957	
965	940	941	
1000	988	987	
1071	1043	1039	
1129	1095	1096	
1152	1159	1186	
1199	1205	1206	
1269	1273	1274	
1330	1311	1312	
1374	1355; 1360	1359	
1401	1384	1384	
1429			
1441	1425	1423	
1462			
1515	1523	1525	
1558	1559	1562	
1639	1645; 1625; 1601	1645;1629;1602	
1706	1726	1724	

gua N9H o.o.p. bending or cyt CO o.o.p. bending
 cyt i.p. skeletal
 gua NH2 o.o.p. bending
 gua NH2 o.o.p. bending; gua i.p. skeletal
 gua o.o.p. skeletal
 gua N1-C2-N3 o.o.p. bending
 cyt NH2 o.o.p. bending
 gua N1H o.o.p. bending
 gua N7-C8-N9 i.p. bending
 cyt C5H, C6H o.o.p. bending
 cyt C5H, C6H, NH2 i.p. bending
 gua C8H, N9H i.p. bending
 cyt C5H, C6H, NH2 i.p. bending
 gua i.p. skeletal
 cyt OH i.p. bending
 cyt C6H i.p. bending
 cyt C5H, C6H, NH2 i.p. bending
 gua N1H, N2H, N9H i.p. bending; gua i.p. skeletal
 cyt i.p. skeletal
 cyt i.p. skeletal, gua N8H i.p. bending
 gua i.p. skeletal
 cyt i.p. skeletal
 gua i.p. skeletal
 cyt NH2 scissor;gua NH2 scissor, N1H i.p. bending;cyt NH2 scissor, cyt skeletal
 gua C=O stretching, gua N1H i.p. bending

Table 6.1: Table of observed frequencies (in cm^{-1}) for the guanine-cytosine complex, the assigned theoretical mode (from structures C and D) and a description of the associated vibration. When an observed resonance is assigned to multiple theoretical modes the line positions and descriptions of these modes are separated by a semicolon. The following abbreviations are used: i.p.: in-plane; o.o.p.: out-of-plane. cyt.: cytosine; gua.: guanine.

CHAPTER 7

THE IR ABSORPTION SPECTRUM OF BENZYL- β -LACTOSIDE

The IR absorption spectrum of the gas-phase disaccharide benzyl β -lactoside is recorded in the 330–1650 cm^{-1} region. The spectrum of the largest system investigated in this thesis using IR-UV double resonance methods still exhibits a very clear and fingerprint-like structure in this spectral region. The combination of the present data with IR spectroscopic data recorded in the O–H stretching vibration region leads to an assignment of the IR spectrum to that of a structure with the lowest calculated energy. This structure has glycosidic torsion angles of ϕ (H1-C1-O-C4') $\sim 180^\circ$ and ψ (C1-O-C4'-H4') $\sim 0^\circ$ which correspond to a rotation of $\sim 15^\circ$ about the glycosidic bond compared to the accepted solution-phase conformation. Strong inter-ring hydrogen bonds rigidify the gas-phase structure.

Adapted from: R. A. Jockusch, R. T. Kroemer, F. O. Talbot, J. P. Simons, L. C. Snoek, P. Çarçabal, M. Havenith, J. M. Bakker, I. Compagnon, G. Meijer, and G. von Helden, *J. Am. Chem. Soc.* **126**, 5709–5714 (2004).

7.1 Introduction

The biological activities of oligosaccharide chains bound in glycoproteins or glycolipids are intimately linked to their structures and conformations [1, 2]. Many selective cell-cell interactions and molecular recognition processes involve glycoconjugates. Specificity is often already present even at the monosaccharide level, and specificity for disaccharides may be a thousandfold higher. Exploration and characterization of the hydrogen-bonded conformational landscapes of oligosaccharides is an essential first step in understanding the origins of their molecular specificity. The component sugar ring units in oligosaccharide chains are generally taken to be rigid, but the same assumption cannot be made about the glycosidic links between them - the types of linkages and torsion angles about these links are the primary determinants of their overall conformation(s). Unfortunately, the assignment of oligosaccharide structure and conformation is a notoriously demanding activity due to the chemical similarity of component monosaccharides, which all contain multiple hydroxyl groups, capable of extensive intra- and intermolecular hydrogen bonding networks. In some circumstances the glycosidic linkages may be 'stiffened' by hydrogen-bonded interactions across them, thereby influencing both their shape and their structural and biological specificity [3, 4]. In others, the glycosidic linkages may be highly flexible. This flexibility hinders crystallographic structural determinations; it also complicates or limits NMR (solution phase) structural assignments based upon time-averaged measurements [5]. Computational studies of (gas-phase) oligosaccharide structure are handicapped by uncertainties in the parameters employed in molecular mechanics calculations, and *ab initio* calculations are restricted by molecular size and complexity constraints [6–9] - though with the current rate of increase in computer power, these restrictions are diminishing rapidly. Calculations of oligosaccharide conformations in solution are constrained by the additional complexity introduced by interactions with the solvent [4, 6, 10]. Taken together, these limitations represent a very significant challenge to experiment and to reliable molecular modeling.

Recently, IR spectroscopy in the near-IR probing the O–H stretching vibrations has been applied to study the structure of two monosaccharides, phenyl- β -D-galactopyranoside and phenyl- β -D-glucopyranoside, and to hydrated clusters of the latter [11–13]. In all cases the combination of IR spectral data with *ab-initio* data proved sufficient for a detailed structural assignment, especially as the O–H stretching vibrations turned out to be very sensitive to local variations. This sensitivity gives rise to optimism about the possibility to identify the structures of even larger systems. For saccharide systems so far no information in the fingerprint region is available, and the interesting question whether other vibrational modes are as sensitive to the environment as the O–H stretching vibrations has not yet been answered. *A priori* one could suspect that the C–O–H twisting or bending vibrations could also be a good identifier of the structure of the system.

Lactose, a very common disaccharide consisting of a glucose and a galactose unit, presents a good choice for an investigation of both the possibility to apply the combination of IR spectroscopy and *ab-initio* calculations to identify the gas phase structure of larger systems, and to the sensitivity of the mid-IR fingerprint region to probe larger hydrogen bonding networks. NMR studies of lactose in solution indicate the dominance ($> 85\%$) of a single conformation in which the hydroxymethyl groups of the two rings adopt a *trans* orientation about the glycosidic linkage [with the glycosidic torsion angles, ϕ (H1-C1-O-C4') $\sim 35^\circ$, ψ (C1-O-C4'-H4') $\sim -21^\circ$ [8, 14, 15]. X-ray diffraction and NMR studies of lactose bound in proteins also indicate the adoption of a *trans* conformation [16]. In contrast, empirical force field and *ab initio* computational studies of lactose and of its near relative, cellobiose (Glc- β -D-Glc), indicate at least three regions of torsional stability about the glycosidic

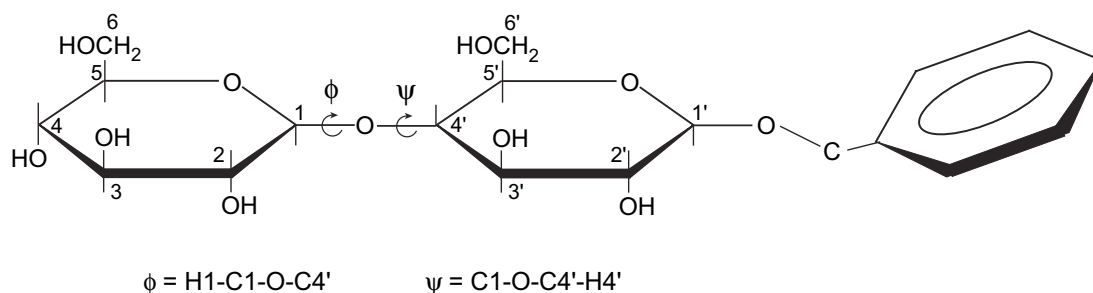


Figure 7.1: Chemical structure of benzyl β -lactoside (*O*-4-benzyl β -D-Gal-(1)- β -D-Glc)

linkage [7–9, 17, 18]. The mimic C-lactose, in which the oxygen bridge is replaced with a CH_2 group, appears to be much more flexible; it populates all three regions of torsional stability in solution and its conformers are differentially selected by different (O-lactose binding) proteins [19].

In this chapter, the IR absorption spectrum of benzyl β -lactoside (*O*-4-benzyl β -D-Gal-(1)- β -D-Glc, depicted in Figure 7.1) is presented. This study is complementary to an investigation in the near-IR by R.A. Jockusch *et al.* [20]. The addition of the benzyl ring to lactose creates a 'spectroscopically friendly' system, which can be probed easily with UV lasers [11, 12]. Addition of the benzyl ring is not expected to disturb the original lactose conformational preferences, as has been shown in ab-initio computed structures of methyl β -lactoside [20].

7.2 Results and discussion

The IR absorption spectrum of benzyl β -lactoside is recorded via IR ion-dip spectroscopy using the laser desorption source. The R2PI spectrum of benzyl β -lactoside contains resonance structure for only a single conformer in the vicinity of 38000 cm^{-1} [20]. Despite the potentially large range of conformations that might have been expected *a priori* in the vapor (different rotamers of the hydroxyl and hydroxymethyl groups [11, 12, 21] in conjunction with the three sets of disaccharide bond torsion angles), only one conformer appears to be abundant. This could be due to its selective population in the desorbed sample or to the relaxation of an initial population distribution into a single conformation as the lactoside is cooled to low temperatures during the free-jet expansion. As temperatures that are involved in the evaporation process (be it oven- or laser desorption based) are rather high and should allow for isomerization between different conformers, it is expected that the latter is the most probable explanation.

In Figure 7.2 the IR absorption spectrum of laser desorbed, jet-cooled benzyl- β -lactoside recorded in the region between 330 cm^{-1} and 1650 cm^{-1} is depicted. The UV probe laser (frequency-doubled dye laser, Coumarin 540A) is tuned to the main feature in the R2PI spectrum at 38000 cm^{-1} . In the spectrum more than 30 separated lines can be identified, whose widths are mainly determined by the FELIX spectral profile. From the line shapes it can be seen that the resonances in the low energy range are the result of single vibrational modes, whereas in the high energy region the resonances are clearly incorporating multiple vibrational modes. All resonance frequencies are indicated in the figure and are also given in Table 7.1.

To assign the observed spectrum to a structure of benzyl- β -lactoside, density functional theory calculations are performed [20, 22]. An ensemble of starting structures for benzyl- β -lactoside was

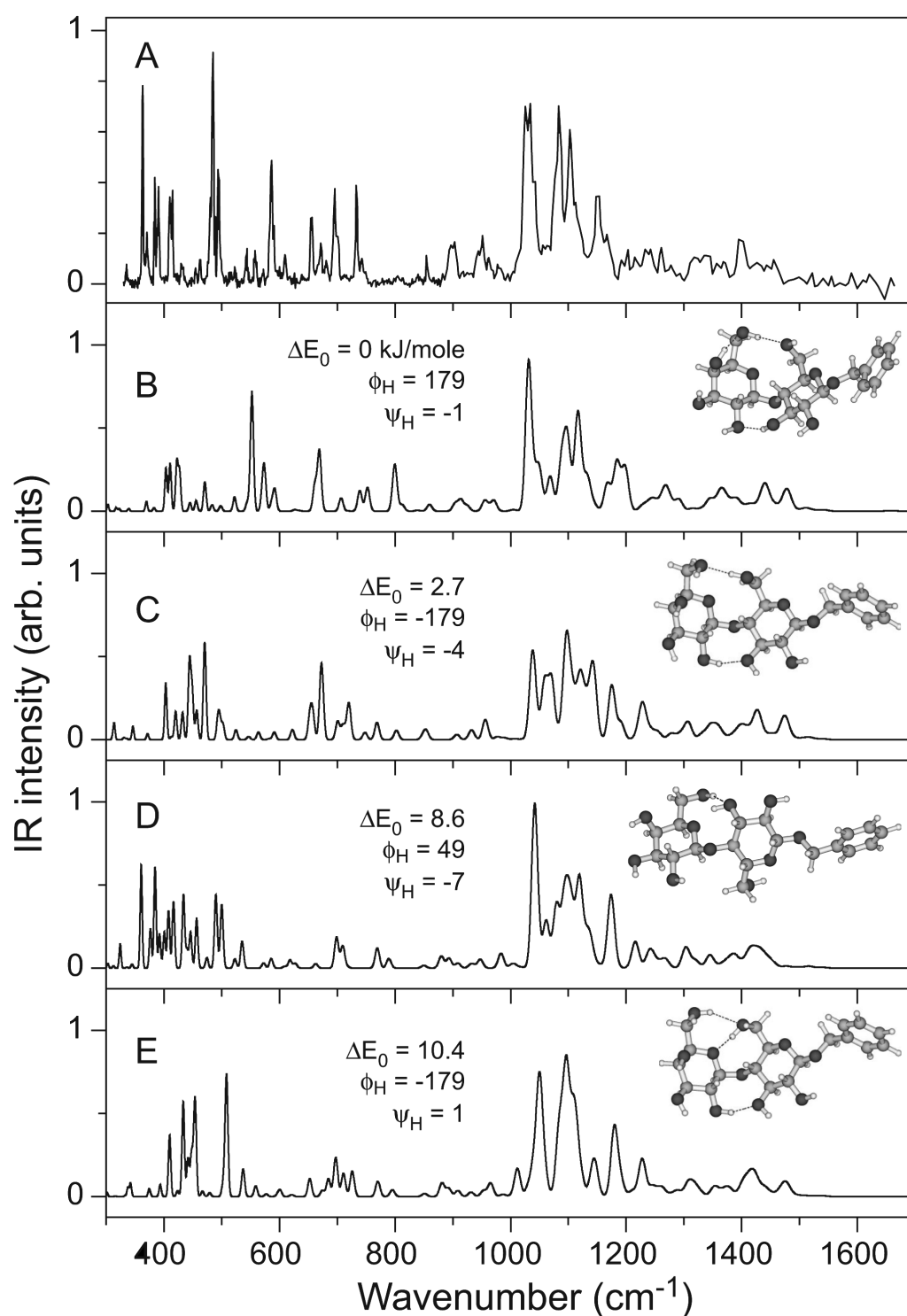


Figure 7.2: The IR absorption spectrum of benzyl β -lactoside (panel A). Below the experimental spectrum four calculated spectra of the shown geometries are displayed. Each structure is characterized by the relative energies (in kJ/mole), calculated at the MP2/6-311++G(d,p) level including zero-point vibrational energy (calculated at the B3LYP/6-31G level) and by the torsional angles describing the glycosidic linkage (in degrees).

generated using the random search procedure implemented in Sybyl 6.5 [23]. In the search, all rotatable bonds (the seven OH groups, the hydroxymethyl groups, the glycosidic linkage and the linkage to the benzyl moiety) were included as were different ring conformations. 10,000 tries/searches were performed, and 214 unique low-energy conformations were identified. Subsequent *ab initio* calculations were done using the Gaussian98 package[24]. The 214 conformers were submitted to full geometry optimization at the HF/3-21G level. For each of the optimized conformers, a single point calculation at the B3LYP/6-31+G* level was carried out. The resulting energies indicated the presence of 20 unique conformers within 25 kJ/mole of the minimum energy conformer. These 20 structures were then re-optimized at the B3LYP/6-31+G(d) level, after which 12 conformers were within the 25 kJ/mole energy cut-off. Harmonic frequencies for each of the remaining 12 conformers were calculated at the B3LYP/6-31+G(d) level of theory. Single-point energies for each of these conformers were evaluated at the MP2/6-311++G(d,p) level and include zero-point energy corrections from the B3LYP/6-31+G(d) frequencies. The four lowest energy structures (depicted in Figure 7.2) have energies within ~ 10 kJ/mole. They all exhibit extensive intra-molecular hydrogen bonds, where it is interesting to note that the hydrogen bonded networks in two lowest energy structures almost completely circle the whole lactose unit.

Below the experimental spectrum the calculated IR spectra associated with each of the four lowest-lying computed conformations are shown. The calculated stick spectra (unscaled frequencies) are convoluted with a Gaussian function representing the FELIX spectral profile. Comparison of the experimental spectrum to the computed spectra does not allow for an unambiguous assignment. The match between experimental and theoretical spectra in the region between 900 cm^{-1} and 1300 cm^{-1} is quite reasonable for all four structures, but much less convincing for the $400\text{--}800\text{ cm}^{-1}$ spectral region. The best agreement appears to be for the structures depicted in panels B and E. Although one is tempted to assign the observed spectrum to the lowest energy structure, the present data do not unambiguously support this assignment.

Given the sensitivity of the O–H stretching vibrational frequencies to the hydrogen bonding environment observed earlier in monosaccharides [11–13], assignment is expected to be much more unambiguous with the data that was recorded in the $3350\text{--}3700\text{ cm}^{-1}$ region [20]. The spectrum of benzyl- β -lactose in the near-IR spectral region by Jockusch and co-workers, is depicted in Figure 7.3, together with the stick spectra for the four lowest energy conformers. It is immediately clear that the data in the near-IR do allow for an unambiguous assignment of the gas-phase IR spectra to the lowest energy structure [20].

In order to understand why the near-IR spectrum proves more telling in the assignment of the structure, the types of vibrations that are probed in the mid-IR need to be known. Therefore, the mid-IR spectrum is now discussed in somewhat more detail. From comparison of the experimental spectrum (panel A) in Figure 7.2 with the calculated spectrum (panel B) one can see that the experimental spectrum seems to fall into two parts. One is the high-energy part between 800 cm^{-1} and 1500 cm^{-1} , where the match with the calculated spectrum is rather good. In this region all resonances can be assigned to a peak (resulting from one or more overlapped vibrational modes) in the calculated spectrum. The vibrations are mostly rather delocalized and contain skeletal distortions of the monosaccharide units or the benzyl ring or coupled C–O–H and C–C–H bending modes. When comparing the experimental and calculated spectra in the second part, at lower frequencies between 300 and 800 cm^{-1} , it appears that the frequencies of the calculated modes have shifted. Although relative intensities seem reasonably well reproduced, when taking this frequency shift into account, several

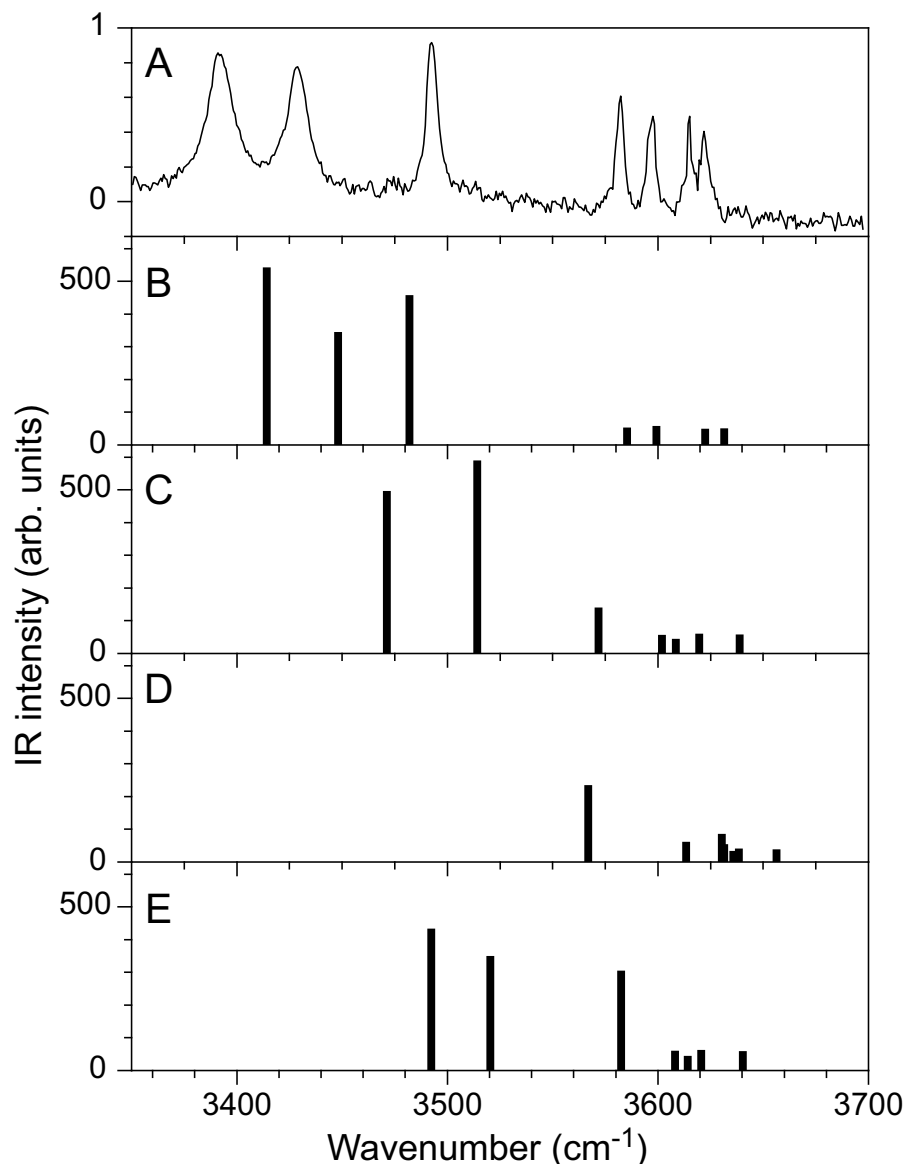


Figure 7.3: IR spectrum of benzyl β -lactoside measured in the $3350\text{--}3700\text{ cm}^{-1}$ range by Jockusch *et al.*[20]. The theoretical stick spectra below the data are shown in the same order as in figure 7.2. The frequencies are scaled by a factor of 0.9734.

calculated lines are predicted to be much stronger than observed. Most of the vibrational modes in this region are also rather delocalized and are associated with twisting motions of the hydroxyl groups coupled through the hydrogen-bond chains. The frequencies of all observed resonances can be found in Table 7.1. For resonances that have a one to one correspondence to theoretical modes, one or more calculated frequencies are included together with a description of the modes.

It is interesting to note that although the mid-IR spectrum contains more lines - and thus intrinsically more information - than the near-IR spectrum, assignment of the mid-IR spectrum to that of a calculated structure is much more ambiguous. When the experimental and theoretical spectrum of the assigned structure are compared in the $800\text{--}1500\text{ cm}^{-1}$ region, which is very congested with vibra-

Observed	Theory	Assignment
335		
363	403	C6'OH, C2'OH twist
370	411	C6'OH, C2'OH twist
384	422	C6'OH, C2'OH twist
390	427	C6'OH twist
410		
415	471	C2OH, C3OH twist
431		
455		
462		
485	552	C2OH, C3OH twist
494	571/574	C4OH, C6OH twist
523		
553		
558		
587	669	C3'OH twist
609	707	phenyl C–H o.o.p. bend
656		
672		
681		
696		
733	800	C4OH, C6OH bend
742		
854	859	Glc skeletal
900	913	Gal skeletal
951	955/971	Glc, Gal skeletal / Glc skeletal
1030	1031/1032	C2'OH, C6'H ₂ , C6'OH bend, C1'OC5' stretching /C2OH, C2C3H, OC1H bend
1083	1089/1098/1099	C2OH, C3OH, C2C3H bend/Gal skeletal/Glc skeletal
1103	1114/1116/1119	benzyl C–C–H i.p./ Glc, Gal, benzyl skeletal / Gal skeletal
1150	1168/1184/1198	Glc skeletal / Glc skeletal / Gal skeletal
1233		
1325		
1397	1439/1441	C6'OH, C5'C6'H bend / C2C3H, C3OH bend
1456	1475/1480	C2C1H, C2OH, CH ₂ (benzyl-link) bend / C6OH, C6'OH, C4'OH bend

Table 7.1: Frequencies of observed resonances (in cm^{-1}) in the IR absorption spectrum of benzyl- β -lactoside together with the calculated frequencies and descriptions of the assigned vibrations.

tional structure, the match can be concluded to be rather good. Therefore, it appears that the current level of theory is good enough to describe the skeletal and bending vibrations, even though many of these are rather delocalized. In principle this region could thus serve well as a spectral fingerprinting region of the molecular conformation. Unfortunately, the spectral properties of FELIX make from the more than 30 expected modes with IR intensity a structured, but not completely resolved spectrum. With the absolute frequency shifts that are predicted for vibrational modes in different geometries, the resulting IR spectra will change mainly in the shape of the resonance structure, but no dramatically changed resonances will appear. This effect is illustrated well when one compares the differences in the calculated spectra between 800 cm^{-1} and 1500 cm^{-1} in Figure 7.2. The highly localized O–H stretching vibrations that are probed in the $3350\text{--}3700\text{ cm}^{-1}$ region form an indirect probe of the intramolecular hydrogen bonds. As these play such an important role in stabilizing the structure, the vibrations that are sensitive to changes in the hydrogen bonding environment are more telling than the more delocalized skeletal modes. The stretching modes consequently exhibit much larger differences in the calculated frequencies, and are thus more suitable for assignment. Moreover, the near-IR spectral region is not as congested as the region of the skeletal vibrations: the region probed spans roughly 400 cm^{-1} and there are only seven modes with IR intensity. In the equally large range of $900\text{--}1250$

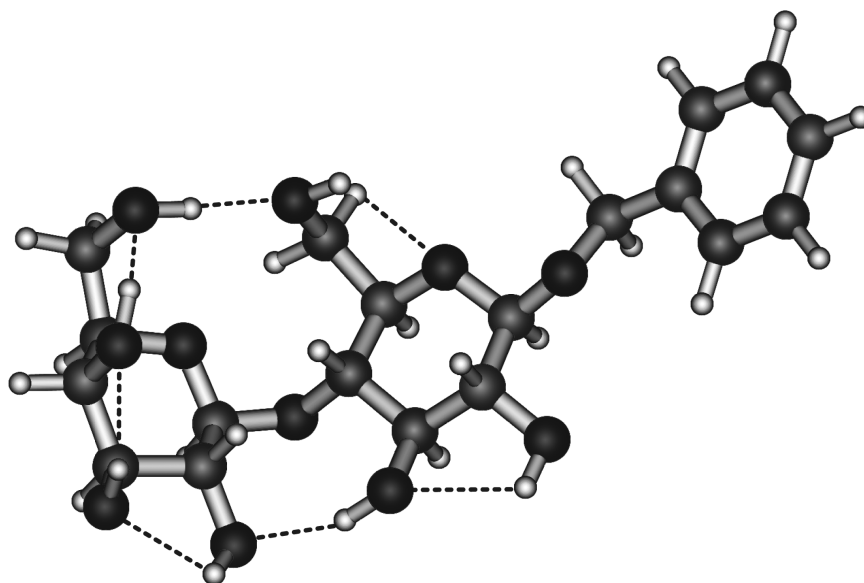


Figure 7.4: Assigned structure of benzyl β -lactoside. The intra-molecular hydrogen bond network that stabilizes the structure is indicated with dashed lines.

cm^{-1} there are 31 calculated modes with appreciable IR intensity.

For the vibrations in the $300\text{--}800\text{ cm}^{-1}$ region the current theoretical techniques do not seem to provide an accurate description of the vibrational modes. All modes found here involve twisting motions of hydrogen atoms that are directly involved in a hydrogen bond. Already in Chapter 4 it was observed that the theoretical methods employed in this work do not reproduce all vibrations involving bonded hydrogens sufficiently accurate. It follows that for a system in which hydrogen bonded networks play such an important role, more advanced methods are required.

The global minimum conformation, depicted in Figure 7.4, is associated with a *cis* orientation of the two hydroxymethyl groups and corresponds to the dihedral angles of $\phi \sim 179^\circ$ and $\psi \sim -1^\circ$. The structure is characterized by a hydrogen-bonded chain, $\text{OH}2'\text{--OH}3'\text{--OH}2\text{--OH}3\text{--OH}4\text{--OH}6\text{--OH}6'$, which circles around the lactose unit. This structure is similar to one of the observed conformations of the mimic C-lactose [19], and it parallels the density functional theory predictions for the analogous β -(1) linked di-saccharide, cellobiose ($\text{Glc-}\beta\text{-(1-Glc)}$) [3, 25]. Calculations using the semi-empirical AMBER force field with a low dielectric constant also favor a *cis* orientation [8]. On the other hand, calculations using another popular semi-empirical force field, MM3, predict a *trans* conformation about the glycosidic linkage to be the global minimum for methyl β -lactoside [26]. Moreover, the gas-phase results presented here contrast with the *trans* glycosidic conformation adopted by (room temperature) methyl lactoside in solution [8], in its crystalline methanol solvate [27] and bound in proteins [16]. The difference is not due to the presence of the benzyl group. Calculated structures of methyl β -lactoside show virtually no change in structure of the galactose structure compared with benzyl β -lactoside [20]. Substitution of the benzyl group by an OH group would most likely simply lengthen the encircling hydrogen-bond chain through formation of a $\text{Glc OH}1'\text{--Glc OH}2$ bond. However, the lactoside structure may well be affected by both the low temperature and the absence of solvent molecules. The *cis* configuration found at low temperature in the isolated lactoside allows the formation of strong inter-ring hydrogen bonds on two sides of the glycosidic

linkage to create a rigid di-saccharide structure and because of this, the enthalpic benefit of the strong hydrogen bonds is somewhat diminished by the loss in flexibility. There is an entropic cost, and it is the *trans* configuration that is favored entropically [18]. Gibbs free energy calculations (room temperature; harmonic frequencies) indeed significantly stabilize the *trans* conformer over the *cis* and predict the *trans* to be the most stable conformer at room temperature by ~ 2 kJ/mole [20]. However, the low-temperature favored *cis* conformer should still be present, at about half the abundance of the *trans* conformer. Specific complexation of the di-saccharide with water molecules may also alter the preferred conformation about the glycosidic linkage [4].

7.3 Conclusions

The IR absorption spectrum of benzyl β -lactoside is recorded in the 330–1650 cm^{-1} region. The previous assignment, based on spectroscopic information in the 3350–3700 cm^{-1} region, to a conformation in which the two monosaccharide units are linked in a *cis*-configuration is confirmed. The observation of benzyl β -lactoside in the *cis*-configuration is in contrast with the generally accepted liquid phase structure (a *trans*-configuration), but it is not unlikely that the stabilization due to a circling network of intra-molecular hydrogen bonds is favored by the cold, isolated environment experienced in the free-jet expansion. The observed vibrational structure could well be used to identify the conformational structure, but the present theoretical methods are as yet insufficient to treat the low-energy torsion-like vibrations that are coupled through the hydrogen bonding network. The present data can thus form a good benchmark for future theoretical methods.

References

- [1] R. A. Dwek, *Chem. Rev.* **96**, 683 (1996).
- [2] H. Lis and N. Sharon, *Chem. Rev.* **98**, 637 (1998).
- [3] J. Yu-Jen Chen and K. J. Naidoo, *J. Phys. Chem. B* **107**, 9558 (2003).
- [4] K. J. Naidoo and J. Yu-Jen Chen, *Mol. Phys.* **101**, 2687 (2003).
- [5] M. R. Wormald, A. J. Petrescu, Y.-L. Pao, A. Glithero, T. Elliott, and R. A. Dwek, *Chem. Rev.* **102**, 371 (2002).
- [6] A. Imberty and S. Pérez, *Chem. Rev.* **100**, 4567 (2000).
- [7] A. D. French, G. P. Johnson, A.-M. Kelterer, M. K. Dowd, and C. J. Cramer, *Int. J. Quantum Chem.* **84**, 416 (2001).
- [8] L. Asensio and J. Jimenez-Barbero, *Biopolymers* **35**, 55 (1995).
- [9] S. B. Engelsen, J. Koca, I. Braccini, C. Hervé du Penhoat, and P. Pérez, *Carbohydr. Res.* **276**, 1 (1995).
- [10] K. J. Naidoo and J. Brady, *J. Am. Chem. Soc.* **121**, 2244 (1999).
- [11] F. O. Talbot and J. P. Simons, *Phys. Chem. Chem. Phys.* **4**, 3562 (2002).
- [12] R. A. Jockusch, F. O. Talbot, and J. P. Simons, *Phys. Chem. Chem. Phys.* **5**, 1502 (2003).
- [13] R. A. Jockusch, R. T. Kroemer, F. O. Talbot, and J. P. Simons, *J. Phys. Chem. A* (2525).
- [14] M. L. Hayes, A. S. Serianni, and R. Barker, *Carbohydr. Res.* **100**, 87 (1982).
- [15] N. W. Cheetham, P. Dasgupta, and G. E. Ball, *Carbohydr. Res.* **338**, 955 (2003).
- [16] H. M. Berman, J. Westbrook, Z. Feng, G. Gilliland, T. Bhat, H. Weissig, I. N. Shindyalov, and P. E. Bourne, *Nucl. Acids. Res.* **28**, 235 (2000).
- [17] F. Cloran, I. Carmichael, and A. S. Serianni, *J. Am. Chem. Soc.* **121**, 9843 (1999).
- [18] S. B. Engelsen and K. Rasmussen, *J. Carbohydr. Chem* **16**, 773 (1997).
- [19] J.-F. Espinosa, F. J. Canada, J. L. Asensio, M. Martín-Pastor, H. Dietrich, M. Martín-Lomas, R. R. Schmidt, and J. Jiménez-Barbero, *J. Am. Chem. Soc.* **118**, 10862 (1996).
- [20] R. A. Jockush, R. T. Kroemer, F. O. Talbot, J. P. Simons, L. C. Snoek, P. Çarçabal, M. Havenith, J. M. Bakker, I. Compagnon, G. Meijer, et al., *J. Am. Chem. Soc.* **126**, 5709 (2004).
- [21] A. Roën, J. I. Padrón, and J. T. Vázquez, *J. Org. Chem.* **68**, 4615 (2003).
- [22] Theoretical calculations for this work are performed by Romano Kroemer.
- [23] M. Clark, R. Cramer, and N. Opdenbosch, *J. Comput. Chem.* **10**, 982 (1989).

- [24] M. J. Frisch, G. W. Trucks, H. B. Schlegel, G. E. Scuseria, M. A. Robb, J. R. Cheeseman, V. G. Zakrzewski, J. J. A. Montgomery, R. E. Stratmann, J. C. Burant, et al., *Gaussian 98, Revision A.7*, Pittsburgh, PA (1998).
- [25] G. L. Strati, J. L. Willett, and F. A. Momany, *Carbohydr. Res.* **337**, 1833 (2002).
- [26] A. Rivet, C. Sabin, K. Mazeau, A. Imberty, and S. Perez, <http://www.cermav.cnrs.fr/> (2003), accessed May 2003.
- [27] R. Stenutz, M. Y. Shang, and A. S. Serianni, *Acta Cryst.* **C55**, 1719 (1999).

SUMMARY AND OUTLOOK

Weak intra- and intermolecular interactions as well as subtle electronic effects can have a large influence on molecular structure. Infrared (IR) spectroscopy can be a useful tool to investigate these effects. In this thesis, a Free-Electron Laser is used to study several molecular model systems using UV-IR double-resonance techniques. The aim is to compare the experimental spectra with results from quantum chemical methods to obtain information on the species studied. Whether this will be of success depends on the answer to two simple questions: a) Is the experiment good enough and b) Is theory good enough.

In the experiments on the gas-phase biomolecules, a key question is whether conformational differences in flexible molecules can actually be observed in the mid-IR wavelength range that is covered by FELIX. Based on the work presented here, this question can be answered positively. In all systems studied, well-discernible IR spectral structure is observed that is sharp enough to be able to differentiate between various conformers. Specifically, in Chapter 5, where three different conformers of a single amino acid are investigated, it is convincingly demonstrated that the spectroscopic techniques are adequate for this purpose. In all other cases, the investigation of single conformers of biomolecules has led to spectroscopic data that are sufficiently characteristic that they could either lead to unambiguous assignments or, at least, to strong evidence for specific classes of conformations.

The second question is whether the currently used (standard) theoretical methods are sufficiently accurate to allow for the spectroscopic data to be evaluated meaningfully. It must be concluded that present theory can be very accurate for certain types of vibrations, but less so for others. For high frequency stretching vibrations (as studied by others) and other strongly localized bending and deformation vibrations, the theoretical methods are adequate. For, mostly low-frequency, de-localized and coupled vibrations, problems can arise. Particularly in the experimental study on benzyl- β -lactoside (Chapter 7), the theoretical treatment of the O–H twisting vibrations, which could be key spectral feature for the derivation of structural conformation, is inadequate. This could potentially be improved by the evaluation of anharmonicities in the calculations of vibrations, a gargantuan task.

For the future use of the here employed techniques, several restrictions can be foreseen: first of all, these studies depend strongly on double-resonance techniques. It is not at all certain that (much) larger molecules facilitate such convenient conformer-specific detection schemes as the ones used here. A possible complication is then the simultaneous probing of several conformers at once.

Second, larger molecules will exhibit more congested IR spectra, as the number of resonances will increase linearly with the number of atoms that form the molecule. For theoretical treatment the increase in number of atoms will be an even more serious problem, as the requirements on compu-

tational resources grow strongly non-linear with molecular size. A possible solution is to resort to carefully parametrized force field molecular mechanics methods.

Thirdly, to bridge the gap between IR spectroscopy of gas-phase biomolecules and the well-established field of liquid-phase IR spectroscopy of solvated biomolecules, it is required to study microsolvation effects, *i.e.*, an extension of the study of gas-phase biomolecules to gas-phase biomolecules that are complexed with one or more solvent molecules. Although already quite some work on this subject has been done in the near-IR, mid-IR spectral studies on such systems are imperative, given the before mentioned spectral congestion that is to be expected and the complications that arise with solvent-induced broadening effects.

It is hoped that the work described in this thesis, together with the work that is being done in the near-IR spectral range, can form a good starting point for future investigations.

Berlin, fall 2004

SAMENVATTING

Op het raakvlak van de biologie en scheikunde bevindt zich het vakgebied dat zich bezighoudt met vraagstukken aangaande de microscopische interacties tussen moleculen die noodzakelijk zijn voor levende organismen, de biomoleculaire chemie. Deze tak van wetenschap stelt zich ten doel biologisch macroscopische processen te vertalen naar intermoleculaire processen. Eén van haar uitgangspunten is het ontrafelen van de driedimensionale structuur van de betrokken moleculen.

In het algemeen zijn moleculen met een biologische functie (kortweg biomoleculen) tamelijk groot. Een typisch eiwit bijvoorbeeld, bevat honderden individuele atomen, gerangschikt in een lang, ketenvormig molecuul. Het is vanzelfsprekend dat een dergelijk lang molecuul een enorme flexibiliteit bezit die het in staat stelt zich te vervormen en als het ware op te rollen tot een compacte kluwen. Er is gebleken dat veel eigenschappen van de intermoleculaire reacties die plaatsvinden direct gerelateerd zijn aan de precieze vorm van de moleculen in kwestie. Veel interacties tussen biologische moleculen vinden plaats op basis van een donor-receptor proces waarbij de partners elkaar door middel van moleculaire patroonherkenning vinden. Een bekend voorbeeld hiervan zijn deoxyribonucleïnezuur (DNA) en ribonucleïnezuur (RNA), de moleculen die verantwoordelijk zijn voor de overdracht van de genetische code van levende organismen. Deze moleculen blijken maar op één unieke wijze met elkaar te wisselwerken. Ook de functionele werking van eiwitten en suikers is vaak uitsluitend bepaald door de driedimensionale structuur van het biomolecuul. De unieke eigenschap van lange ketenmoleculen in het algemeen en biomoleculen in het bijzonder is dat ze, ondanks het enorme aantal vrijheidsgraden dat ze bezitten, tijdsgemiddeld eigenlijk altijd in één zelfde opgerolde toestand ofwel conformatie worden aangetroffen. Dit bepaalt voor een belangrijk deel de functionele werking van de moleculen.

Om een beschrijving mogelijk te maken van de driedimensionale structuur van biomoleculen wordt de gehele structuur van biomoleculaire clusters in vier lagen aangeduid. Allereerst bestaat er de primaire structuur, die beschrijft hoe het molecuul met covalente bindingen uit de individuele atomen is gevormd. Het is ook gebruikelijk met de primaire structuur aan te duiden hoe macromoleculen uit individuele kleinere moleculen zijn opgebouwd. Men spreekt dan ook vaak van de ketenvolgorde of sequentie. Een veelgebruikte onderzoeksmethode in de biochemie is het ontwarren van de primaire structuur door middel van het *sequencen*, het bepalen van de volgorde van de bouwmonomeren.

Van secundaire structuur spreekt men om de (vaak locale) ruimtelijke oriëntatie van verschillende zijgroepen ten opzichte van elkaar te karakteriseren. Deze secundaire structuur wordt hoofdzakelijk bepaald door zwakkere interatomaire wisselwerkingen zoals elektrostatische (waterstofbruggen) en dispersieve interacties. Typisch zijn deze wisselwerkingen een ordegrrootte zwakker dan de covalente

bindingen waardoor de primaire structuur wordt bepaald. Voorbeelden van secundaire structuren zijn de α -helixstructuur, de β -geplooid bladstructuur en de verschillende bochtstructuren.

Een verdere karakterisatie vindt plaats met de tertiaire structuur, die op grotere schaal de substructuren binnen het macromolecuul beschrijft. De quartaire structuur tenslotte, beschrijft de conformatie van meerdere in elkaar verwikkelde biomoleculen.

Voor een goed begrip van de eigenschappen van biomoleculen is het van belang dat de inherente eigenschappen van de moleculen die de secundaire en hogere orde structuren bepalen in detail worden bestudeerd met een focus op de inter- en intramoleculaire krachten. De laatstgenoemde interacties worden sterk beïnvloed door de aanwezigheid van watermoleculen in de natuurlijke, waterige omgeving van biologische systemen. Deze zogenaamde oplosningseffecten versluieren de fundamentele eigenschappen van de biomoleculen, hetgeen het onderscheid tussen de bijdragen van het molecuul zelf en die van de watermoleculen aan de stabilisering van één bepaalde conformatie bemoeilijkt. Om dit onderscheid wel te kunnen maken worden in dit proefschrift experimenten beschreven aan moleculen die in de gasfase geïsoleerd zijn van hun omgeving. Op deze wijze zijn de fundamentele eigenschappen van de moleculen zelf ontdaan van oplossingsgerelateerde effecten. In eventuele vervolgstudies kunnen dan clusters van biomoleculen en watermoleculen worden bestudeerd waarbij bij sequentiële toevoeging van watermoleculen de oplosningseffecten als het ware worden opgebouwd.

Voor de karakterisatie van de structuren van biomoleculen in de gasfase wordt in dit proefschrift gebruik gemaakt van infraroodspectroscopie. Het infraroodspectrum is zeer nauw verbonden met de structuur van een molecuul aangezien het door de moleculaire vibraties wordt bepaald, en dus ook door de daaraan sterk gerelateerde moleculaire bindingen. Daarom wordt met behulp van verschillende spectroscopische technieken van gasfase moleculen het infraroodspectrum opgemeten ter bepaling van hun driedimensionale structuur.

Beschrijving van de experimenten

Om de infraroodspectra van de moleculen in kwestie te meten worden de moleculen samen met een inert draaggas door een gepulste klep in een vacuümkamer gelaten. Daar ondergaat de gaswolk een adiabatische expansie. De interne energie van de gaswolk wordt omgezet in kinetische energie. Alle moleculen in het gas staan door middel van binaire botsingen met draaggasatomen hun interne energie af totdat ze zich in hun elektronische en vibrationele grondtoestand bevinden. Een gedeelte van de uitzettende gaswolk wordt een tweede vacuümkamer ingelaten. Hier vindt interactie plaats met de verschillende laserbronnen.

Aangezien het geen triviale zaak is om alle typen moleculen intact in de gasfase te brengen, worden er verschillende technieken gebruikt om dit te bewerkstelligen. Van sommige moleculen heeft de vastestof of vloeistof een voldoende hoge dampdruk om een dichte wolk voor het experiment te creëren. Bij andere moleculen moet de vastestof worden verhit om de gewenste dampdruk te bereiken. Helaas blijken biomoleculen in het algemeen slecht bestand tegen verhitting, omdat er fragmentatie plaatsvindt voordat sublimatie vanuit de vastestof kan optreden. Voor deze moleculen is een techniek ontwikkeld, waarbij de moleculen op een goed gedefinieerd tijdstip vanuit een grafieten matrix met een gepulste desorptielaser in de gasfase worden gebracht. Dit proces gebeurt op een dusdanige plaats en tijd dat de biomoleculen onmiddellijk worden meegevoerd in de nog expanderende draaggaswolk en vrijwel al hun interne energie kwijtraken door botsingen met de draaggasatomen.

De infraroodspectra van de moleculen worden gemeten met twee verschillende spectroscopische

technieken. De eerste techniek, infrarood geïnduceerde fotodissociatie, wordt gebruikt voor geladen systemen. Hierbij wordt het spectrum van een heel precies geprepareerd molecuulion dat een complex vormt met een inert edelgasatoom gemeten. Aangenomen wordt dat de aanwezigheid van het edelgasatoom een verwaarloosbaar kleine invloed op het spectrum heeft. Het resulterende infraroodspectrum is dus in zeer goede benadering gelijk aan dat van het kale ion.

De tweede techniek, infrarood *ion-dip* spectroscopie, is universeel toepasbaar om de infraroodspectra van neutrale moleculen te meten. In deze techniek wordt de moleculaire populatie van de grondtoestand van het molecuul bemonsterd door in het molecuul een zeer goed gedefiniëerde elektronische overgang te induceren met een ultraviolet foton. Een tweede foton ioniseert dan het molecuul waarna het wordt gedetecteerd in een massaspectrometer. Kort voordat de elektronische overgang wordt geïnduceerd vindt er een interactie plaats tussen de moleculen en de infraroodlaser. De laatste kan een vibrationele overgang in de moleculen induceren. Wanneer dit het geval is, dan wordt een deel van de bevolking vanuit de grondtoestand naar een vibrationeel geëxciteerde toestand overgebracht. Dit heeft tot gevolg dat er minder moleculen in de grondtoestand achterblijven die bemonsterd kunnen worden door de ultravioletlaser en leidt tot een vermindering van het aantal geproduceerde en gedetecteerde ionen, een *ion-dip*. Door nu het aantal ionen te meten als een functie van de infraroodgolflengte wordt het infrarood *ion-dip* spectrum verkregen. Dit kan weer tot een infrarood absorptiespectrum worden geconverteerd. Aangezien de elektronische overgangen die door de ultravioletlaser worden geïnduceerd voor elk conformeer van een molecuul anders zijn wordt voor een gekozen ultraviolette golflengte slechts het infraroodspectrum van één molecuulair conformeer gemeten.

Een uniek gegeven voor dit werk is de beschikbaarheid van de vrije-elektronenlaser FELIX als bron voor afstembare infraroodstraling. FELIX is een bij uitstek geschikt instrument voor het uitvoeren van spectroscopisch werk aan moleculen in het mid- tot verinfrarode golflengtegebied (ruwweg van 5 μm tot 250 μm) aangezien zich in dit gebied het merendeel van de vibraties bevindt. Naast het grote bereik van de golflengte maken de continue golflengteafstembaarheid, de resulterende lichtenergie die beschikbaar is voor de gasfase experimenten (typisch 100 mJ in 5 μs) en de voor vibrationele spectroscopie zeer acceptabele bandbreedte dit instrument tot een ideaal hulpmiddel.

Voor de interpretatie van de gemeten spectra worden quantumchemische berekeningen uitgevoerd. Van een aantal verschillende conformaties van het molecuul wordt het infraroodspectrum uitgerekend waarmee het gemeten spectrum vergeleken kan worden. Op basis van een gevonden gelijkenis kan het gemeten spectrum dan aan een specifieke structuur worden toegekend.

Resultaten

Alhoewel alle experimenten die in dit proefschrift worden beschreven als modelsysteem kunnen worden beschouwd, kan het eerste toch als een klassieker worden beschouwd: in hoofdstuk 2 wordt het infraroodspectrum van het benzeenion gemeten door middel van infrarood fotodissociatie. Het mag verbazing wekken dat van een zo belangrijk molecuul het infraroodspectrum van het ion aan het einde van de 20^e eeuw nog niet bekend is. De huidige meetmethoden nemen de barrière weg om het infraroodspectrum van het benzeenion te bestuderen. Daarnaast lenen de experimenten zich uitstekend voor een verkenning van de mogelijkheden van de beschikbare methoden. Bovendien is het benzeenion een klassiek modelsysteem voor bestudering van het Jahn-Tellereffect, een quantummechanisch effect waarin door middel van een koppeling tussen elektronische en bepaalde vibrationele toestanden

de hoogsymmetrische structuur van benzeen wordt vervormd.

De in dit proefschrift beschreven experimenten aan het benzeenion dragen bij tot een quantitatief begrip van de vibratie-eigenschappen van dit belangrijke molecuul-ion. Ook wordt aangetoond dat de invloed die het edelgasatoom heeft op het infraroodspectrum miniem is in het geval van neon als gebonden edelgasatoom, maar dat er aantoonbare verschillen bestaan als argon wordt gebruikt. Tenslotte wordt beschreven dat het er sterk op lijkt dat in het systeem benzeen- Ar_2^+ ook de twee argonatomen, die zich aan weerszijden van het benzeenmolecuul bevinden, onderhevig zijn aan het Jahn-Tellereffect.

In hoofdstuk 3 wordt het neutrale benzeen dimeer bestudeerd. Van dit systeem, dat model staat voor de interactie tussen twee moleculen door puur dispersieve krachten, bestaan twee voorspelde structuren: een T-vormige, waarbij één van de benzeenmoleculen de stam en één de dwarsbalk van de T vormt, en een parallelle structuur waarin de benzeenmoleculen enigszins van elkaar afgeschoven zijn. Historisch zijn er zowel voorstanders van de T-vormige als van de parallel verplaatste structuren geweest. De hier beschreven experimenten wijzen in de richting van een T-vormige structuur. Er zijn zelfs tekenen die op een enigszins vervormde T-structuur wijzen. Tevens blijkt dat het infraroodspectrum van het dimeersysteem nauwelijks afwijkt van dat van het monomeer, een bewijs van de slechts uiterst kleine invloed van de dispersieve krachten die het dimeer stabiliseren op de individuele monomeren waaruit het dimeer bestaat.

Na de studie van de invloed van dispersieve krachten op het infraroodspectrum wordt in hoofdstuk 4 een systeem onder de loep genomen dat door middel van twee waterstofbruggen verbonden is: het benzoëenzuur dimeer. De verschillen tussen de spectra van het monomeer en van het dimeer zijn aanzienlijk. Hieruit blijkt dat de aanwezigheid van een dubbele waterstofbinding het infraroodspectrum sterk beïnvloedt.

Omdat dit een berekeningstechnisch nog vrij klein systeem is geldt het als een proeve voor de rekenmethodes die gebruikt kunnen worden voor grotere systemen. De gebruikte theoretische methode slaagt goed in de voorspelling van de infraroodspectra van zowel monomeer als dimeer en kan dus met vertrouwen gebruikt worden in meer gecompliceerde systemen. Eén aspect van de – vaak gebruikte – theoretische methode blijkt niet toereikend in de beschrijving van dit moleculair systeem: de berekende frequentie van de vibratie waarbij de beide waterstofatomen in de $\text{C}-\text{O}-\text{H} \cdots \text{O}=\text{C}$ bindingen door het vlak van de moleculen bewegen wijkt sterk af van de geobserveerde.

In hoofdstuk 5 wordt het zeer flexibele molecuul tryptofaan bestudeerd. Tryptofaan kan in een groot aantal verschillende conformaties, die worden gekenmerkt door intramoleculaire waterstofbindingen, voorkomen. Van drie van de in totaal zes ooit waargenomen conformeren is het infraroodspectrum gemeten en er blijken tussen de spectra van verschillende conformeren grote verschillen te bestaan. De in hoofdstuk 4 geteste theoretische methode blijkt wederom in staat om op basis van de vergelijking tussen berekende en gemeten spectra de gemeten spectra uniek toe te kennen aan bepaalde berekende structuren. Nadat in eerder onderzoek in het midinfrarode golflengtegebied al was gebleken dat de spectra gevoelig waren voor conformatieverschillen, bewijst dit eerste onderzoek van een zo flexibel molecuul in het midinfrarode golflengtegebied dat ook hier structurele identificatie goed mogelijk is.

Een zeer interessant biologisch systeem wordt onderzocht in hoofdstuk 6: het gasfasecluster van guanine en cytosine, twee van de vier nucleobases in DNA. De meest interessante vraag is hier of de nucleobases in afwezigheid van de suiker-fosfaat keten die de helixstructuur stabiliseert nog altijd dezelfde drievoudige waterstofverbinding aangaan in de gasfase. Uit de vergelijking van het experi-

menteel waargenomen spectrum met berekende spectra voor verschillende configuraties van guanine-cytosine blijkt dat niet de klassieke “Watson-Crick” configuratie wordt waargenomen. Het hier waargenomen guanine-cytosine complex bevat een tautomeer van guanine. Een definitieve toekenning van het geobserveerde spectrum aan een bepaalde configuratie blijkt in het hier bestudeerde golflengtebereik niet mogelijk te zijn. Hoogstwaarschijnlijk komt de “Watson-Crick” configuratie wel voor in de bundel, maar is het de UV detectie die observatie niet mogelijk maakt.

Tenslotte worden in hoofdstuk 7 experimenten beschreven aan de gesynthetiseerde disaccharide benzyl- β -lactoside. De experimenten tonen aan dat ook moleculen met een dergelijke omvang nog een uniek infraroodspectrum bezitten dat aan de hand van theoretisch berekende spectra toegekend kan worden aan een unieke conformatie. Helaas blijkt hier wel dat met de huidige voorhanden zijnde theoretische modellen bepaalde typen vibraties niet adequaat berekend worden en dat het wenselijk is deze beschrijving te verbeteren.

In grote lijnen bewijst het werk dat is beschreven in dit proefschrift dat het toepassen van midinfrarode straling voor de identificatie van structurele conformaties van flexibele (bio)moleculen een succesvolle methode is waarmee de intra- en intermoleculaire interacties op gedetailleerde wijze bestudeerd kunnen worden. In alle beschreven experimenten blijkt unieke identificatie aan de hand van een midinfrarood absorptiespectrum mogelijk. Een toekomstige belemmering zou wel eens kunnen bestaan uit het falen van theoretische berekeningen aan gekoppelde en sterk gedelocaliseerde vibraties, alsmede uit de afwezigheid van een geschikt detectiemechanisme met ultraviolet laserlicht. Niettemin vormt de grootte van het molecuul in ieder geval nog geen belemmering voor identificatie.

De in dit proefschrift beschreven methoden bewijzen daarmee dat infraroodspectroscopie een krachtig instrument vormt in de identificatie van flexibele moleculaire structuur in de gasfase.

DANKWOORD

Vroeger ging ik promoveren. Dat zou gebeuren op een dag ver, ver in de toekomst. Tot die tijd zou ik wat rondlummelen in een laboratorium, af en toe wat lasers uitlijnen, spectra van moleculen opmeten en de ermee samenhangende, lastige problemen proberen te doorgronden. Wie weet zou ik er zelf een bijdrage toe leveren dat zulke problemen beter begrepen zouden kunnen worden. Eén ding was zeker: de weg naar de promotie zou lang, en vooral zwaar zijn. Loodzwaar.

Het bleek een vergissing. Ik heb rondgelummeld, uitgelijnd, opgemeten en doorgrond. Ik heb een bijdrage kunnen leveren om natuurwetenschappelijke problemen van beter begrip te voorzien. Maar zwaar? Zwaar was het niet. Het was een feest.

Op mijn feest waren een heleboel gasten. Sommigen waren er de hele tijd, anderen kwamen even snel gedag zeggen om naar een volgende afspraak te gaan. Van ieders aanwezigheid heb ik genoten.

Het feest is nu over, de lichten gaan aan. Het laatste biertje wordt getapt, wie weet volgt straks nog koffie. Het uur is gekomen om na te praten, om de uitnodigingen voor een volgende gelegenheid te sturen. Maar vooral om te bedanken voor de aanwezigheid op mijn feest.

Laat ik beginnen de feestzaal te complimenteren. Wat een mooi instituut is dat Rijnhuizen toch! Met zijn prachtige kasteel, zijn tuin en zijn rustige omgeving een ideale plek om een promotie te volbrengen. Ik wil hier alle afdelingen van het instituut bedanken voor de prachtige tijd die ik heb mogen doorbrengen tussen jullie. Dankzij jullie hulpvaardigheid, inspiratie of gewoon koffie met kletspraat heb ik zo'n mooie tijd gehad.

Dan de ceremoniemeester, Gerard Meijer. Gerard, in de afgelopen vier jaar heb je je voor mij bewezen als een Weltklasse wetenschapper, motivator en manager. Al duurden je bezoeken aan mijn lab in de regel niet langer dan 5 minuten, in die tijd bleek je altijd in staat je enthousiasme voor moleculen over te brengen. Je enorme parate kennis, al dan niet doorspekt met een portie bluf die je in het westen niet zou misstaan, wist je altijd wel aan te wenden om me in de goede richting te duwen als het weer eens ergens wat stroever liep. Ook toen je transfer naar Berlijn allang in kunnen en kruiken was bleek je met een verbluffende efficiëntie in staat me bij te staan. Ik heb er dan ook een vol vertrouwen in dat de komende periode minstens zo succesvol zal zijn. Dat je me ooit nog eens zult poorten, waag ik overigens te betwijfelen.

Een ambitieuze hoogleraar verpoost veel van zijn tijd onderweg om zijn ideeën te verkopen. In Gerards afwezigheid ontpopte Gert von Helden zich als de drijvende kracht in de groep. Gert, ik vond het een groot plezier met je te werken. Vooral in de overgang van het eeuwigdurende benzeen naar de biomoleculen heb ik je enthousiasme en je ijzersterke kwaliteiten op het vlak van quantum chemische berekeningen leren kennen. Met je galgehumor en je eeuwige geklaag over de Nederlandse gebruiken

en eetgewoontes was je daarnaast ook een voortdurende inspiratiebron voor wetenschappelijk misschien minder verantwoorde maar des te vermakelijkere gesprekken.

Onze groepstechnicus Jan Pluygers heb ik eeuwigvaak lastiggevalen voor hulp op het praktische vlak. Jan, je werd nooit (te) moe van me en hebt me vele malen van mijn twee linkerhanden gered. Het is voor mij zonneklaar dat zonder jou dit boekje niet tot stand was gekomen.

Avec Isabelle Compagnon j'ai fait beaucoup de voyages nocturnes entre Utrecht et Amsterdam après des shifts pleins de beaux résultats sur les biomolécules. Isabelle, j'ai apprécié les derniers shifts, et j'ai confiance que tu emporteras beaucoup de succès avec mon expériment.

Dat ik Isabelle heb kunnen inwijken in de fijne kneepjes van het werken met FELIX, is onder andere de verdienste van Hans Piest. Hans heeft me in een maand of vier alle nukken en eigenaardigheden van de opstelling geleerd. Hans, bedankt!

Middenin kreeg ik de kans mijn eigen pedagogische vaardigheden uit te oefenen op een Franse gaststudent, Luke Mac Aleese. Luke, ç'a marché pas mal, eh? Merci pour cette période et bonne chance avec tes études, toi-même.

Toen ik begon in de groep Moleculaire Dynamica liep daar zo'n druk, opgewonden standje rond, Deniz van Heijnsbergen. In de 3 jaar sindsdien hebben we met groot plezier het instituut verlevendigd, variërend van 'hulp' bij Gerts interne verhuizing en Gerards computerproblemen tot de verkeersherstructurering binnen het instituut. Dat we ook na onze promoties goede vrienden blijven is voor mij buiten twijfel. Daar helpt zelfs verhuizen naar New York niet tegen.

Samen met Rob Satink deelden Deniz en ik lange tijd een kamer. Rob, dat je al het gekleuter hebt weten te overleven mag een klein wonder heten. Anderzijds heb we ook binnen de kamer enorme lol gehad. Dankzij jouw eerdere werk aan benzeen en het Jahn-Teller effect kon ik een vliegende start maken.

Van mijn laatste kamergenoot, Dave Moore, heb ik veel plezier gehad. Nooit heb ik een Amerikaan zo snel na aankomst in Nederland zo goed Nederlands horen praten. Voor elk probleem had hij één ontstellend lang, dan wel meerdere antwoorden. Bij al zijn Amerika-bashing zou je bijna vergeten dat hij zelf Amerikaan is.

Ook de mensen binnen de groep met wie ik minder direct samengewerkt heb, Nick Polfer, André Fielicke, Karine Demyk, Britta Redlich en Jos Oomens bedank ik voor de uitstekende sfeer en behulpzaamheid.

Bij alle experimenten beschreven in dit proefschrift is gebruik gemaakt van de vrije-elektronen laser FELIX. De hulp van de FELIX-staf, bestaande uit Lex van der Meer, Britta Redlich (daar is ze weer), Giel Berden, René van Buuren, Wim Mastop, Peter Delmee en Theo Ram, is daarvoor onontbeerlijk geweest. Ik dank jullie allen nogmaals voor de uitstekende omstandigheden waaronder ik heb kunnen werken en voor de bereidheid om me tot vaak diep in de nacht al dan niet telefonisch uit de brand te helpen.

Aan de andere kant van het gebouw was een tweede groep gespecialiseerd in molecuulfysica, de Koude Moleculen. In willekeurige volgorde Rick Bethlem, Floris Cromptvoets, Jacqueline van Veldhoven, Bas van de Meerakker, Rienk Jongma, Sophie Schlunk, Jochen Küpper, Dave Carty, Allard Mosk, Wieland Schöllkopf, Boris Sartakov, Paul Smeets en André van Roij bleken een uitstekende bron van kennis, materialen en plezier. Ik heb ondertussen wel gezien dat Bas, nu hij niet meer zo hoeft te steunen om het Amsterdam-Rijnkanaal over te fietsen, een enorm succesvolle fysicus gaat worden.

Mochten er ondanks of dankzij voornoemde mensen toch nog enige frustraties hebben bestaan,

dan was er dinsdags en donderdags alle gelegenheid om die af te reageren op de bal. Menige poeier heb ik daar uitgedeeld, en het was fijn dat Rob, Deniz, Aad, Anton, Frank, Dick, Jan-Cornelis, Toon, Dave, David en Jochen daar ook waren om me nog wat verder geïrriteerd te krijgen.

Halverwege mijn promotie heb ik een kleine tweeëneenhalve maand doorgebracht in de groep van Mattanjah de Vries aan de University of California in Santa Barbara. Van Mattanjah's promovendus Ali Abo-Riziq heb ik de zwarte magie van de laser-desorptie geleerd die onontbeerlijk is gebleken voor het slagen van dit proefschrift. Later heeft Mattanjah een succesvol tegenbezoek gebracht waarvan onder andere Hoofdstuk 6 het resultaat is. Mattanjah and Ali: thanks very much for both your hospitality and the generosity to let me have a look into your kitchen. Especially Ali's mastery of the machine and his will power to force the experiments his way were a true inspiration.

Voor het laatstgenoemde hoofdstuk zijn de berekeningen uitgevoerd door Pavel Hobza en Martin Kabeláč van het Institute of Organic Chemistry and Biochemistry, van de Tsjechische Academie der Wetenschappen in Praag. Martin and Pavel, it was a pleasure to be able to collaborate.

De zomer van 2003 bestond niet. Althans, niet dat ik weet. Het grootste deel van de maand augustus heb ik opgesloten in de FELIX kelder doorgebracht met Isabelle, Lavina Snoek en Pierre Çarçabal van het Physical and Theoretical Chemistry Laboratory van de Universiteit van Oxford. Succesvolle experimenten aan tryptofaan-water clusters en aan benzyl- β -lactoside (zoals beschreven in Hoofdstuk 7 behoorden tot onze bezigheden. With much pleasure I think back to this period, in which we shared the fears whether the airco would hold it and the continuous battle for signal. I especially cherish the valuable lessons by Pierre on the proper treatment of liquid nitrogen. After much correspondence on the benzyl- β -lactoside experiments I finally got to meet with Rebecca Jockusch, Romano Kroemer (who put all his efforts in calculating the structure of benzyl- β -lactoside), Francis Talbot and John Simons at a lavish Christmas dinner in Oxford.

Ook de herfst van 2003 was druk: buiten begonnen de bladeren alweer te vallen, maar daar had ik geen erg in. Oktober 2003 zat ik weer in de kelder, deze keer met Christian Plützer, Isabel Hünig en Karl Kleinermanns van de Heinrich-Heine Universiteit uit Düsseldorf. Weliswaar is werk uit deze periode niet opgenomen in dit proefschrift, een publicatie zal hiervan zeker verschijnen. Christian, Isabel und Carlo, es war mir ein wahres Vergnügen mit euch zu arbeiten.

Het lijkt wel alsof er buiten het lab geen leven was. Dat was bijna zo. 's Ochtends was er gelukkig altijd het welkome "mogguh" vanaf de spam. Bruce, Vins, Len, Alec, Tors, Frey, Peet, Tom: "mogguh trug". Voor verdere onzin en goede raad kon ik terecht bij Suus en Died. In Amsterdam viel er zeker eens in de zoveel tijd van concertjes, lekker eten en drinken te genieten met Kirsten, Freya en Joris.

's Zondags had ik altijd het team der teams om naar uit te kijken: VVA/De Spartaan Zondag 4. Ondanks de mislukte poging om de Knudde Cup te veroveren heb ik vertrouwen in de toekomst, en ik weet jullie te vinden, bij welke club jullie dan ook weer rondzwerven.

Thuis op de Biesbosch moeten ze er ook van genoten hebben: vier jaar lang zo'n 5 tot 10 keer in de maand die fiets uit Utrecht weer op de overloop omdat Joost weer zo nodig moest meten. Alec, Tom, Marcel en Jo, ik zou nooit van mijn leven meer in dat kot willen wonen, maar denk er met enorm veel plezier aan terug.

Pa, moe, Erin, Mirte en Theo, ik dank jullie voor het vertrouwen dat jullie altijd in me gehad hebben, al was ik er zelf nooit zo zeker van.

En Lou natuurlijk. Kom Lou, het is af. We gaan bierdrinken!

CURRICULUM VITAE

Ik ben geboren op 8 oktober 1975 in het Noord-Hollandse Uitgeest, waar ik mijn hele jeugd heb gewoond. Na de lagere school in Uitgeest heb ik mijn middelbare schooltijd doorgebracht aan het Murmellius Gymnasium in Alkmaar. Zomer 1993 haalde ik mijn diploma en begon in Amsterdam de studie Natuurkunde aan de Universiteit van Amsterdam. Mijn afstudeerwerk heb ik uitgevoerd aan het FOM instituut voor Atoom- en Molecuulfysica (AMOLF) in Amsterdam in de groep van Bart Noordam. Onder begeleiding van Diederik Maas en Marcel Warntjes deed ik studies aan getsjilpte excitatie van rubidium (Rb) en de dynamica van Rydbergtoestanden van stikstofmonoïxide (NO).

Na deze studie heb ik een jaar (1998-99) in de FEL groep van Alan Schwettman aan Stanford University in Palo Alto, Californië, Verenigde Staten gewerkt. Hier werkte ik onder andere aan de ontwikkeling en karakterisatie van een nieuwe methode om staaroperaties te kunnen uitvoeren.

Na terugkomst begon ik op 1 januari 2000 aan het FOM instituut voor Plasmafysica “Rijnhuizen” aan het onderzoek wat tot deze promotie zal leiden. Hiertoe voerde ik in de groep “Moleculaire Dynamica” van Gert von Helden en Gerard Meijer metingen uit aan de infrarood eigenschappen van kleine modelsystemen van moleculen met een biologische relevantie. De resultaten van dit werk zijn beschreven in dit proefschrift.

Sinds 1 maart 2004 werk ik in de groep van Achim Peters van de Humboldt Universiteit in Berlijn aan de constructie van een magneetval voor ultrakoude moleculen die met de techniek van buffergas koeling geladen kan worden. Dit project wordt uitgevoerd op het Fritz-Haber-Institut der Max-Planck-Gesellschaft en is een samenwerkingsverband tussen de groepen van Achim Peters en Gerard Meijer.

PUBLICATIELIJST

- [1] Joost M. Bakker, Christian Plützer, Isabel Hünig, Thomas Häber, Isabelle Compagnon, Gert von Helden, Gerard Meijer, and Karl Kleiner, *Folding structures of isolated peptides as revealed by gas-phase mid-infrared spectroscopy*, Chem. Phys. Chem. , in press.
- [2] Isabelle Compagnon, Jos Oomens, Joost M. Bakker, Gerard Meijer, and Gert von Helden, *Vibrational spectroscopy of a non-aromatic amino acid-based peptide: identification of the γ -turn motif of the peptide backbone*, submitted for publication .
- [3] Pierre Çarçabal, Romano T. Kroemer, Lavina C. Snoek, John P. Simons, Joost M. Bakker, I. Compagnon, Gerard Meijer, and Gert von Helden, *Hydrated complexes of tryptophan: ion dip infrared spectroscopy in the molecular fingerprint region, 100–2000 cm^{-1}* , Phys. Chem. Chem. Phys. **6**, 4546 (2004).
- [4] Joost M. Bakker, Isabelle Compagnon, Gerard Meijer, Gert von Helden, Martin Kabeláč, Pavel Hobza, and Mattanjah S. de Vries, *The mid-IR absorption spectrum of gas-phase clusters of the nucleobases guanine and cytosine*, Phys. Chem. Chem. Phys. **6**, 2810 (2004).
- [5] Rebecca A. Jockush, Romano T. Kroemer, Francis O. Talbot, John P. Simons, Lavina C. Snoek, Pierre Çarçabal, Martina Havenith, Joost M. Bakker, Isabelle Compagnon, Gerard Meijer, and Gert von Helden, *Probing the glycosidic linkage: UV and IR ion-dip spectroscopy of a lactoside*, J. Am. Chem. Soc. **126**, 5709 (2004).
- [6] Joost M. Bakker, Luke Mac Aleese, Gerard Meijer, and Gert von Helden, *Fingerprint IR spectroscopy to probe amino acid conformations in the gas phase*, Phys. Rev. Lett. **91**, 203003 (2003).
- [7] Joost M. Bakker, Luke Mac Aleese, Gert von Helden, and Gerard Meijer, *The infrared absorption spectrum of the gas phase neutral benzoic acid monomer and dimer*, J. Chem. Phys. **119**, 11180 (2003).
- [8] Jos Oomens, Joost M. Bakker, Boris G. Sartakov, Gerard Meijer, and Gert von Helden, *The infrared spectrum of the benzoyl cation*, Chem. Phys. Lett. **367**, 576 (2003).

- [9] Rob G. Satink, Joost M. Bakker, Gerard Meijer, and Gert von Helden, *Vibrational lifetimes of aniline-noble gas complexes*, Chem. Phys. Lett. **359**, 163 (2002).
- [10] Joost M. Bakker, Rob G. Satink, Gert von Helden, and Gerard Meijer, *Infrared photodissociation spectroscopy of benzene–Ne,Ar complex cations*, Phys. Chem. Chem. Phys. **4**, 24 (2002).
- [11] J.A. (Hans) Piest, Jos Oomens, Joost Bakker, Gert von Helden, and Gerard Meijer, *Vibrational spectroscopy of gas-phase neutral and cationic phenanthrene in their electronic groundstates*, Spec. Acta A **57**, 717 (2001).
- [12] A.H. Chin, J.M. Bakker, and J. Kono, *Ultrafast electroabsorption at the transition between classical and quantum response*, Phys. Rev. Lett. **85**, 3293 (2000).
- [13] J.B.M. Warntjes, F. Robicheaux, J.M. Bakker, and L.D. Noordam, *Autoionizing Rydberg states in NO in strong electric fields*, J. Chem. Phys. **111**, 2556 (1999).